PULSED CHEMICAL LASER SCIENCE AND TECHNOLOGY

Avco-Everett Research Laboratory,
Incorporated

Prepared for:

Air Force Weapons Laboratory
Advanced Research Projects Agency

October 1973

UNCLASSIFIED
Security Classification

AD-769040

DOCUMENT CONTROL DATA - R & D

(Security classification of title, body of abstract and indexing annotation must be entered when the overall report is classified)

1. ORIGINATING ACTIVITY (Corporate author) Avco-Everett Research Laboratories 2385 Revere Beach Parkway Everett, Massachusetts 02149	2a. REPORT SECURITY CLASSIFICATION UNCLASSIFIED 2b. GROUP

3. REPORT TITLE

PULSED CHEMICAL LASER SCIENCE AND TECHNOLOGY

4. DESCRIPTIVE NOTES (Type of report and inclusive dates)

Final report; 8 November 1971-1 December 1972

5. AUTHOR(S) (First name, middle initial, last name)

6. REPORT DATE October 1973		7a. TOTAL NO. OF PAGES ~~190~~ 185	7b. NO. OF REFS 38
8a. CONTRACT OR GRANT NO. F29601-72-C-0017 new		9a. ORIGINATOR'S REPORT NUMBER(S) AFWL-TR-73-40	
b. PROJECT NO. 0870			
c. Task No. 06		9b. OTHER REPORT NO(S) (Any other numbers that may be assigned this report)	
d. ARPA Order No. 870			

10. DISTRIBUTION STATEMENT

Approved for public release; distribution unlimited.

11. SUPPLEMENTARY NOTES	12. SPONSORING MILITARY ACTIVITY AFWL (LRT) Kirtland AFB, NM 87117

13. ABSTRACT

(Distribution Limitation Statement A)

Research is described on a pulsed chemical laser operating on the reaction between hydrogen and fluorine at pressures above the second explosion limit. A laser energy density of 80 joules/liter-atm was demonstrated for a mixture of 10% F_2/10% H_2/80% He at 1.1 atm total pressure. This corresponds to a chemical efficiency of 8% and an overall electrical efficiency of 1.3% for our particular photolysis initiation. The highest vibrational level observed to give laser action is v = 6, and it is concluded that rapid deactivation of the upper vibrational levels is occurring. It was also experimentally determined that a high energy electron beam could dissociate F_2 with an expenditure of about 12 eV of energy per F-atom produced. When this number is coupled with the initial F-atom concentration required for good laser performance, overall electrical efficiencies of greater than 100% are predicted. Attempts have also been made to develop (1) fast yet accurate computer programs which contain the essential physics for the calculation of the vibration-relaxation cross section in an atom molecule collision, and (2) theoretical model of the propagation of a collimated pulsed laser beam in an absorbing medium. The energy absorbed by the medium causes heating, leading to an index-of-refraction change which causes self-defocusing.

DD FORM 1 NOV 68 1473

UNCLASSIFIED
Security Classification

14. KEY WORDS	LINK A		LINK B		LINK C	
	ROLE	WT	ROLE	WT	ROLE	WT
HF pulsed chemical laser Flash photolysis reaction initiation Electron beam-fluorine interaction						

AFWL-TR-73-40

AIR FORCE SPECIAL WEAPONS CENTER
Air Force Systems Command
Kirtland Air Force Base
New Mexico 87117

When US Government drawings, specifications, or other data are used for any purpose other than a definitely related Government procurement operation, the Government thereby incurs no responsibility nor any obligation whatsoever, and the fact that the Government may have formulated, furnished, or in any way supplied the said drawings, specifications, or other data, is not to be regarded by implication or otherwise, as in any manner licensing the holder or any other person or corporation, or conveying any rights or permission to manufacture, use, or sell any patented invention that may in any way be related thereto.

DO NOT RETURN THIS COPY. RETAIN OR DESTROY.

AFWL-TR-73-40

PULSED CHEMICAL LASER SCIENCE AND TECHNOLOGY

Avco-Everett Research Laboratory, Inc.
2385 Revere Beach Parkway
Everett, MA 02149

TECHNICAL REPORT NO. AFWL-TR-73-40

Final Report for Period 8 November 1971-1 December 1972

Prepared for

Advanced Research Projects Agency
1400 Wilson Blvd
Arlington, VA 22209

is

FOREWORD

This report was prepared by Avco-Everett Research Laboratory, Everett, Massachusetts, under Contract F29601-72-C-0017. The research was performed under Program Element 62301D, Project 0870, Task 06, and was funded by the Advanced Research Projects Agency (ARPA) under ARPA Order 870.

Inclusive dates of research were 8 November 1971 through 1 December 1972. The report was submitted 31 August 1973 by the Air Force Weapons Laboratory Project Officer, Captain William E. Thompson III (LRT).

The following scientists at AERL contributed to this report: Dr. Raymond L. Taylor; Dr. Jack Wilson; Dr. Hao-Lin Chen; Mr. Paul Lewis; Dr. Ramesh Sharma; Dr. James Wallace; and Mr. Walter Fyfe. The work on electron-beam dissociation of fluorine was done in collaboration with Dr. Roger Little and Mr. Robert Lowell of Simulation Physics, Inc., of Bedford, Massachusetts.

This technical report has been reviewed and is approved.

William E. Thompson, III

WILLIAM E. THOMPSON III
Captain, USAF
Project Officer

JOHN C. RICH
Lt Colonel, USAF
Chief, Advanced Technology Branch

RUSSELL K. PARSONS
Colonel, USAF
Chief, Laser Division

ABSTRACT

(Distribution Limitation Statement A)

Research is described on a pulsed chemical laser operating on the reaction between hydrogen and fluorine at pressures above the second explosion limit. A laser energy density of 80 joules/liter-atm was demonstrated for a mixture of 10% F_2/10% H_2/80% He at 1.1 atm total pressure. This corresponds to a chemical efficiency of 8% and an overall electrical efficiency of 1.3% for our particular photolysis initiation. The highest vibrational level observed to give laser action is v = 6, and it is concluded that rapid deactivation of the upper vibrational levels is occurring. It was also experimentally determined that a high energy electron beam could dissociate F_2 with an expenditure of about 12 eV of energy per F-atom produced. When this number is coupled with the initial F-atom concentration required for good laser performance, overall electrical efficiencies of greater than 100% are predicted.

Attempts have also been made to develop (1) fast yet accurate computer programs which contain the essential physics for the calculation of the vibration-relaxation cross section in an atom molecule collision, and (2) theoretical model of the propagation of a collimated pulsed laser beam in an absorbing medium. The energy absorbed by the medium causes heating, leading to an index-of-refraction change which causes self-defocusing.

TABLE OF CONTENTS

LIST OF ILLUSTRATIONS

LIST OF TABLES

SECTION I

PULSED HF CHEMICAL LASER

1.1 INTRODUCTION

Since the first demonstration by Pimentel,[1] chemical lasers have offered the promise of being the ultimate laser device. Because they use the chemical energy of reaction to produce the population inversion, high specific power is possible with chemical laser devices. By employing a chain reaction, high efficiency is also possible. Finally, by producing laser action in species such as DF or HCl, transitions within the region of the 4 μ atmospheric window are possible, thus assuring good atmospheric propagation. All of the above advantages, while significant, are accompanied by various disadvantages compared to CO_2 or CO lasers. For example, the most promising chemical lasers utilize halogen or halogen containing compounds with all the attendant handling problems, corrosiveness, and toxicity of such species. Chemical lasers in general are high gain systems and undoubtedly this fact will be a major technological problem in the development of large size, high power devices for military applications. Finally, and probably most important, chemical lasers, due to their very nature, necessitate more kinetic information and detail than most other laser systems. Frequently, it is the lack of these scientific data that has slowed the development of chemical lasers and forced this field of research to be fairly empirical in practice.

These disadvantages of chemical laser systems have undoubtedly slowed their development and enthusiastic support, but recent advances appear to have overcome some of these factors. It is the purpose of this report to describe the results of this research which has advanced the development of chemical lasers for military applications.

The work described herein is the second year of a two-year program to study the pulsed H_2/F_2 laser. The motivation for this work was the belief that an efficient, high energy laser could be developed from the rapid H_2/F_2 reaction (this is often referred to as an explosion laser). The Soviets[2] were the first to demonstrate that mixtures of H_2 and F_2 could be initiated rapidly and made to lase. It is intriguing to realize that after this early publication, no further reports on this type of laser have been noted from the Soviet Union.

The rationale for this type of laser is straightforward. There is considerable exothermicity in the reaction of H_2 with F_2 to form HF - about 6 eV/mole of reactants. It is known from the work of Polyani[3] that more than 50% of this exothermicity ends up in vibrational/rotational excitation of the product HF, and, therefore, in principle is available for

extraction as laser energy. Furthermore, the reaction mechanism involves a propagating chain; the production of a few F-or H-atoms can cause the entire mixture to react to completion. A chain reaction is important if one is to obtain high overall electrical efficiency, e. g., greater than 100% conversion of electrical energy into laser photons. By replacing H_2 with D_2, lasing on DF can be obtained in the spectral region of 4 μ, a good atmospheric window. It is known that H_2 and F_2 can react spontaneously (i. e., explosively) upon mixing. There are regions of pressure and temperature where "stable" gas mixtures can be prepared. In our investigations we have chosen to work at high pressures, above the second explosion limit. This requires that the gases be premixed before initiation of reaction in order to avoid a mixing limited situation. However, the advantage to be gained by high pressure operation is a great savings in overall system weight due to the minimal pumping requirements. Hence, the final objective of this research would be a chemical laser device operating on D_2/F_2 gas premixed at about atmospheric pressure and volumetrically initiated for scalability. For high power applications, such a device would have to be repetitively pulsed, and hence would involve flow and mixing of the gases upstream of the laser cavity.

During the first year's research effort the major accomplishments were (a) demonstration of the ability to produce stable mixture of $H_2 + F_2$ + various diluents at room temperature and pressure around one atmosphere, and (b) the demonstration of laser action in some of these mixtures initiated by flash photolysis of the F_2. The overall laser energy and efficiency obtained were small. It was found that more reproducible stable mixtures could be produced in a slow flow, mixing device. The data obtained in the first year's study indicated that increased laser efficiency and energy should be obtainable by increasing the photolysis of the F_2 to produce more F-atoms in order to speed up the chain reaction and by increasing the optical cavity length to increase the rate of stimulated emission.

Thus, the second year's program started with the objective of improving the overall energy density and efficiency of the pulsed, atmospheric pressure H_2/F_2 laser. A larger laser cavity device was constructed using coaxial flash lamps for photolysis with improved optical coupling to the cavity. With this device a parametric study of laser performance was investigated. To understand and correlate the trend of the data and to provide overall insight into the laser phenomenology a theoretical modeling effort was also performed and compared where possible to the experimental data. In support of the modeling effort, a theoretical calculation of important kinetic cross sections was undertaken. Besides the study of the laser itself, an experimental investigation was also carried out of the efficiency of a high energy electron beam as a possible volumetric initiation scheme.

The major conclusion of this second year's research program are the following:

A laser energy density of 80 joules/liter-atm was demonstrated for a mixture of 10% F_2/10% H_2/80% He at 1.1 atm total pressure. This corresponds to a chemical efficiency of 8% and an overall electrical efficiency of 1.3% for our particular photolysis initiation.

The main features of the laser performance appear to be understandable and predictable via our theoretical model. However, the agreement with data is only qualitative and certain important effects, such as the influence of rotational non-equilibration and optical output coupling, remain to be understood.

It was experimentally determined that a high energy electron beam could dissociate F_2 with an expenditure of about 12 eV of energy per F-atom produced. When this number is coupled with the initial F-atom concentration required for good laser performance, overall electrical efficiencies of greater than 100% are predicted. These results are very significant because they indicate that a high efficiency, scalable chemical laser operating at atmospheric pressure is close to reality.

The following sections present the significant results of this investigation of the pulsed, atmospheric pressure, HF laser. Section 1.2 describes the experimental details including the various diagnostics used to study laser performance and summarizes the experimental data obtained on the laser device. Section 1.3 describes the analytic model on laser performance and comparisons with data. Section 1.4 summarizes the conclusions on laser performance and understanding. Section 1.5 describes a theoretical approach to calculate vibrational energy exchange for species such as HF. Section 1.6 presents the experimental data on laser initiation techniques including a pin discharge and a high energy electron beam. Section 1.7 presents some overall comments on laser scalability and future device development.

1.2 EXPERIMENTAL

1.2.1 Description of Laser Experiments

1.2.1.1 Experimental Setup and Laser Operations

The Avco Everett Research Laboratory, Inc., experiments with the pulsed H_2/F_2 chemical laser had shown [5] that the requirements for improved chemical efficiency were, (i) a longer optical path length to increase stimulated emission, and (ii) a higher concentration of fluorine atoms produced by the flash lamps to trigger the reaction. Thus, under the present contract the apparatus was modified to increase the optical path length. In an attempt to increase the fluorine atom concentration, coaxial flash lamps were also used. Since these coaxial lamps surround the gas that is to be photolysed, they offer improved optical coupling to the cavity, whereas the geometry of the linear lamps used previously was such that only a small fraction of their output was coupled into the gas. Due to their lower inductance, the coaxial lamps also have a much shorter pulse length. It appears from the experimental results that a higher fluorine atom concentration is indeed obtained; the efficiency achieved is about two times higher than before, and larger output energies are also observed.

A diagram of the laser apparatus is given in Fig. 1. Fluorine and hydrogen are each premixed with diluent helium in separate storage tanks at pressures above ten and five atmospheres respectively. During a run, fast acting, electrically operated valves open to admit these gases to a mixing manifold which distributes the gases in the mixing region in alternate sheets 2 mm thick. The cross section of this mixing region is 12 x 10 cm. The storage tanks, lines and valves are of stainless steel, the mixing region is made of aluminum and Teflon sheets. The mixed gases pass into two coaxial Xe flash lamps and then exhaust into a 4-liter dump tank. A Kistler pressure gauge mounted upstream of the optical cavity is used to confirm that the xplosion originated in the cavity (see Fig. 1). Figure 2 shows a typical oscillogram of the pressure gauge signal. Note that the abrupt change in pressure, indicating reaction, occurs coincident with the flash lamp firing. On completion of a run, the fast acting valves close and other valves open to admit helium to the manifolds and to exhaust the dump tank. The system is thus flushed automatically at the end of each run.

The optical cavity is composed of an 8-m radius confocal copper mirror and various other elements such as sapphire, salt, germanium, or silicone plate reflectors. Both plate and mirror are installed in aluminum housings at the ends of the flash lamps, and are protected from the corrosive gases by a helium bleed flow. Figure 3 shows the diagram of the porous wall bleed system used in the experiment. The flash lamps have an internal diameter of 17 mm, and an active length of 25 cm; the active length of the cavity is therefore about 50 cm. The lamps have a duraction (full width at half height) of about 1 μsec, and are each energized by a 1.5 μf capacitor at 20 kV, giving 300 joules per lamp. Figure 4 shows a typical flash signal monitored by an IP28 photomultiplier.

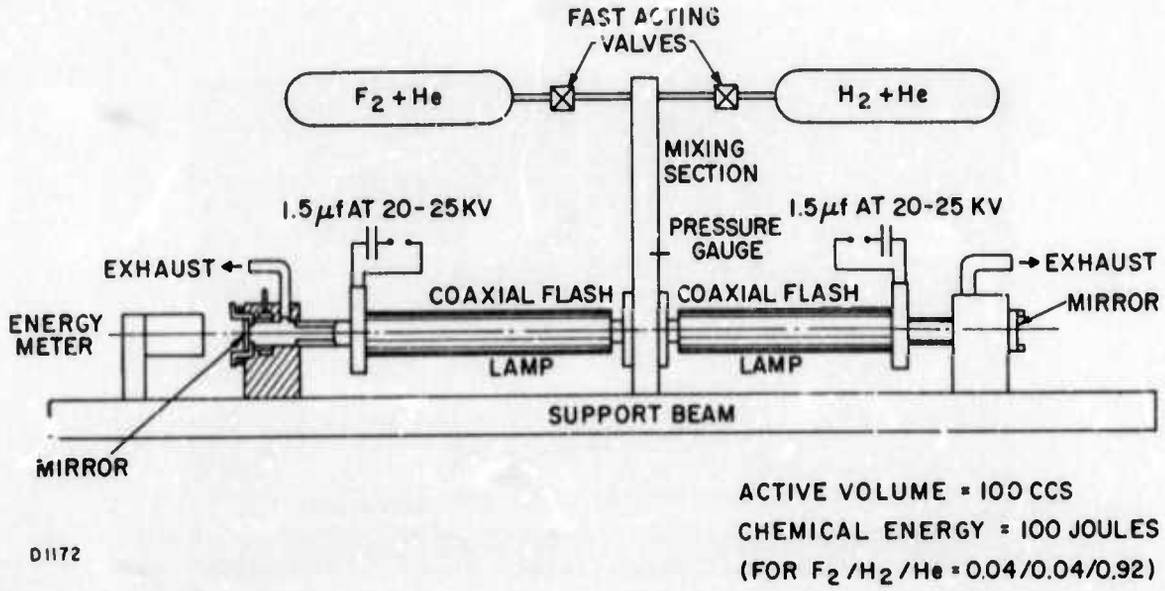

Fig. 1 Schematic of Flash Photolysis Laser Experiment

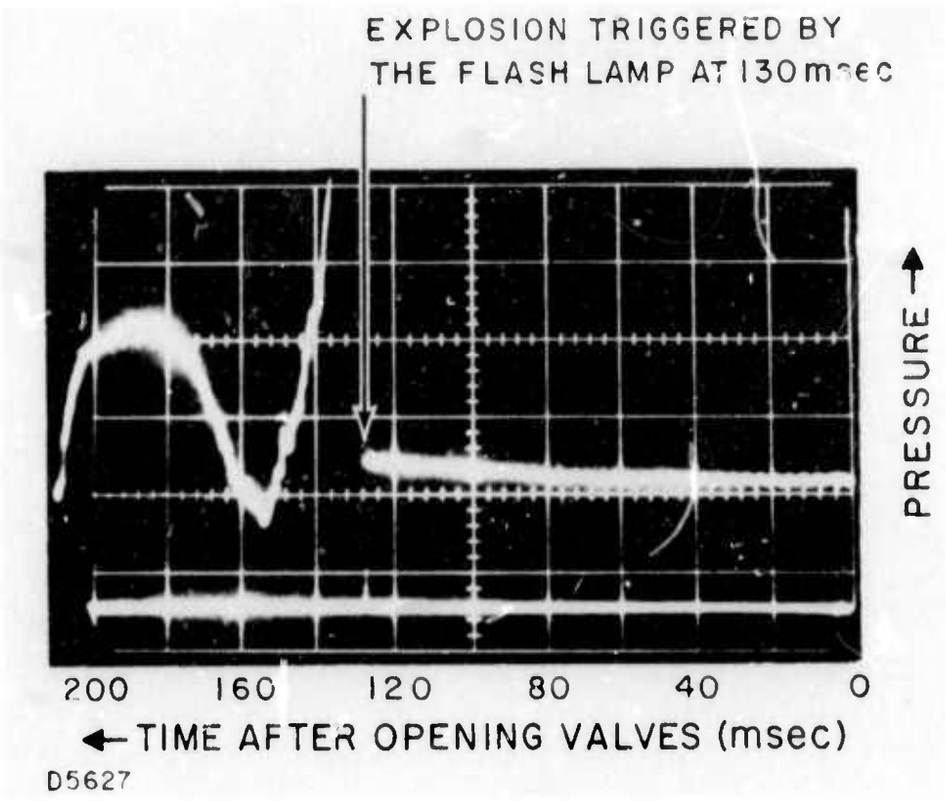

Fig. 2 Oscillogram of the Pressure Gauge Signal

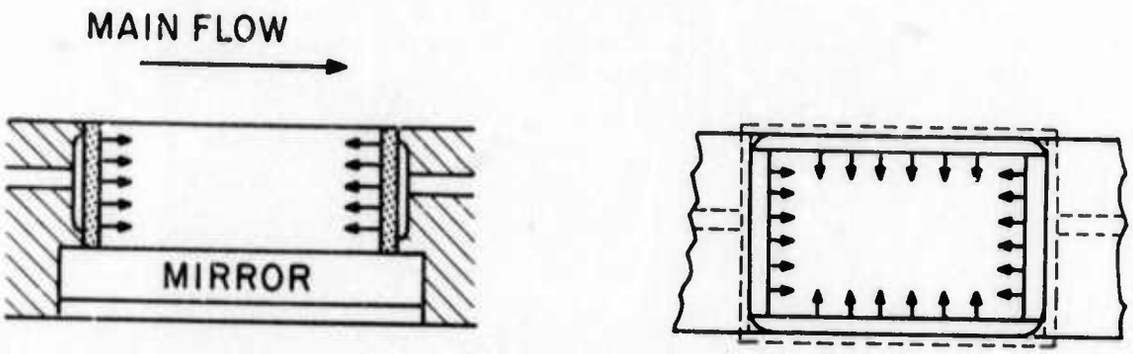

Fig. 3 Diagram of the Bleed System Used to Protect the Mirrors from Chemical Attack

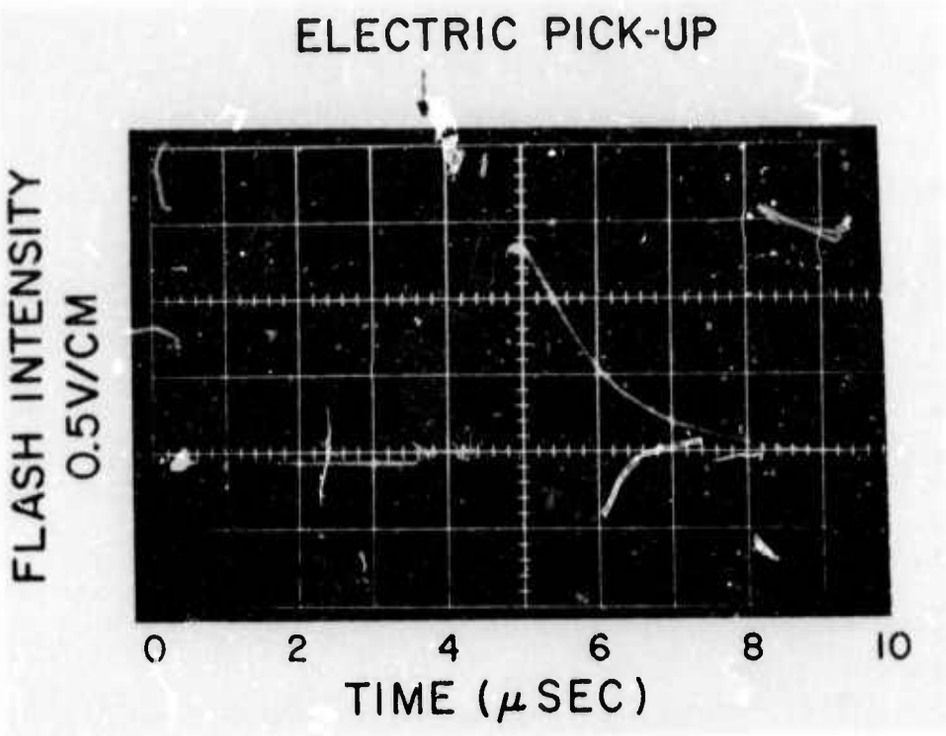

Fig. 4 The Pulse Shape of the UV Signal Emitted by the Flash Lamp

Measurements of the laser output energy were made with a calorimeter. The details of construction of this calorimeter are described later. The temporal variation of the laser duration was monitored with an InSb PEM detector viewing scattered radiation from the calorimeter surface. For spectral analysis, an 0.5 meter Jarrell-Ash monochromator fitted with a gold-doped germanium detector was used. The signals from the detectors are amplified, displayed on an oscilloscope and photographed.

Matheson prepurified grade H_2 (99.95%), high purity grade He (99.95%), and high purity grade O_2 (99.95%) were used without further purification. The reason for using O_2 in the mixtures is given in Section 1.2.2.1. In order to remove any HF contamination (~1%) from the F_2 tank, F_2 gas (98%), supplied from Matheson, was passed through an NaF_2 adsorber prior to the preparation of F_2/He mixtures. It was found that more than 90% of the HF in F_2 could be removed by this technique. The temperature of both the laser cavity and mixing bottles was room temperature in all experiments.

1.2.1.2 Diagnostic Experiments

1.2.1.2.1 Measurement of the Percent of F_2 Dissociation Produced by the Flash Lamp

Since the rate of the H_2/F_2 reaction depends upon the value of the concentration of F atoms [F] initially produced, a precise measurement of [F] or % F_2 dissociation is very important. Two efforts were made to measure the initial fluorine atom concentration. First, an ultraviolet He-Cd laser (Coherence Radiation Corp.) operating at 3250 Å was used to measure the fluorine molecule concentration with the object of determining the percentage dissociation of F_2 caused by the flash lamps. This experiment was unsuccessful due to (i) the small initial percentage dissociation (<1%) and hence the small change in 3250 Å absorption and (ii) the large inherent fluctuation in intensity of the laser signal (>10%). Clearly a much more stable He-Cd laser is needed for this measurement. Due to lack of resources, no effort was expended in attempting to stabilize the He-Cd laser.

The second technique was to react the F atoms initially produced by the flash with $HC\ell$ to form HF

$$F + HC\ell \rightarrow HF + C\ell \qquad (1)$$

and measure the concentration of HF with a probe HF laser. In this technique no H_2 is used in the gas mixture, so that in principle no chain reaction occurs. The quantity of HF produced is then exactly the number of fluorine atoms present initially. The [HF] can be measured after sufficient delay for vibrational relaxation, by absorption of an HF laser pulse.

Figure 5 shows the experimental arrangement used. The HF $1P_4$ transition was generated by an AVCO C950 N_2 laser operated on a

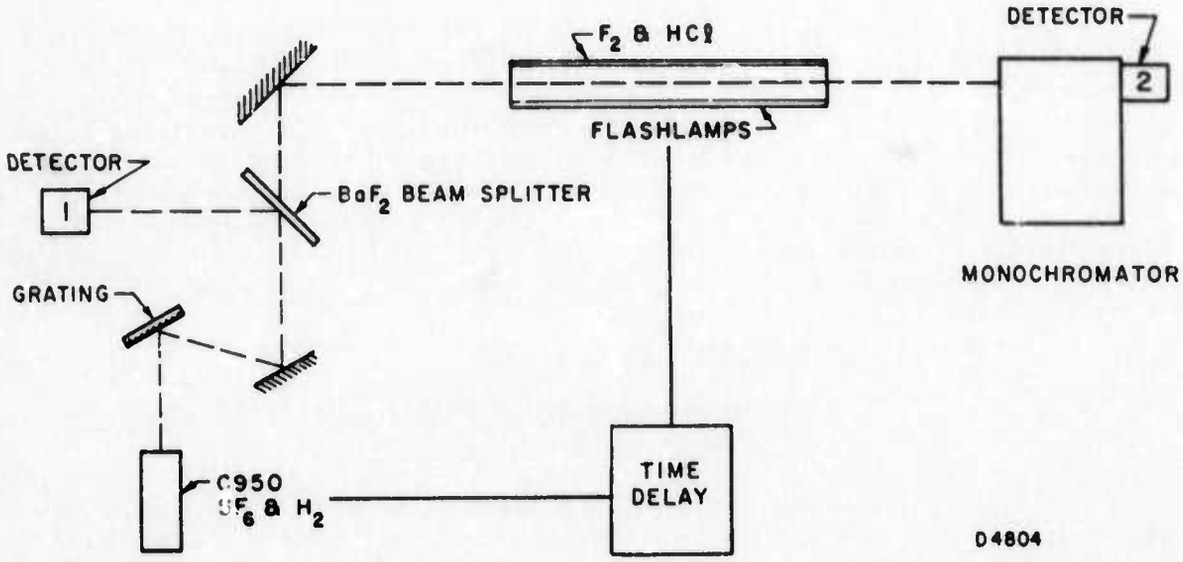

Fig. 5 Diagram of Apparatus Used for Determination of Concentration of HF Produced by Reaction of F + HCl → HF + Cl

mixture of SF_6 and H_2. The BaF_2 beam splitter reflects about 10% of the $1P_4$ line into Ge-Au detector #1 and transmits 90% through the test cell and thereafter into the monochromator and Ge-Au detector #2. The test cell is the actual laser cavity with two BaF_2 windows. The experimental sequence is identical to that of the laser experiment except that H_2 is replaced by $HC\ell$ in one mixing tank. A time delay generator was used to produce a desired delay for firing the probe laser after the flash lamp initiation. Thus, detector #1 monitors the value of I_o (initial signal) and detector #2 monitors the intensity I with absorption simultaneously. For mixtures containing 0.1 atm F_2 an optical path length of about 50 cm is used. For higher F_2 pressures, an optical path of 5 cm was used. An averaged absorption coefficient for the $1P_4$ HF line determined previously[5] was used; this value is 3 cm^{-1} $torr^{-1}$. The results of this experiment are discussed in Section 1.2.2.5.

1.2.1.2.2 Measurement of the Rate of the $H_2 + F_2$ Reaction by Monitoring the Transient F_2 Concentration

There has been a controversy in the literature[6] concerning the possibility of chain branching reactions in the H_2/F_2 explosion. Unfortunately, no detailed information on the rate constants of the branching reaction(s) is known. The fact that a second explosion limit exists in the H_2/F_2 system indicates that chain branching does participate in the reaction. Russian scientists[7] have claimed that this chain branching occurs through the reaction

$$HF\ (v \geq 4) + F_2 \rightarrow HF + 2F \qquad (2)$$

which indicates that HF vibrationally excited in states greater than v = 3 can participate in dissociating F_2. It is not obvious whether such a reaction should increase or decrease laser efficiency: by speeding up the reaction, it should increase the efficiency, however, the increased reaction rate is accomplished by removing vibrationally excited HF, which should decrease efficiency. However, if branching did occur with a reasonably fast rate, the H_2/F_2 reaction could proceed much more rapidly than without branching. The temperature of the reacting gas would also increase more rapidly, and, hence, the laser duration would be shorter. In order to experimentally estimate the overall rate of reaction in our H_2/F_2 system, the transient concentration of F_2 was measured.

Figure 6 shows the experimental set up. An AVCO C950 N_2 laser, producing 2-kW pulses at 3371 Å was used as a stable light source. The reflected 3371 Å beam from the front surface of the back sapphire window was monitored by the 1P28 photomultiplier equipped with a 100 Å bandpass UV transmission filter centered at 3371 Å. The detector is located 11 meters away from the flash lamp. To avoid any flash lamp light scattering into the detector, a 10-meter long black box with small (5 mm diameter) entrance and exit holes was placed between the photomultiplier and the flash lamp. The overall response time of the detector and amplifier are less than 0.2 μsec. A time delay box was used to control

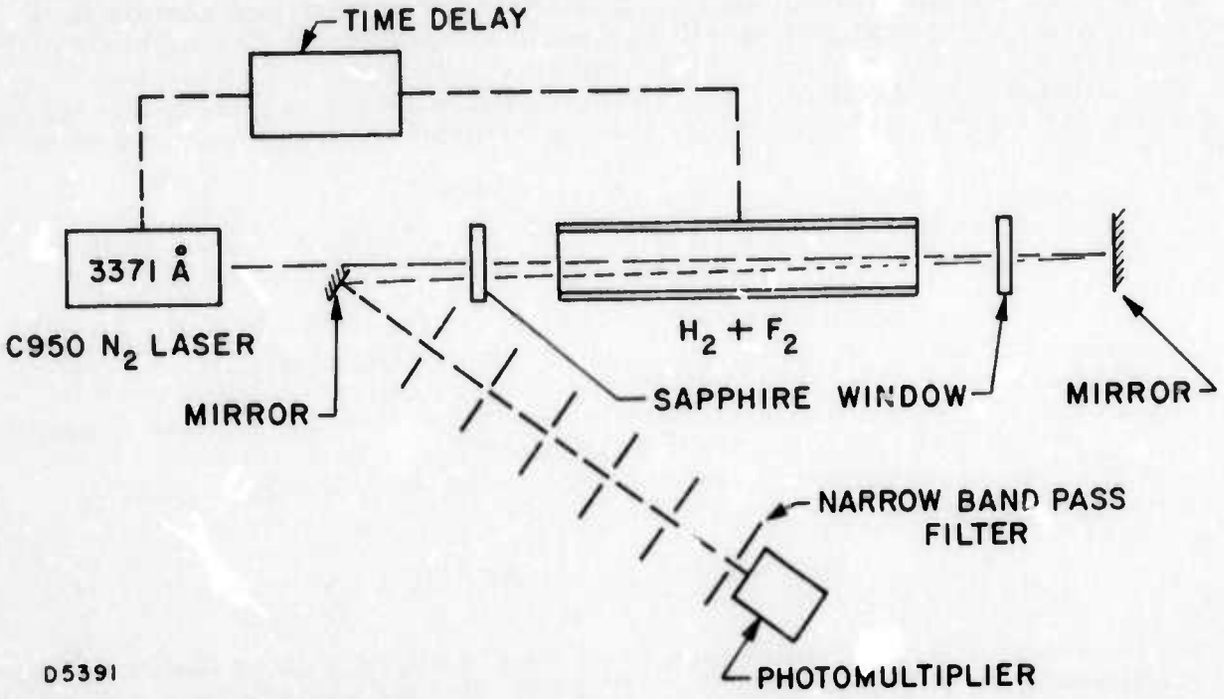

Fig. 6 Diagram of Apparatus Used for Determination of the Transient Concentration of F_2 in the Mixture

the firing tine of UV laser after the flash lamp initiation. The transient percentage absorption of the 3371 Å line by F_2 molecules in the laser cavity is repeatedly measured with varying time delays after flash initiation. Based on these data, the fraction of F_2 reacted at various times and hence the rate of the H_2/F_2 reaction is calculated. The results are given in Section 1.2.2.7.

1.2.1.2.3 Measurement of Laser Output Spectra

For a better understanding of the detailed reaction kinetics involved in the H_2/F_2 system, we have investigated the time-dependent spectra of our HF laser. Figure 7 shows the optical set up for measuring both total laser output energy and laser transitions simultaneously. An InSb PEM detector was used to monitor HF IR laser emission. The operating time constant was less than 0.1 μsec. Transition wavelengths were identified on a 0.5-meter Jarrell-Ash monochromator (Model 82-000) equipped with a 4 μ-blaze grating and calibrated with a visible He-Ne laser. Laser pulse energies were measured with a calibrated AVCO made energy meter (see next section). Limited experiments on D_2/F_2 laser action were also performed. The results are given in Section 1.2.2.4 and 1.2.2.5.

1.2.1.2.4 Construction and Calibration of an Energy Meter

The energy meter used previously was a commercial product (TRG model 100) which had an input aperture of only 1-cm diameter. If the output beam were considerably larger than this, clearly erroneous readings would be obtained. It was decided that a large size energy meter was required for this experiment, placed as close to the output mirror as possible. Such energy meters are available commercially, but only with a long *delivery time*, and at quite high cost. These commercial meters employ a polished cone to collect the radiation, and although the manufacturers claim that they are equally responsive to all wavelengths, it was not clear that this claim had been verified. Moreover, at high input energies, a cone will focus the radiation, creating an air breakdown which prevents the meter from receiving all the energy. It was decided, therefore, that it would be better to build an energy meter.

The general arrangement of the resulting meter is shown in the top half of Fig. 8. Radiation is absorbed by the grooved anodized face of a thin piece of aluminum 5-cm diameter. On the back of the aluminum are attached 19 thermocouple junctions, and 19 junctions are also attached to a similar reference slug of aluminum, wired in series as indicated in Fig. 8 to increase the output signal. The meter is supported by lucite stand-offs inside a copper shield to prevent air currents from affecting the signal. The output signal is fed to a micro voltmeter. This calorimeter is capable of detecting a millijoule of energy.

It was calibrated by both calculations of the heat rise experienced by the aluminum on absorbing a given quantity of energy, and, in addition, a set of HF laser pulses from an AVCO C950 laser operating on

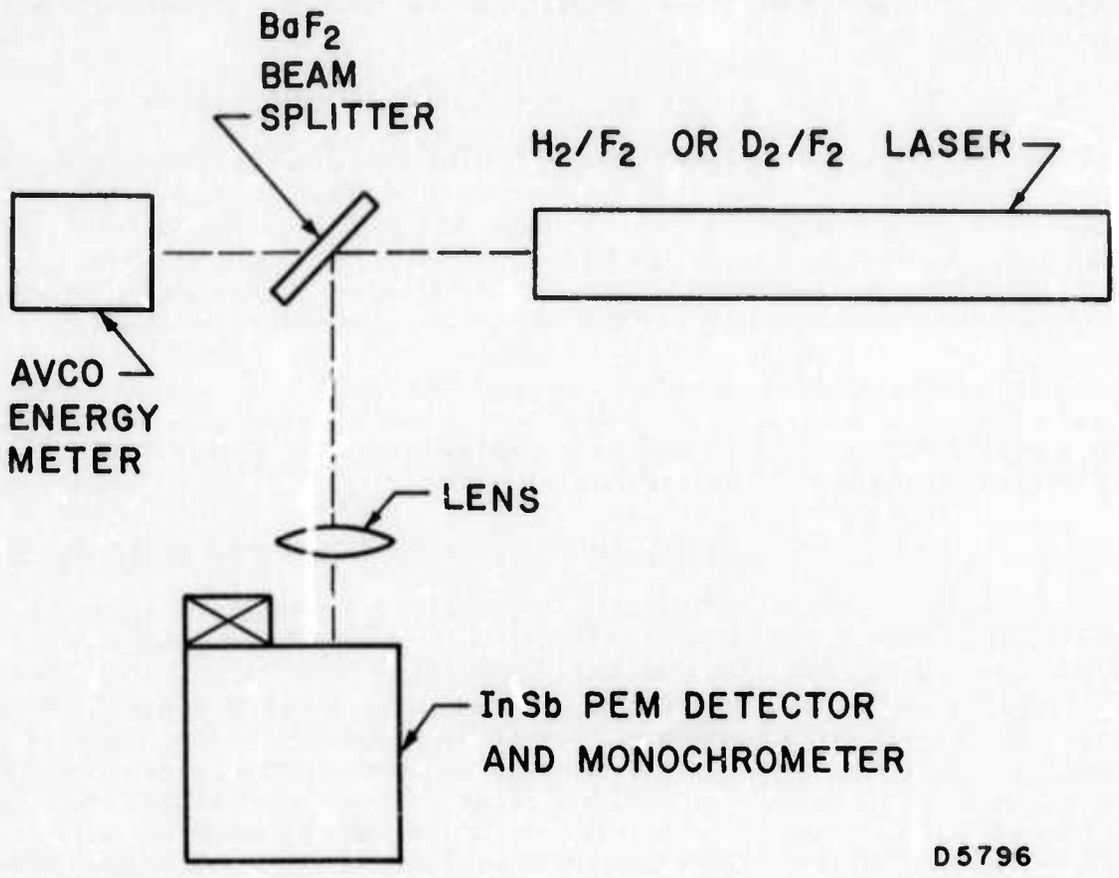

Fig. 7 The Optical Set Up Used for Measuring Laser Output Energy and Laser Transitions

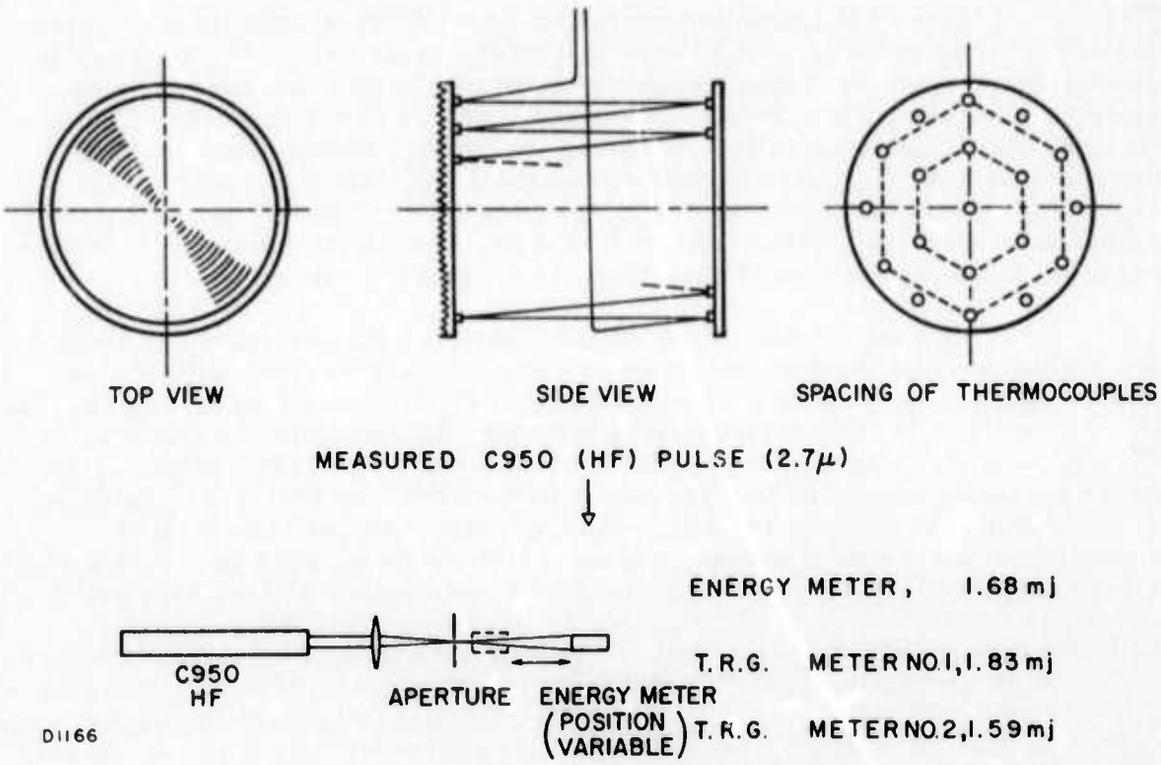

Fig. 8 Diagram of Energy Meter and the Calibration Tests of the Energy Meter

SF_6 and H_2 was directed onto the meter after being focused down and passed through an aperture (see lower half of Fig. 8). This aperture was smaller than the entrance aperture of two available TRG meters, and these were also used to measure the energy of the HF pulses. The energy of a single HF laser pulse as measured by each instrument is given in Fig. 8, and shows good agreement for all 3 meters.

The 19 thermocouples on the back of the aluminum slug were spaced so they each served an approximately equal area. In this case it can be shown that the signal is independent of whether the energy is applied at a single point, or over the whole surface of the detector. This was verified experimentally by moving the energy meter away from the aperture so that the pulse spread to fill the entire aluminum slug. Provided the size of the laser spot was not greater than the meter face, the signal was identical whether the meter was close to the aperture, with the pulse only falling on a small region of the meter, or far away.

Before actually building the energy meter, tests were made of the reflectivity of various surfaces at various wavelengths, with the objective of finding a surface that was fully absorbing at all wavelengths. It was known that black anodized aluminum was an excellent absorber at 10.6 μ, so a flat sample of this was chosen as the reference point. Two other surfaces with circular grooves were made, one with a 30° half-angle groove, the other with a 15° half-angle groove, and both were black anodized. These two surfaces, plus the flat surface, were measured with a reflecting attachment on a Perkin Elmer spectrophotometer between 2 and 11 μ. Unfortunately, we possess no instrument for making total reflectivity measurements. Nor, despite the abundance of manufacturers of optical accessories in the Boston area, was it easy to find anyone else who had one. Finally, one was located at EG&G, and this firm kindly agreed to run the samples for us. Their instrument, however, could only measure between 1 and 2.7 μ. However, the traces taken showed a remarkable independence of wavelength within their measuring range, and it was felt safe to extrapolate this result to longer wavelengths. The results are presented in Fig. 9. Where N.M. appears, it means no measurement was made. The measurements on the flat sample showed that there is a considerable diffuse reflectivity which is reduced somewhat by the 30° half-angle grooves, and considerably reduced by the 15° half-angle grooves. On the basis of these tests, the black anodized surface with 15° half-angle grooves was considered to be equivalent to a fully absorbing surface, and was used as the collecting surface of the energy meter that we constructed.

1.2.2 Results

1.2.2.1 Gas Mixture Stabilization

During the course of our experimentation, it had been noticed that different results were obtained with different bottles of fluorine -- some bottles showing spontaneous reaction on mixing, others being more stable. Since the work of Levy and Copeland[8] had shown that oxygen

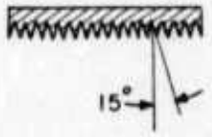

$\lambda(\mu)$	2 – 2.7	4	10.6	2 – 2.7	10.6	2.0 – 2.7	10.6
SPECTRAL	~ 3	.24	0	N.M.	N.M.	0	0
TOTAL	.75	N.M.	N.M.	.45	N.M.	.05	N.M.

D1168

Fig. 9 Results of Spectral and Total Reflectivity Measurements of Three Different Surfaces

inhibits the spontaneous reaction of H_2/F_2, it seemed natural to suspect that varying amounts of oxygen in the fluorine tanks were causing this effect. The manufacturer claimed a maximum oxygen level of 2% in the fluorine. Consequently, amounts of oxygen up to 2% of the fluorine were added to a mixture that exhibited spontaneous reaction. The reaction was monitored by the Kistler pressure gauge as the gases flowed through the cavity. The results were:

i) Additions of oxygen to the hydrogen mixing tank did not affect the mixture stability.

ii) Addition of oxygen to the fluorine mixing tank enhanced the mixture stability, increasing the time to spontaneous explosion on mixing, until at 0.4% of the total mixture, the gas was completely stable, i.e., it did not react at all unless triggered.

Next, the effect of oxygen addition on laser output was studied. Using a gas mixture composition of $H_2/F_2/He = 0.08/0.04/0.88$, various amounts of oxygen were added. The actual technique was to use helium to which oxygen had been admixed. The laser energy was measured using a stable semi-confocal cavity with a barium fluoride output coupling flat. The results are shown in Fig. 10, indicating a steep rise in energy as the mixture becomes less stable, i.e., less added O_2. With a fairly unstable mixture an energy of 1.8 joules was obtained. However above 0.2% of added O_2 the mixture is very stable, and the output energy is independent of oxygen concentration. Since the reproducibility is the most important thing in any systematic study, we have used gas mixtures with 0.2 or 0.4% of added O_2 for all our subsequent experiments.

Possible reasons for the stabilization of H_2/F_2 mixture by molecular oxygen may be postulated as follows:

$$F_2 + M \xrightarrow{k_1} 2F + M \text{ (where M is surface)} \qquad (3)$$

$$F + O_2 + M' \xrightarrow{k_2} FO_2 + M' \text{ (where M' could also be a surface)} \qquad (4)$$

followed by

$$FO_2 + F \xrightarrow{k_3} F_2 + O_2 \qquad (5)$$

For steady-state conditions, the following relations hold:

$$\frac{d[F]}{dt} = \frac{1}{2} k_1 [F_2] [M] - k_2 [F] [O_2] [M'] - k_3 [FO_2] [F] = 0 \qquad (6)$$

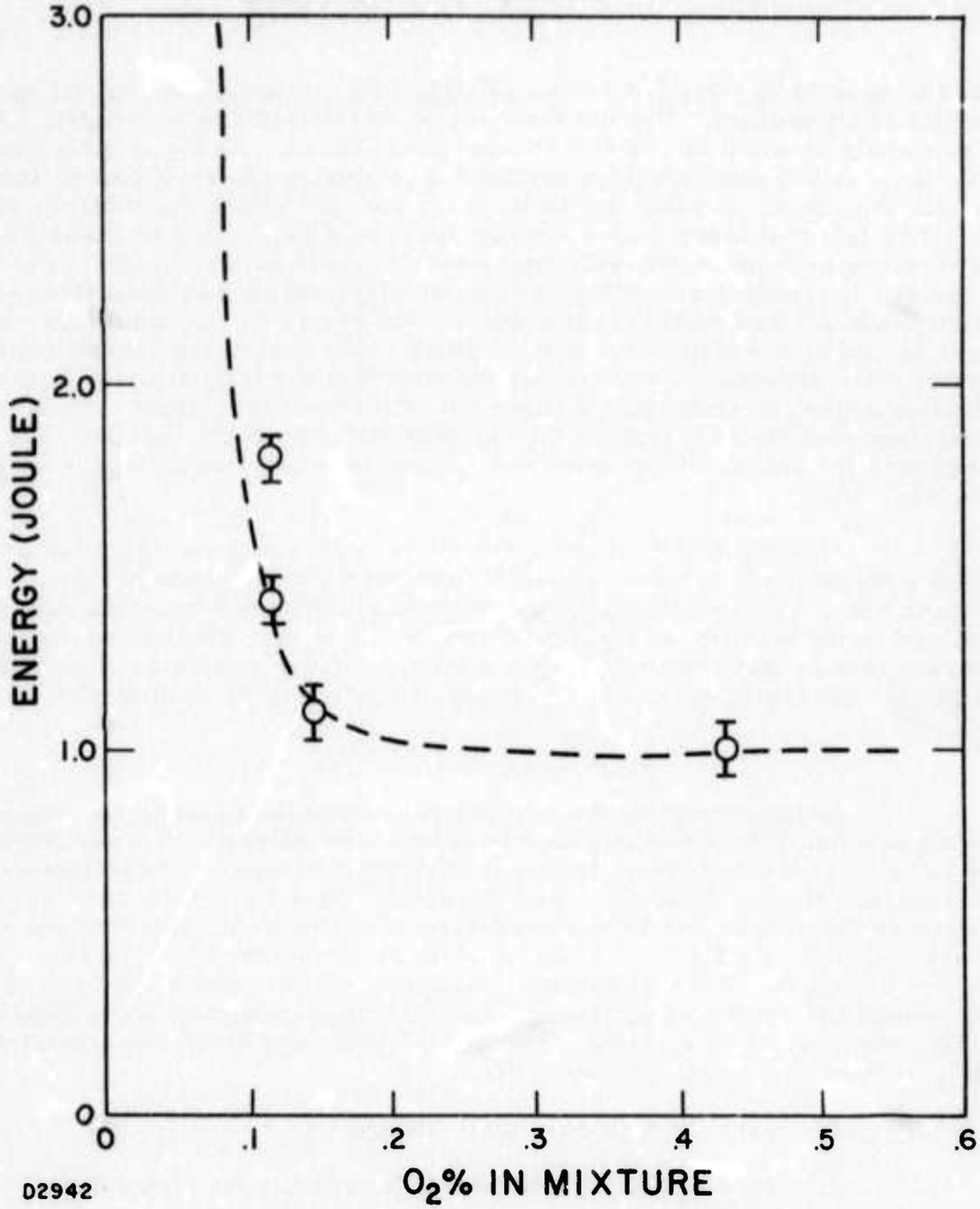

Fig. 10 The Effect of O_2 Additive to the Laser Output Energy Observed in a $H_2/F_2/He$ Mixture

$$[F]_{s.s.} = \frac{\frac{1}{2} k_1 [F_2] [M]}{k_2 [O_2] [M'] + K_3 [FO_2]} \qquad (7)$$

For the case of $k_2 [O_2] [M'] \ll k_3 [FO_2]$, $[F]_{s.s.}$ does not depend on the amount of O_2 present. But for the case of $k_2 [O] [M'] \gg k_3 [FO_2]$, $[F]_{s.s.}$ is inversely proportional to the amount of O_2 added. As O_2 is added to the gas, the F-atom concentration decreases to a value where it can no longer initiate the chain. Further addition of O_2 does not affect the mixture stability. The fact that laser output energy decreases as O_2 is increased (and the mixture becomes noticeably more stable) could be due to the presence of the small steady-state concentration of FO_2 produced by Reaction (4) which could act as a chain terminator via Reaction (5). O_2 could also affect laser action by the formation of H_2O which could deactivate vibrationally excited HF. However, calculations indicate that the formation of H_2O is too slow under our conditions to have an effect on laser output. This is consistent with the observation that further addition of O_2, beyond that necessary for stabilization, does not appear to reduce laser output energy (see Fig. 10).

Unfortunately, none of the above-mentioned rate constants by which a more quantitative discussion could be made are known. At the present time, we can only speculate that this may be the reaction scheme involved in the stability of H_2/F_2 mixtures. However, it is of considerable interest to note that additional laser energy might be available if stability could be achieved by other than addition of O_2, e.g., by cooling the gas.

1.2.2.2 Output Energy Measurements

Experience with the earlier version of the pulsed, flowing laser had shown that nitrogen is inferior to helium as a diluent. This is probably due to the fact that helium is less effective than nitrogen in deactivating vibrationally excited hydrogen fluoride.[9] We have therefore used only helium as the diluent in our experiments. The optimum ratio found previously, namely $H_2/F_2/He = 0.04/0.04/0.92$ was normally used as a standard mixture. Runs were also made with various other mixture ratios, with deuterium replacing hydrogen, and with other mixed halogen fluoride compounds in place of fluorine. HF and DF laser radiation was systematically studied in several different ways:

1. Varying the flash lamp energy,
2. Varying the F_2 concentration with the H_2 concentration fixed,
3. Changing the initial F-atom concentration by introducing additives,
4. Changing both the H_2 and F_2 concentrations simultaneously,

5. Varying the output coupling, and

6. D_2/F_2/He mixture results.

The results can be summarized as follows:

1.2.2.2.1 The Effect of Varying Flash Lamp Energy

The laser pulse energy was measured at various flash lamp energies (and hence at various initial F-atom concentrations) for a gas mixture of H_2/F_2/He = 0.12/0.04/0.84 at a total pressure of 1.1 atm and 90% output coupling obtained with a total reflecting copper mirror at one end and a BaF_2 plate at the other. The H_2 enriched mixture was used to assure that all the F-atoms produced by the flash lamp would react with the excess H_2 molecules. In this way a direct correlation between the lamp energy and laser output energy can be obtained. In Fig. 11 the measured laser pulse energy is plotted against the energy of the flash lamp capacitor bank. As one can see, up to the maximum flash energies available with this apparatus (700 J) the laser energy is still increasing with flash energy or equivalently initial F-atom concentration.

1.2.2.2.2 The Effect of Varying F_2 Concentration

Another means of varying the F-atom concentration is to change the F_2 concentration at fixed flash energy. These measurements were done at fixed H_2 concentration and variable F_2 ratios. The experimental conditions are exactly the same as described above, namely a 90% output coupling and a total pressure of 1.1 atm. Figure 12 shows the dependence of output energy as a function of F_2 concentrations. An increase in laser energy as F_2 concentration increases is observed. The slope gives a value of 40 joules of laser photons/atm of F_2 used in an active volume of 0.1 liter at the described experimental conditions.

1.2.2.2.3 The Effect of Increasing F-atom Concentration by Introducing Additives such as MoF_6

Molecular MoF_6 has been noted to have a large absorption coefficient in the UV spectral region where the xenon flash lamps emit. Hess has recently reported[10] that an enhancement in HF laser output energy was observed as MoF_6 was added to his H_2/F_2 system. It is believed that this enhancement was due to the additional initial F-atoms generated by the MoF_6 flash photolysis. Since both of our experiments above indicate that the output energy will increase with $[F]_i$, a trace of MoF_6 (0.1%) was added to the 0.12/0.04/0.84 mixture. Runs were made at various values of capacitor flash lamps energy. The result is shown in Fig. 13. Again, it is found that the laser output increases with the flash lamp energy, but less energy is observed with MoF_6 than without it. At low flash lamp energy, the opposite result is obtained. The addition of MoF_6 should increase the $[F]_i$, as should an increase in the flash lamp energy. If the extra fluorine atoms produced by MoF_6 were actually

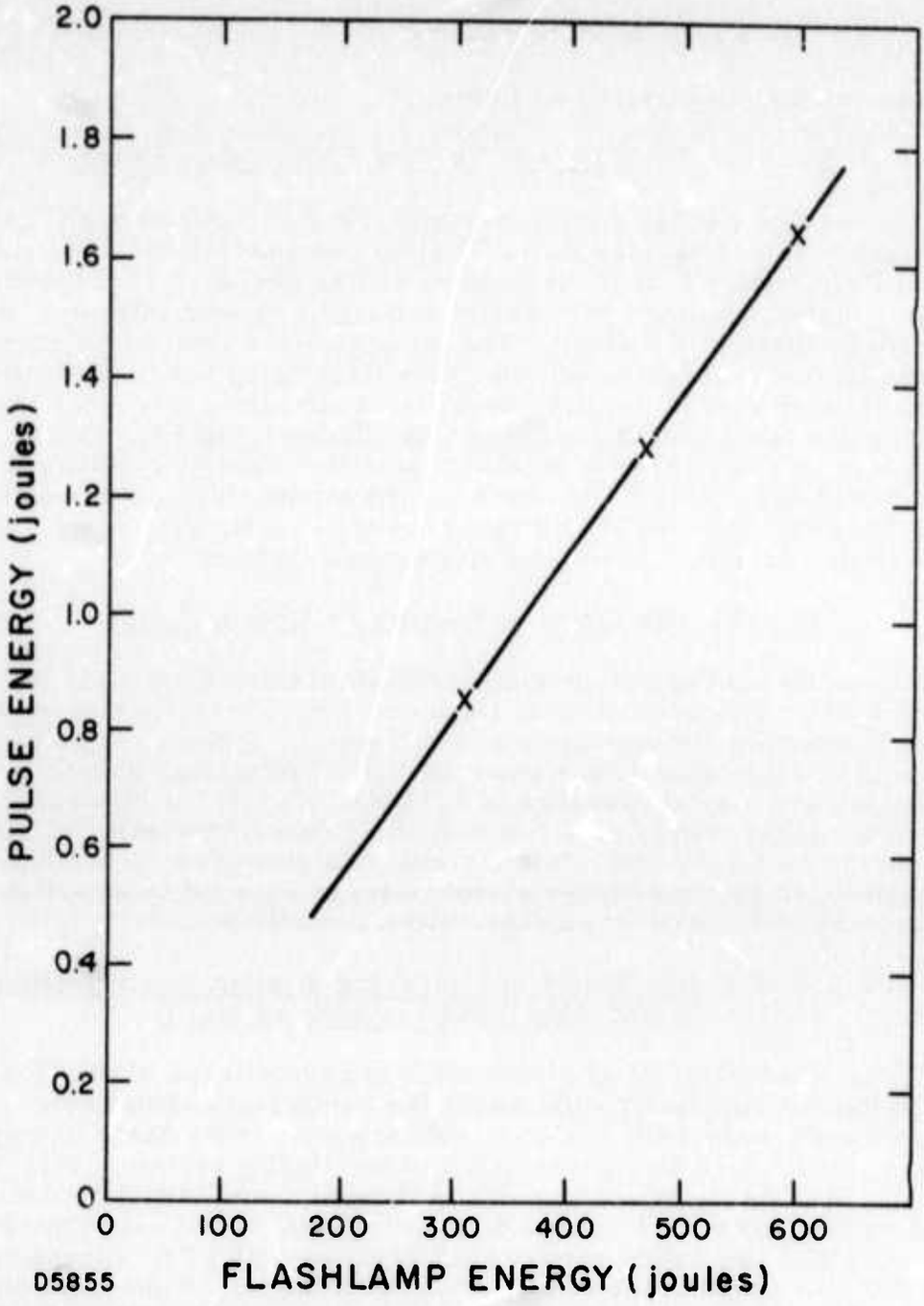

Fig. 11 The Effect of Changing Flash Lamp Energy to the Laser Output Energy Observed in the $H_2/F_2/He$ Mixture

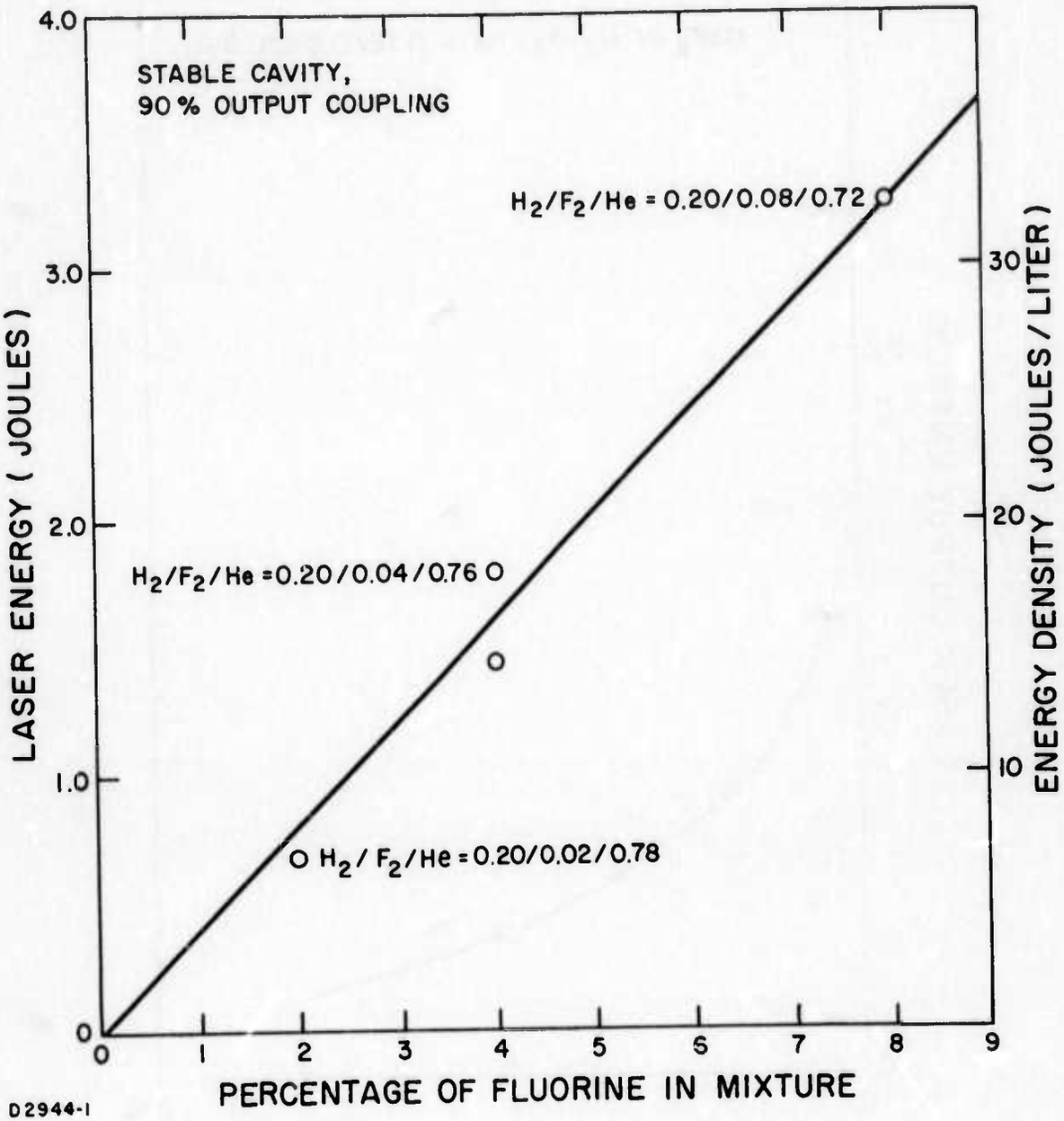

Fig. 12 The Effect of Changing F_2 Concentration to the Laser Output Energy Observed in the $H_2/F_2/He$ Mixture

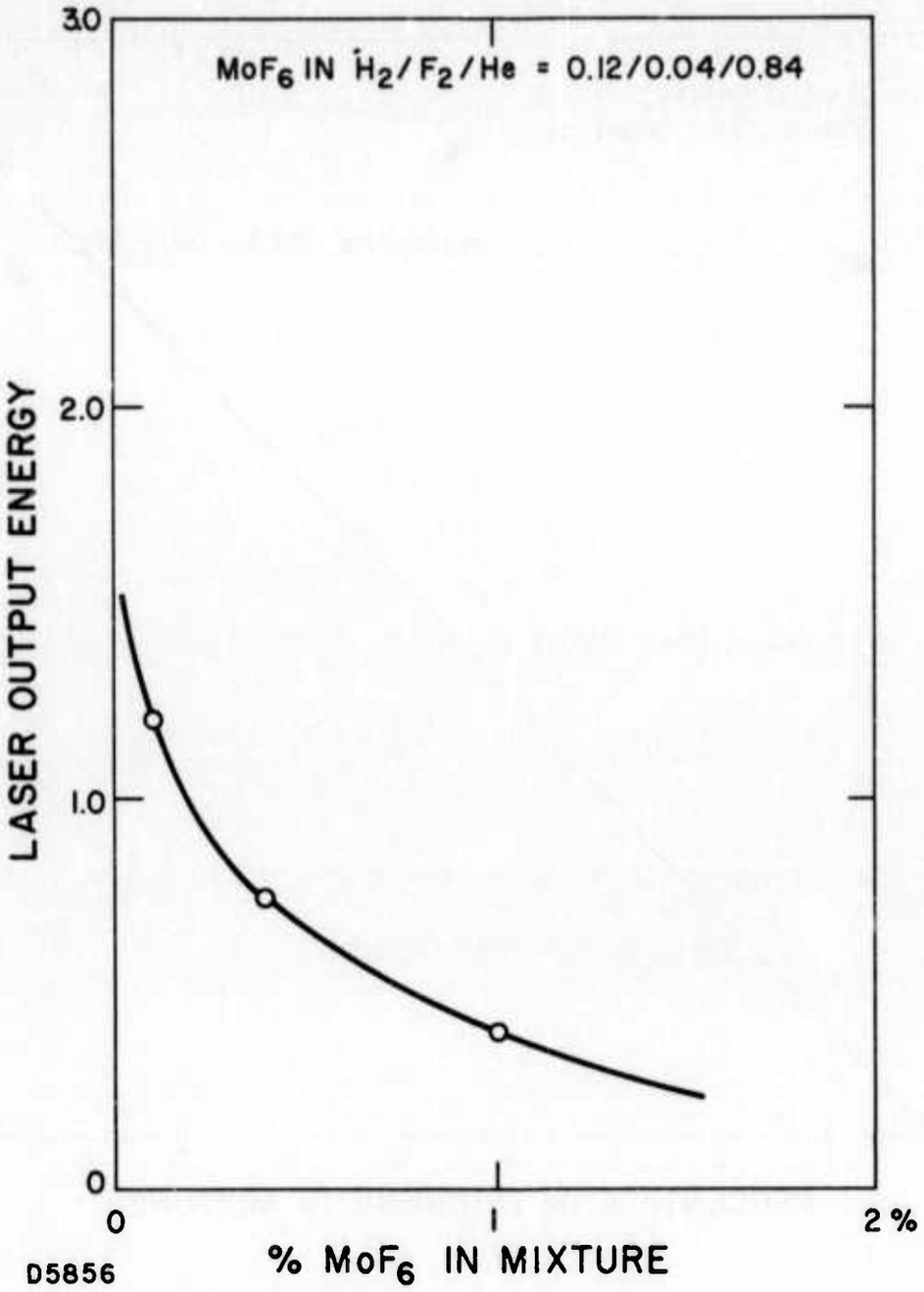

Fig. 13 The Effect of Changing MoF_6 Concentration to the Laser Output Energy Observed in the $H_2/F_2/He$ Mixtures

deactivating the HF, one would expect the laser energy to fall at high flash lamp energy. It is not likely that MoF_6 has extremely high quenching efficiency for vibrationally excited HF molecules.

The interpretation of this result is not very clear. One possible explanation is that some kind of chain terminating reaction is introduced as MoF_6 is added to the system. For example, radicals like MoF_5 generated from flash photolysis of MoF_6

$$MoF_6 \xrightarrow{\text{flash}} MoF_5 + F \tag{8}$$

could serve as a chain terminating reactant

$$MoF_5 + F \rightarrow MoF_4 + F_2 \tag{9}$$

This could result in a lower laser energy although $[F]_i$ might be higher. Another possibility is that MoF_6 could act as an effective quencher for rotational deactivation of HF. Process like

$$\begin{aligned} &HF\ (v=n,\ J=\ell) + MoF_6\ (v_i=o) \\ &\rightarrow HF\ (v=n,\ J=\ell\ -1 \text{ or } \ell-2) + MoF_6\ (v_i=1) \end{aligned} \tag{10}$$

could be quite fast due to the close resonant rotation-to-vibrational energy transfer between MoF_6 and HF. As will be apparent later, rotational equilibration effects can be important in the H_2/F_2 laser.

If rotational relaxation of HF by MoF_6 is responsible for the observed decrement in laser output energy, a similar effect should also be expected for H_2/F_2 mixtures with SF_6 additive. Since both SF_6 and MoF_6 have low lying vibrational energy levels, both should be capable of removing rotational energy of HF by the process of near resonant rotation-to-vibration energy transfer. However, SF_6 is not dissociated via the flash and should not act as a chain terminator. Figure 14 shows the effect of SF_6 additive to the H_2/F_2 laser output energy. A drop in output energy was observed as more and more SF_6 was added. Molecular SF_6 has long been noted to be rather inefficient in the vibrational deactivation of HF.[11a] This drop in output energy can only be explained by a possible $R \rightarrow V$ process which changes the HF rotational distribution and hence the laser kinetics.

1.2.2.2.4 The Effect of Changing Both H_2 and F_2 Concentrations Simultaneously

The laser pulse energy for gas mixtures with both H_2 and F_2 varied at a fixed flash lamp energy was measured. The laser energy is coupled out with a sapphire plate with a copper mirror at the other end. The results are shown in Fig. 15. It is found that, in general, the output

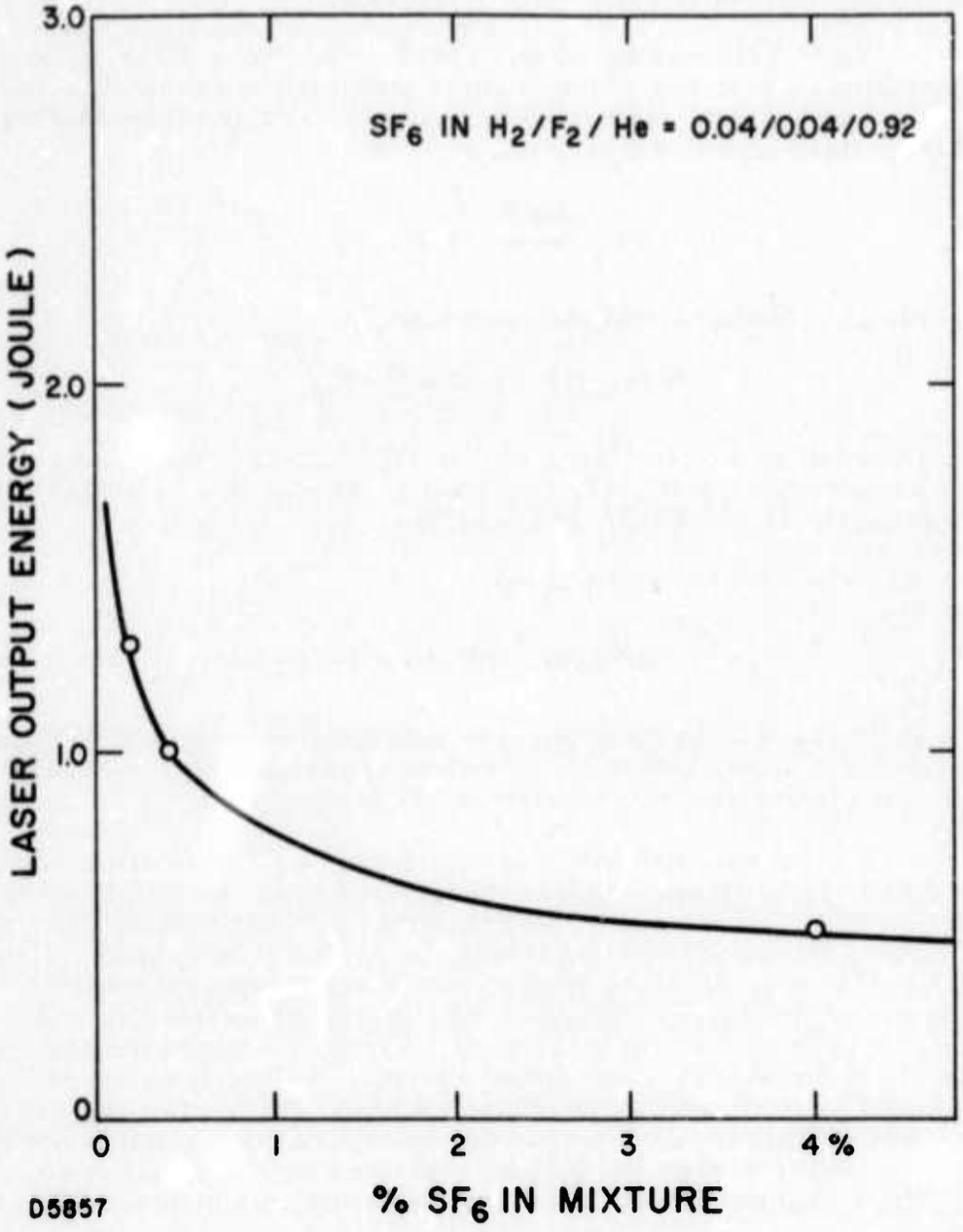

Fig. 14 The Effect of Changing SF_6 Concentration to the Laser Output Energy Observed in the $H_2/F_2/He$ Mixture

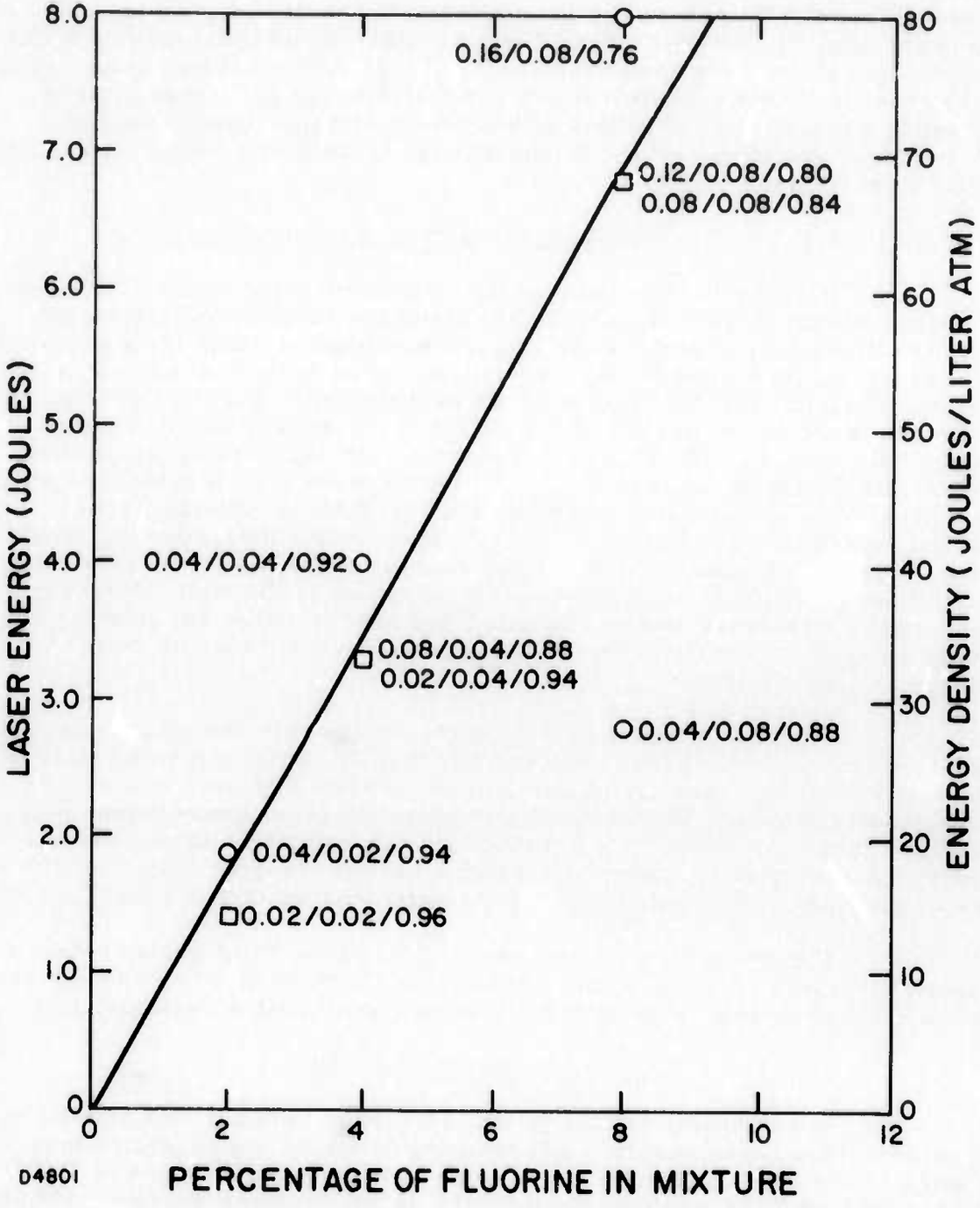

Fig. 15 The Effect of Changing Both H_2 and F_2 Concentration to the Laser Output Energy Observed in the $H_2/F_2/He$ Mixture

energy is limited by the smaller constituent of the mixture. The ratio of [laser energy]/[F_2 pressure] in an active volume of 0.1 liter is about 80 joules/atm F_2, which is about twice of what we had obtained in the BaF_2-copper optical coupling experiment. Since both BaF_2 and sapphire windows have about the same transmission and reflectivity at 2.7 μ region, it is certainly surprising to note this difference in measured laser energy. More discussion of the effect of output coupling on laser energy will follow in the next section.

1.2.2.2.5 The Effect of Varying the Output Coupling

In order to determine if the difference noted above also exists for other window materials which have about the same transmission and reflectivity at 2.7 μ laser energy measurements were made for a gas mixture of H_2/F_2 He = 0.04/0.04/0.92 with a copper mirror at one end and a variety of partial transmitting windows at the other. Table I lists the averaged laser output energy observed for these optical cavities using either KBr, NaCl, LiF, CaF_2, BaF_2, quartz or sapphire as the partial transmitting window. All of these cavities have about 90% output coupling. A difference in output energy between Ge, IRTRAN IV, and Si flats as partial transmitting windows (which give about 50% output coupling) was also observed. It was found that Si is the best of the latter materials and among the 90% output coupling windows, sapphire is the best. However, in comparing sapphire and silicon windows, for the same gas mixture and every other condition the same, sapphire couples out twice as much energy as that of silicon.

The performance of an unstable resonator was also tested. An unstable cavity should have the advantage that the mode can completely fill the active medium, thereby minimizing the tendency of parasitic oscillation and also allowing efficient energy extraction from the medium. The unstable cavity consisted of a 2.5 cm diameter concave mirror, and a 1.3 cm diameter convex mirror mounted on a barium fluoride output window. This cavity had 14% coupling and gave a pulse energy of 0.9 joules.

Figure 16 summarizes these data on the relationship between laser energy and output coupling observed in the 0.04/0.04/0.92 mixture. A full discussion of this phenomena will be given in later sections.

1.2.2.2.6 D_2/F_2/He Mixture Results

In replacing H_2 by D_2, the laser output energy was slightly decreased but the pulse duration was found to be either unchanged or longer. Figure 17 shows a typical DF laser pulse observed in a mixture of D_2/F_2/He = 0.04/0.04/0.92 and using a sapphire output coupling window. The laser energy monitored by the AVCO energy meter was found to be 1.6 joule. Since the rates of vibrational relaxation of DF are considerably slower than that of HF, the pulse duration is expected to be longer. However, the energy of 1.6 joule appears to be too low in comparison with the value of 3.4 joule obtained in the H_2/F_2/He mixture using an identical experimental condition. If equal number of photons were emitted from both gases, a DF laser energy of 3.4/1.4 = 2.4 joules should be obtained.

TABLE I

LASER OUTPUT ENERGY FOR VARIOUS COUPLING SCHEMES

Material	% Transmission at 2.7μ	Measured Laser Output Energy For Cavity Length, L, cm	
		L = 50	L = 25
Sapphire	87	3.6±.4	-
KBr	92	1.8±.3	-
NaCℓ	92	2.4±.3	-
BaF_2	93	2.7±.3	1.0±.1
CaF_2	94	2.7±.3	-
LiF	95	3.2±.4	-
Si	54	2.2±.3	-
IRTRAN IV	50	0.6±.2	-
Ge	47	0.4±.1	.3±.05
BaF_2 - BaF_2	99	0.7±.1	(From both ends)

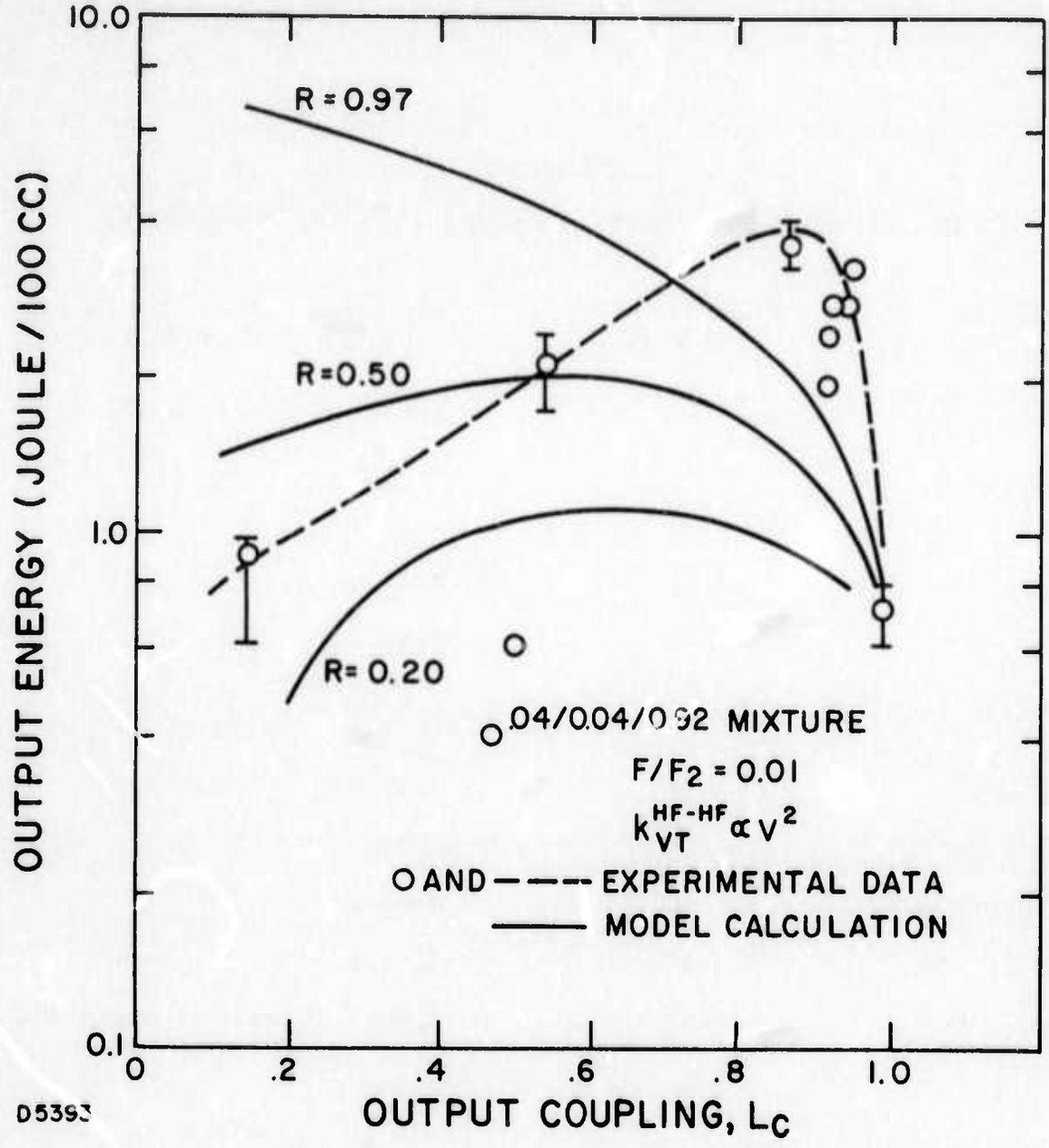

Fig. 16 Laser Output Energy as a Function of Output Coupling II-14

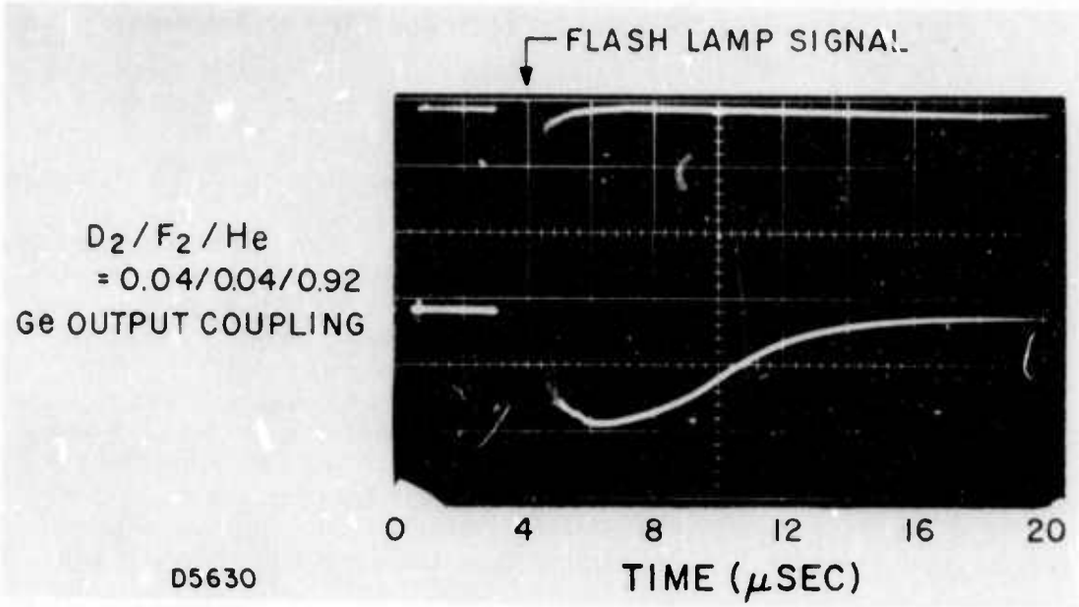

Fig. 17 Time Dependence of DF Laser Output Pulse Observed in $D_2/F_2/He$ Mixture

1.2.2.3 Temporal Behavior of Laser Pulses

The transient behavior of laser photons has been systematically studied in two ways;

i) Comparing the total pulse shape for various gas mixtures,

ii) Comparing the total pulse shape for various output couplings.

The results are summarized as follows:

1.2.2.3.1 The Effect of Gas Composition on Pulse Duration

A typical oscillogram of the HF laser pulse (overall transitions) observed in mixture of $H_2/F_2/He = 0.04/0.04/0.92$ and sapphire output coupling is shown in Fig. 18. The upper trace is the flash lamp output, showing a pulse length less than 2 μsecs. The laser output, shown in the lower trace, lasts for 4 μsecs. The fact that the laser pulse is longer than the flash lamp indicates that the chain reactions are operative in this laser. From the overall time of the individual chain reactions it can be estimated that approximately 10 chain steps are possible during laser action. Figure 17 shows the shape of a typical DF laser pulse observed from a $D_2/F_2/He = 0.04/0.04/0.92$ mixture using a sapphire output coupling window. The observed laser duration is somewhat longer than for HF - about 6 μsec.

Figure 19 shows representative HF laser pulses observed in various gas compositions. It is clear that the duration of laser pulse decreases with increasing $H_2/F_2/He = 0.12/0.08/0.80$ the laser duration is only 2 μsec long, but for mixtures with 0.02/0.02/0.96 composition, the duration is longer than 5 μsecs.

1.2.2.3.2 The Effect of Output Coupling on Pulse Duration

Figure 20 shows the shapes of HF laser pulses obtained in mixture of $H_2/F_2/He = 0.04/0.04/0.92$ using either sapphire or silicon output coupling windows. It is found that both pulses have about the same shape and duration regardless of their differences in optical transmission, reflection, and therefore output coupling.

1.2.2.4 Spectra Analysis of Pulsed HF Laser

The spectral transitions of the HF laser pulses were investigated in two different optical regions:

i) The short wavelength infrared region between 2.5-3.5 μ, and

ii) The far infrared region between 15-30 μ.

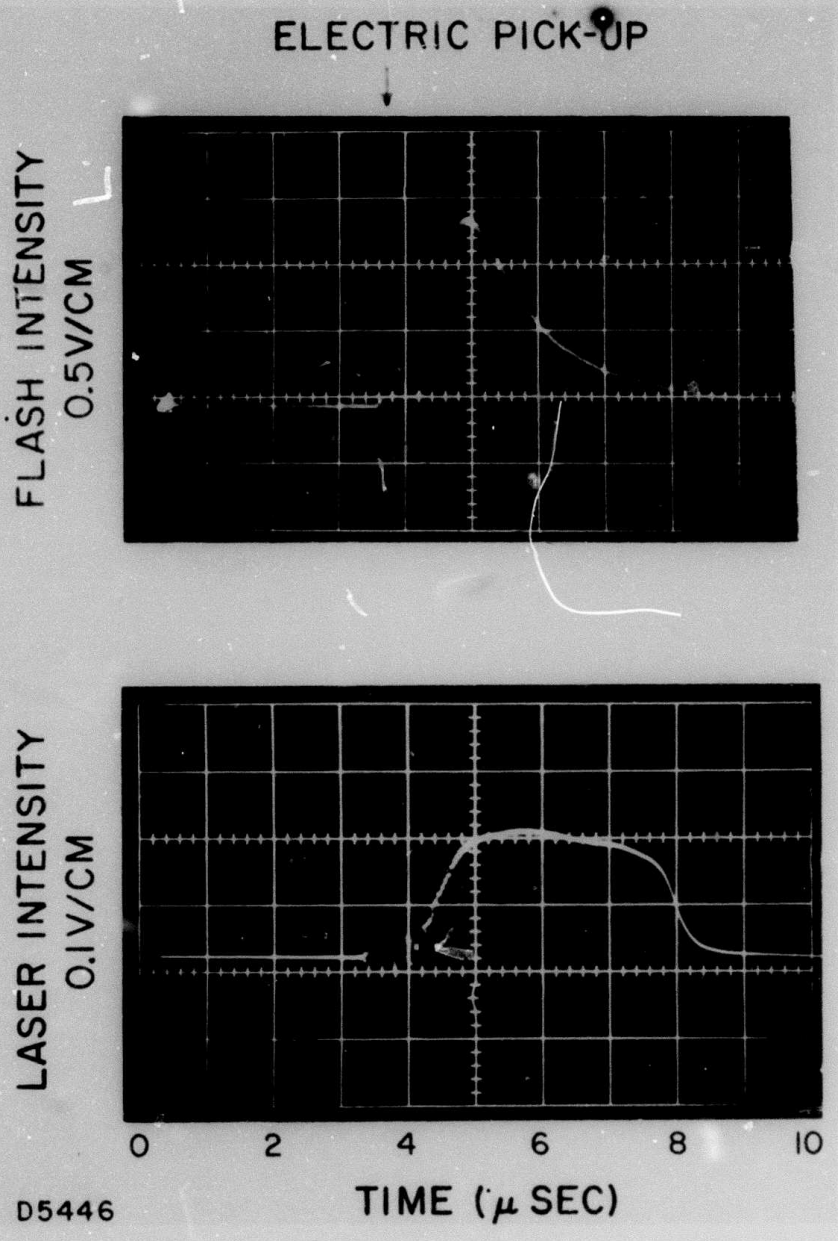

Fig. 18 Time Dependence of HF Laser Output Pulse Observed in $H_2/F_2/He$ Mixture

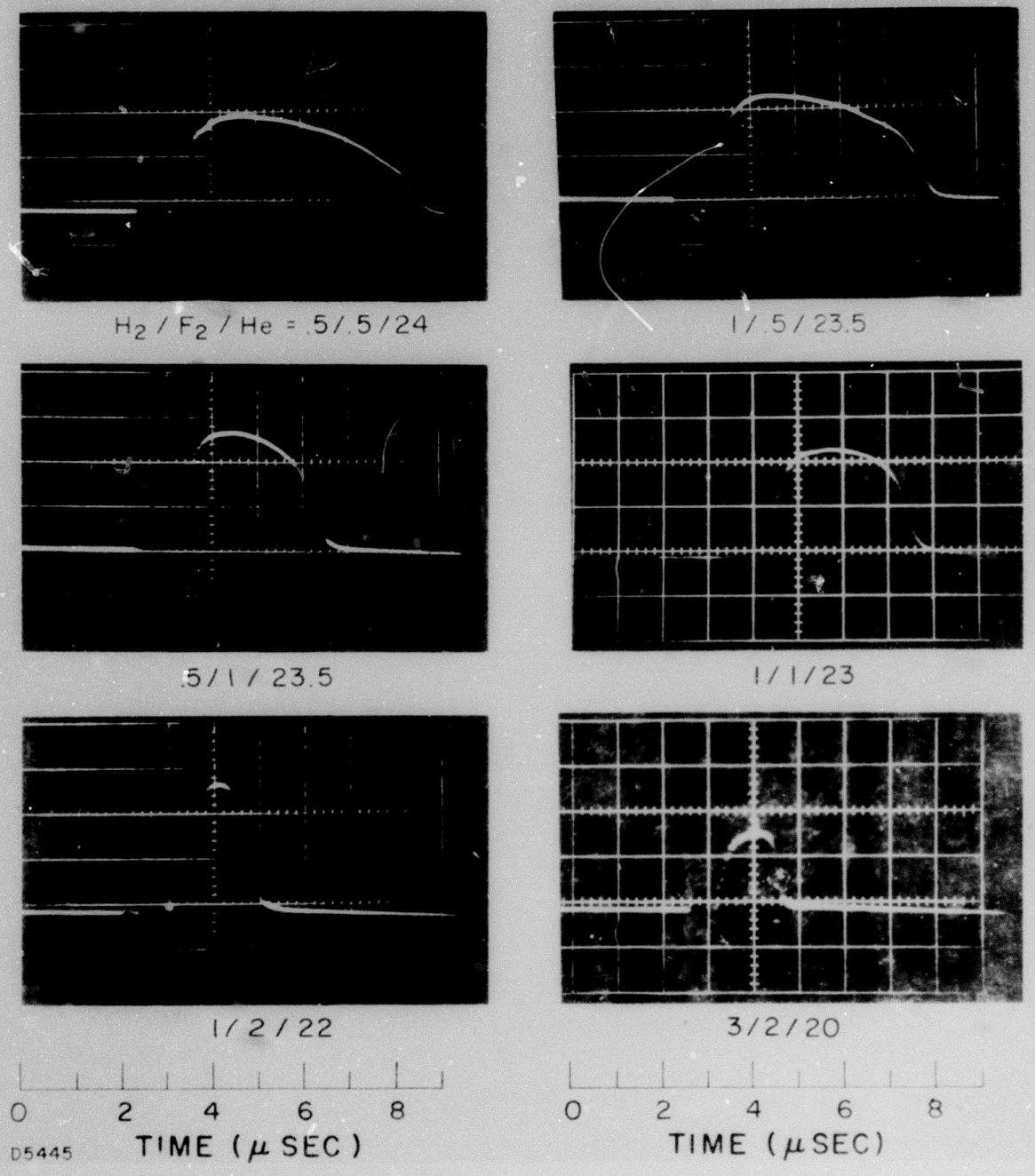

Fig. 19 Time Dependence of HF Laser Output Pulses Observed in Various $H_2/F_2/He$ Compositions

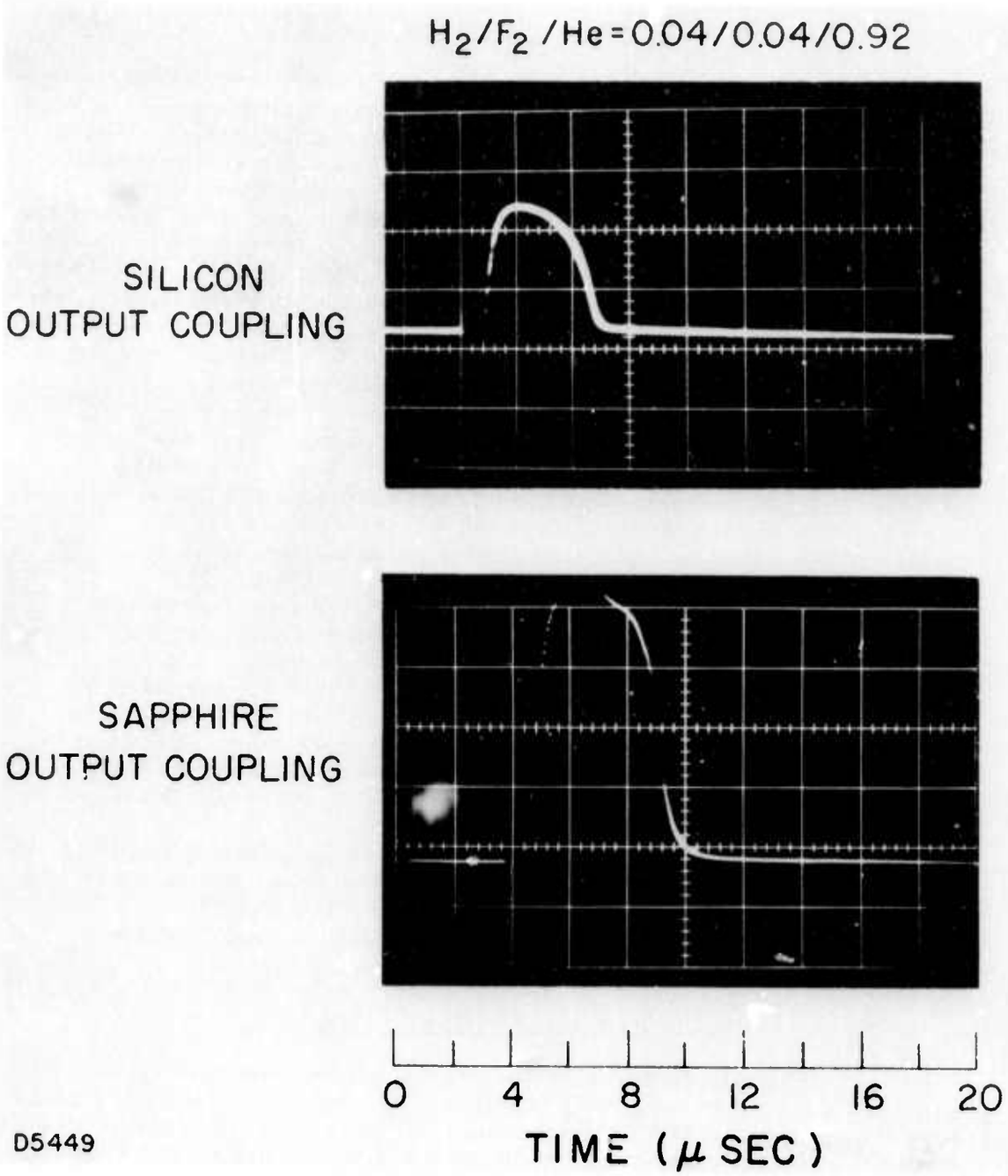

Fig. 20 The Shapes of HF Laser Pulses Observed in $H_2/F_2/He$ Using Either Sapphire or Silicon Output Coupling Windows

The results obtained by the experimental technique discussed in Section 1.2.1.2.3 are the following:

1.2.2.4.1 Short Wavelength Infrared Laser Transitions

Table II lists the various P and R branch transitions observed in the standard H_2/F_2/He mixture using a sapphire output coupling window. It is seen that vibrational transitions are observed for V=6→5, 5→4, 4→3, 3→2, 2→1 and 1→0. The fact that 6→5, 5→4 and 4→3 are present indicates that the hot reaction is operative. Furthermore, the observation of R branch transitions indicates an absolute population inversion at least for certain vibrational/rotational states.

Figures 21, 22, 23, 24, 25, 26 and 27 show the temporal behavior of the 1P, 2P, 3P, 4P, 5P, 6P and R branch transitions observed in the standard mixture of H_2/F_2/He = 0.04/0.04/0.92 using a sapphire output coupling window. There are two features that are noteworthy;

i) Among all the P branch transitions, there are definitely two noticeable trends that reach lasing threshold. For transitions involving low J states (below J=8), the lowest J transition always reaches threshold first and higher J transitions occur later. For transitions involving high J states (above J=8), there are definitely two pulses in each transition. A pulse occurs at early time, and the second pulse arrives later (e.g., see Fig. 21, $1P_9$ transition). The first pulses reach threshold almost as early as the lowest transition for the low J transition (below J=8). The second pulse appears to follow the temporal trend of the low J transitions.

ii) The R branch transitions reach threshold quite early and only lase on the low J states where the P branch lasing action does not occur. This is similar to what Prof. John Polanyi predicted six years ago.[11b]

1.2.2.4.2 Far Infrared Laser Transitions

HF laser radiation in the far-IR region has been reported from both the $SF_6 + H_2$ and $CF_4 + H_2$ reactions.[12] Since (a) the H_2/F_2 reaction favors the population of high rotational states for lower vibrational levels and (b) the rate of rotational relaxation of the high J states of HF could be very long, i.e., comparable to the vibrational relaxation time, it is quite possible that population inversion may also exist between rotational energy levels. In order to determine if there was any far-IR radiation in our H_2/F_2 laser system, a black polyethylene cloth was used to cover the energy meter, and the transmitted energy was measured. It was found

TABLE II

OBSERVED LASER TRANSITIONS

BAND	P BRANCH	R BRANCH
1 → 0	P (3) (4) (5) (6) (7) (8) (9)	NONE
2 → 1	P (3) (4) (5) (6) (7) (8) (9) (10) (11) (12) (13) (14) (15) (16)	R(0)
3 → 2	P (4) (5) (6) (7) (8)	NONE
4 → 3	P (4) (5) (6) (7)	R (1), R (4)
5 → 4	P (3) (4) (5) (6)	R(0)
6 → 5	P (1) (2) (3) (4) (5)	NONE
7 → 6	NONE	NONE
8 → 7	NONE	NONE

* Underlines indicate the strongest transition observed in the band

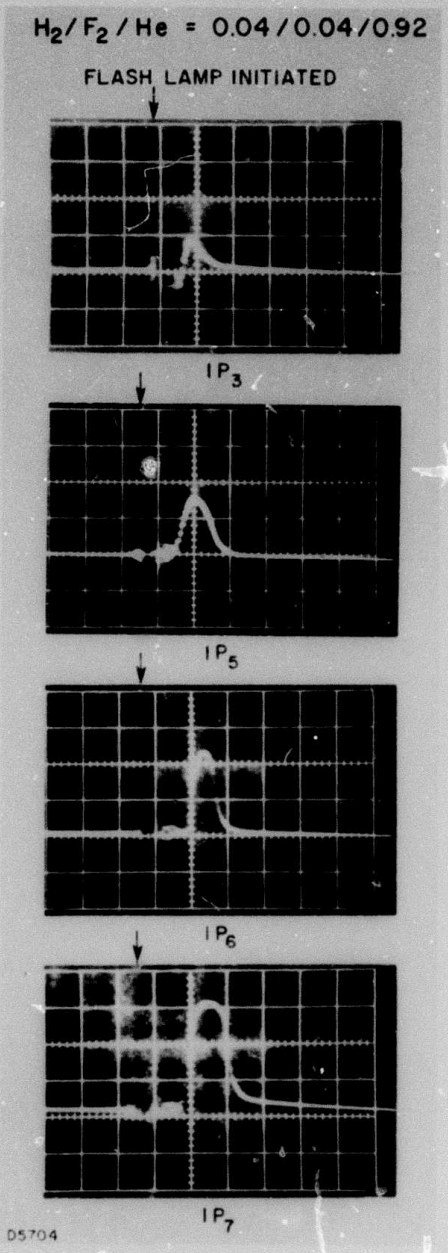

Fig. 21a The Temporal Behavior of 1P Transitions

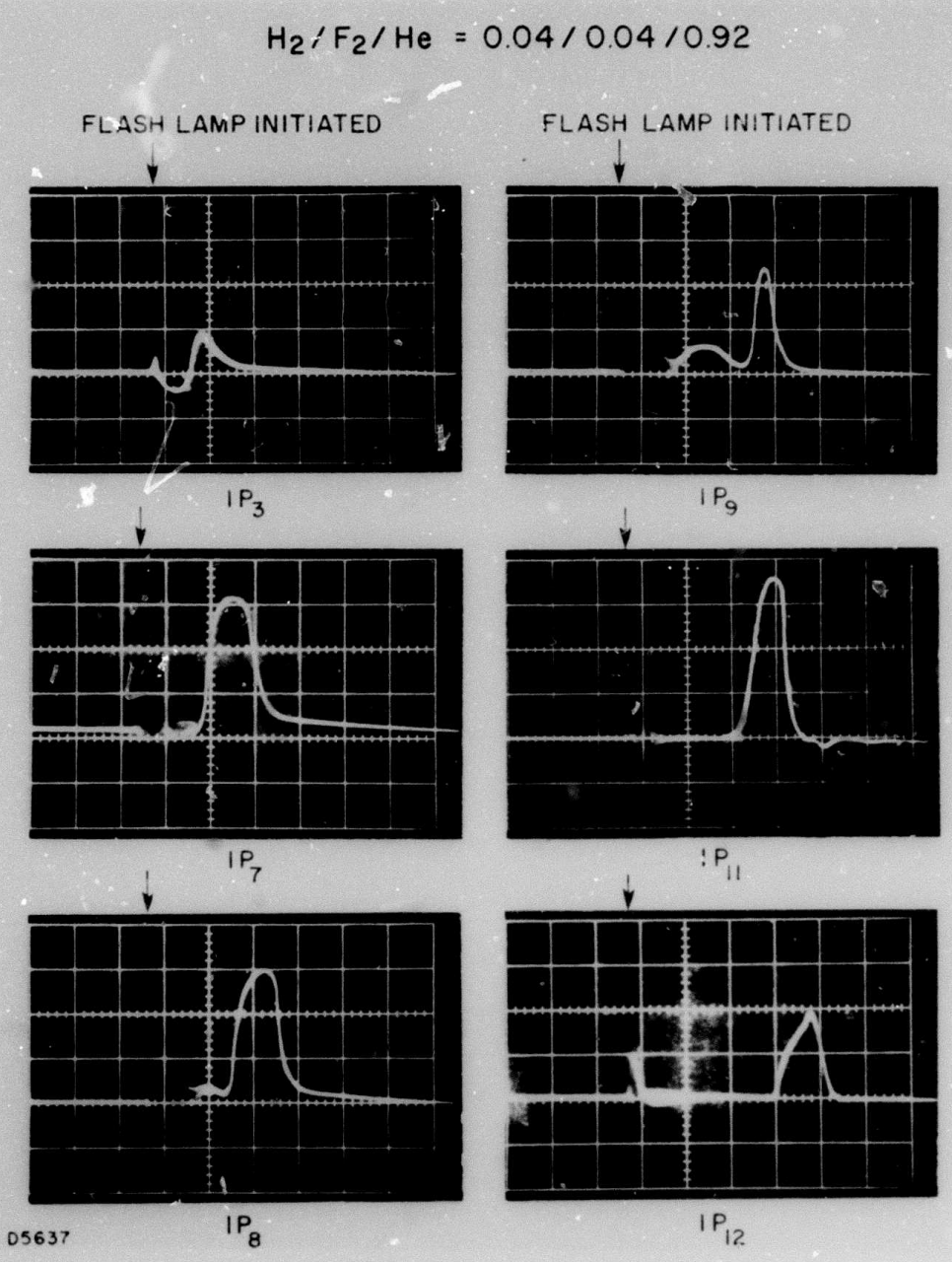

Fig. 21b The Temporal Behavior of 1P Transitions

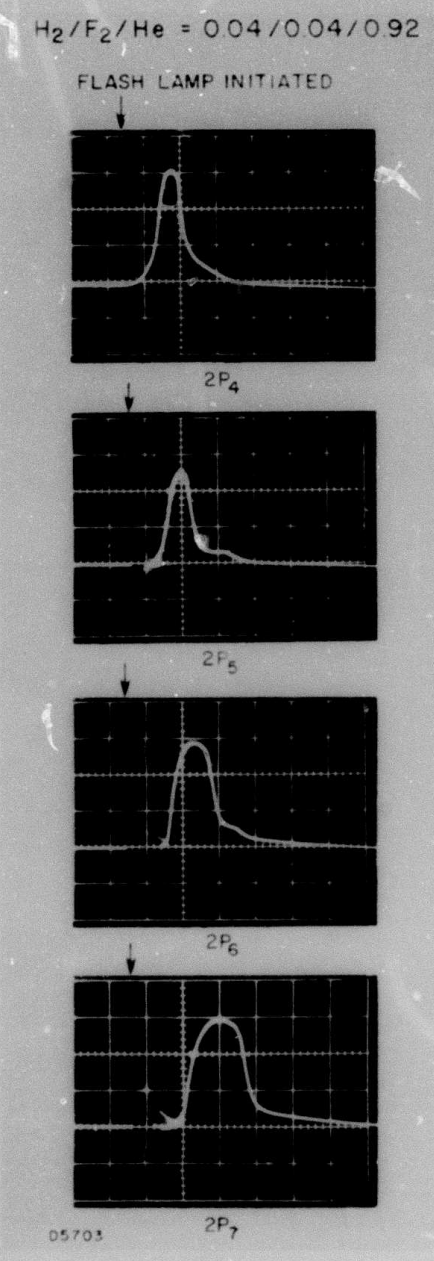

Fig. 22a The Temporal Behavior of 2P Transitions

$H_2 / F_2 / He = 0.04 / 0.04 / 0.92$

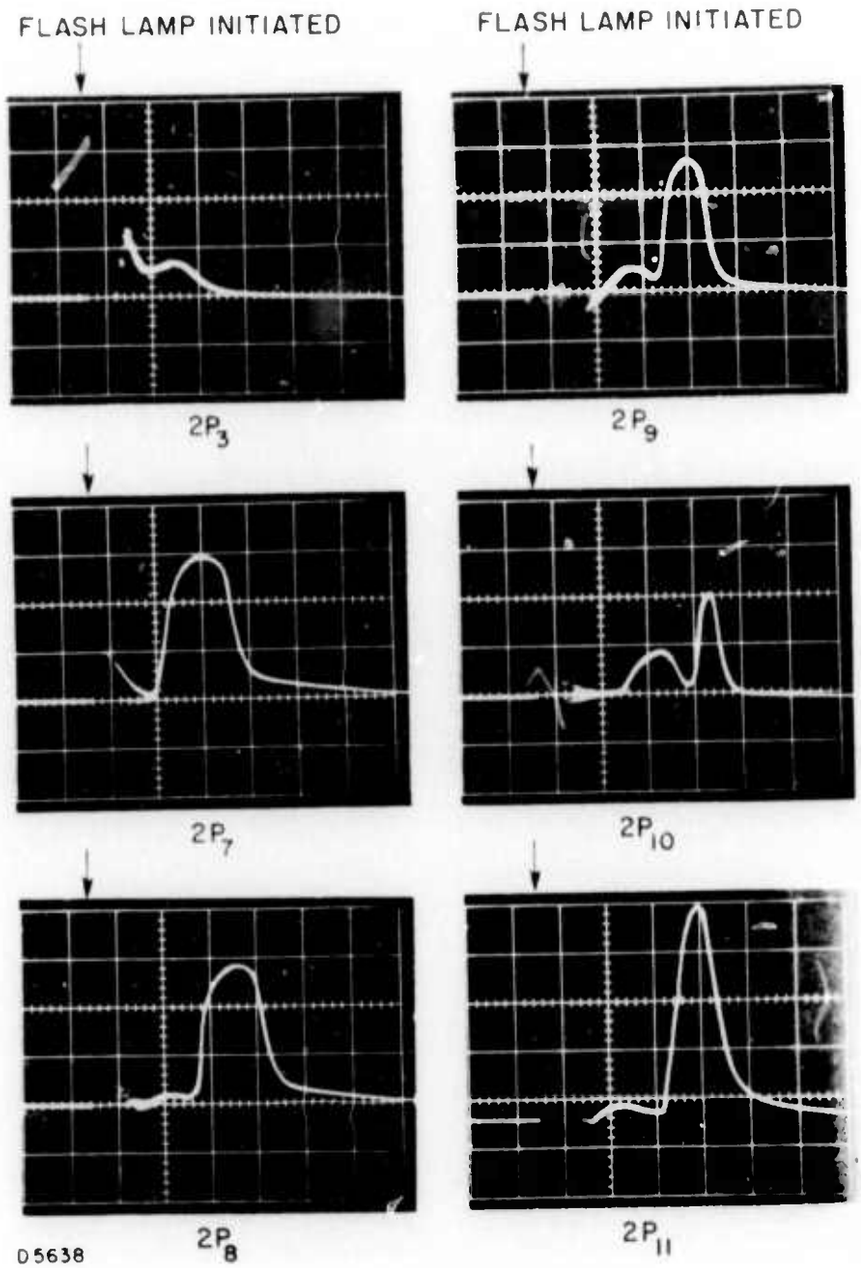

Fig. 22b The Temporal Behavior of 2P Transitions

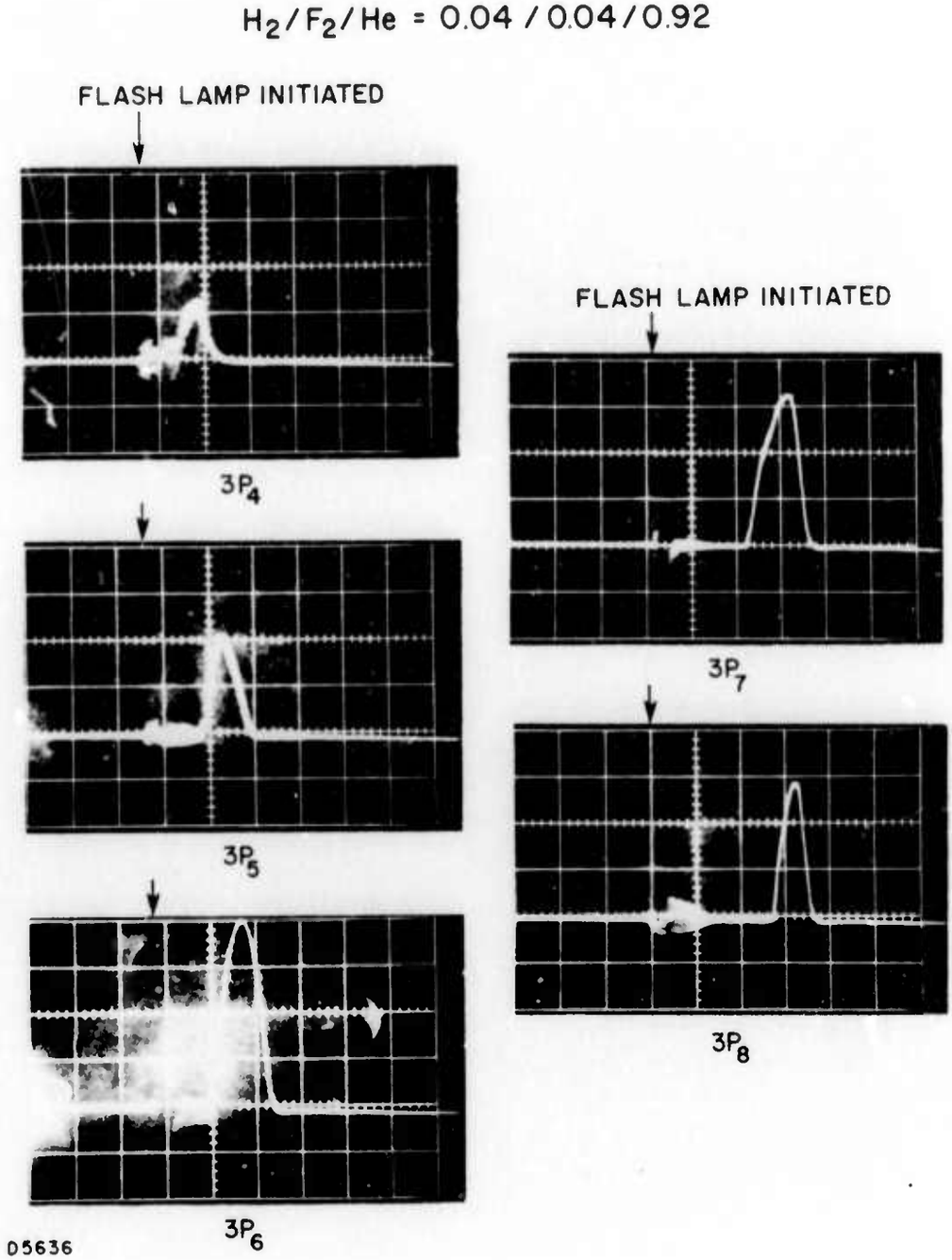

Fig. 23 The Temporal Behavior of 3P Transitions

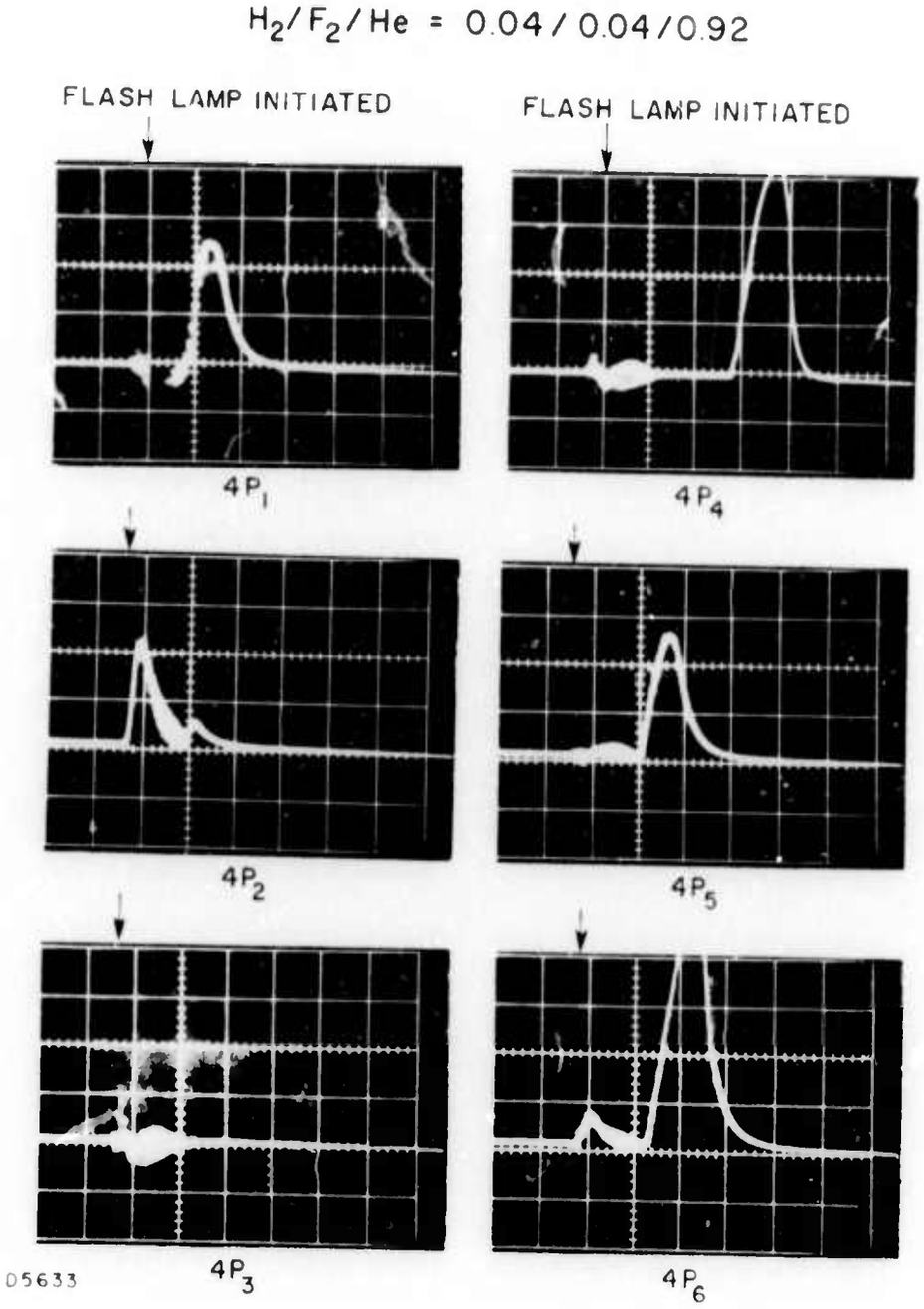

Fig. 24 The Temporal Behavior of 4P Transitions

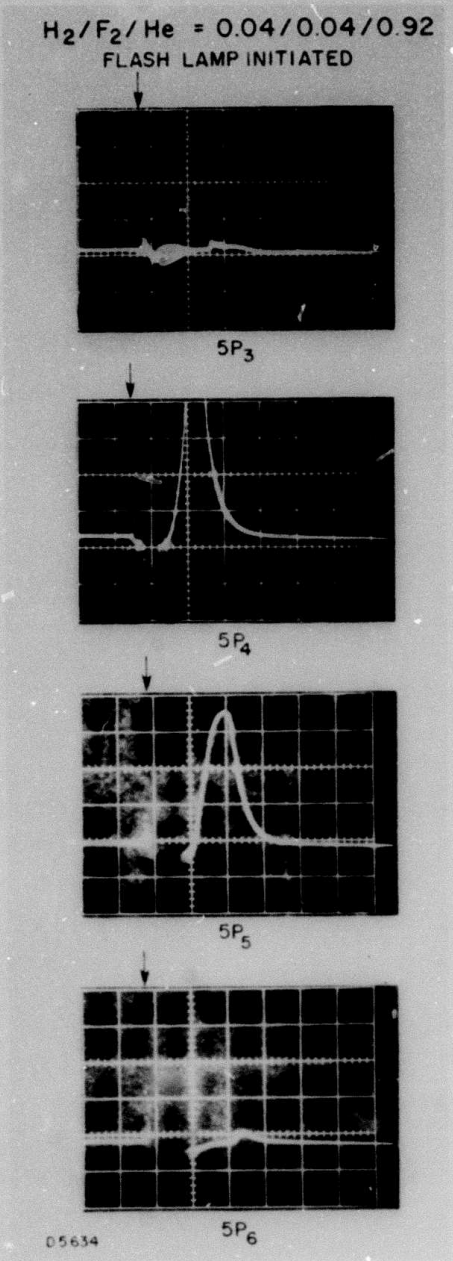

Fig. 25 The Temporal Behavior of 5P Transitions

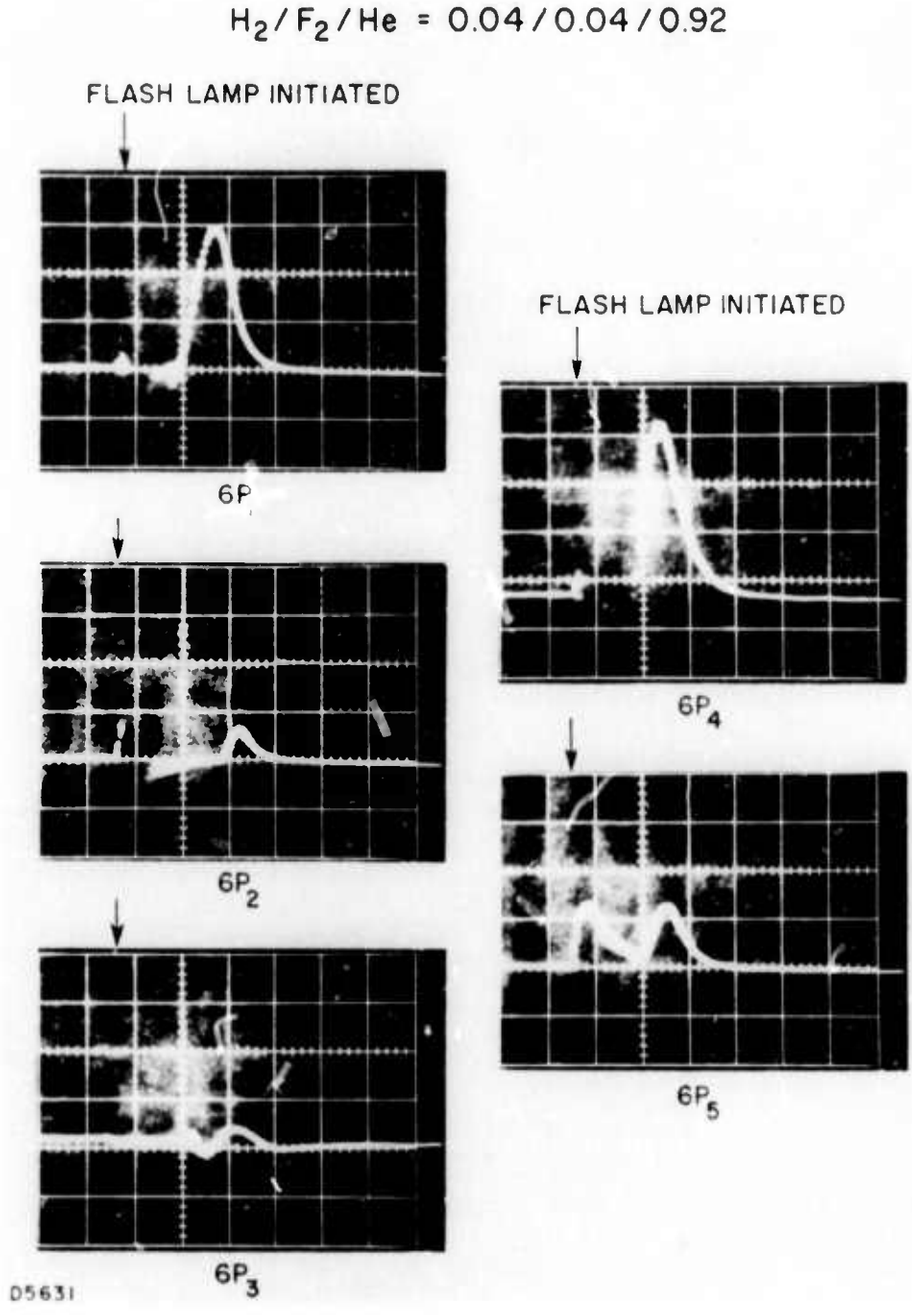

Fig. 26 The Temporal Behavior of 6P Transitions

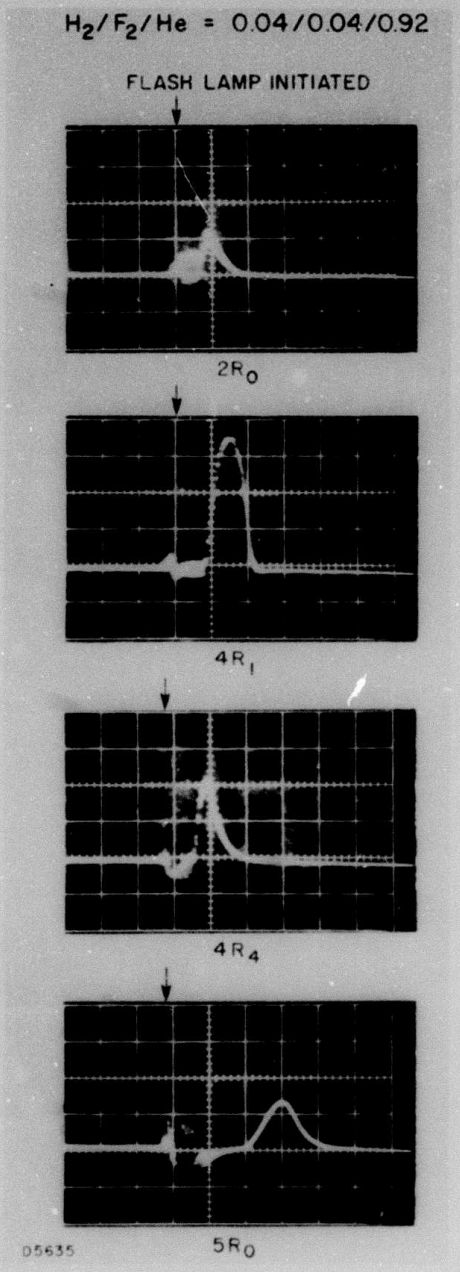

Fig. 27 The Temporal Behavior of R Branch Transitions

that for a total 1.5 joule HF laser pulse, about 0.3 joules of energy were transmitted through the black polyethylene. Since black polyethylene only starts to transmit above 15 μ, these 0.3 joules of energy are the contribution of laser photons with a wavelength greater than 15 μ and most likely above the 20 μ region. Unfortunately, without a spectroscopic study in the far-IR region, it is not possible to conclude which particular rotational levels are involved, and to determine if the rotational laser action has proceeded before, during or after the vibration-rotational laser transitions at shorter wavelength. This spectroscopic study was not performed.

1.2.2.5 F_2 Dissociation Produced by Flash Photolysis

The result obtained by the titration technique discussed in Section 1.2.1.2.1 is shown in Fig. 28. This plot of F/F_2 ratio vs F_2 pressure in the $HC\ell/F_2$/He mixture shows a constant value over the F_2 pressure studied. $HC\ell$ enriched mixtures were used to assure that all the F atoms photolized by the flash reacted with $HC\ell$ to form molecular HF. The data show a dissociation of F_2 of about 1% independent of F_2 partial pressure. This lack of F_2 concentration dependence is interpreted as a result of the gas being optically thin under these experimental conditions.

In order to determine if side reactions like

$$C\ell + F_2 \rightarrow C\ell F + F \qquad (11)$$

also occur and produce additional HF molecules, measurements with both $HC\ell$ and F_2 enriched mixtures were tested. It is found that the amount of HF formed does not increase linearly or quadratically with the concentration of $HC\ell$ present. Figure 29 shows the fraction of F-atoms produced as a function of $HC\ell$ pressure. Above 2 torr of $HC\ell$, the data flatten out and yield a constant result, namely, 1% F_2 dissociation or $F/F_2 = (8 \pm 2) \times 10^{-3}$. Based on our previous photylysis results using the linear flash lamps and less efficient optical coupling, the coaxial lamps appear to yield about a factor of two more F-atoms.

1.2.2.6 The Rate of $H_2 + F_2 \rightarrow 2HF$ Overall Reaction

The results obtained from the experiment described in Section 1.2.1.2.2 are shown in Fig. 30 where the ratio of

$$\left([F_2]_{t=o} - [F_2]_t\right)/[F_2]_{t=0}$$

is plotted against the time t after flash lamp initiation. By adopting the F/F_2 ratio previously determined and the rate constants of both "hot" and "cold" reactions reported in the literature,[13] the rate of the overall $H_2 + F_2 \rightarrow 2HF$ reaction is computed and plotted along with the experimental values. It is clearly evident that the consumption of F_2 molecules in the cavity proceeds with a speed comparable to that predicted from the

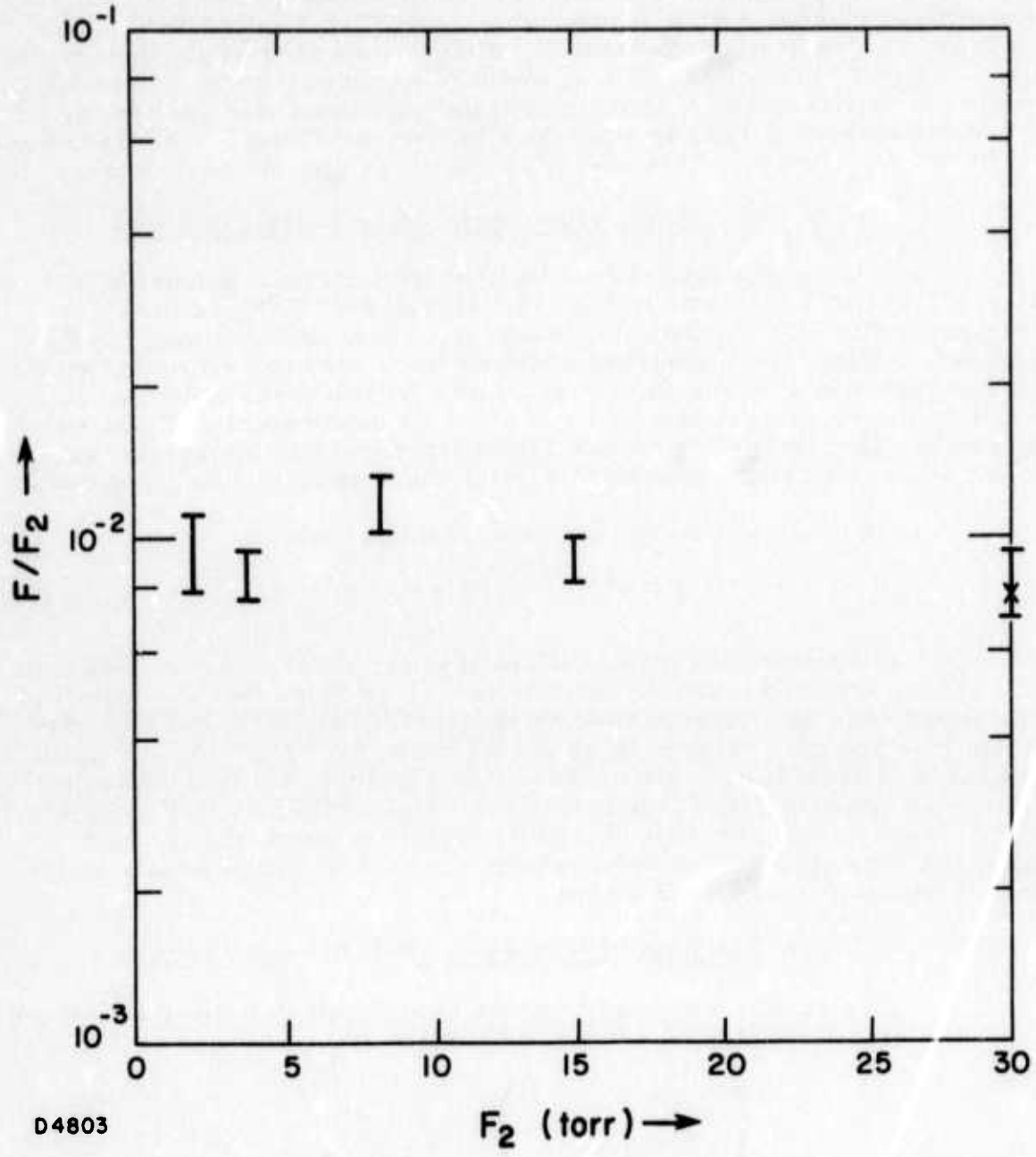

Fig. 28 The Measured F/F_2 Ratio as a Function of F_2 Pressure in Mixture $\overline{\mathrm{I}}$ for Mixture with 0.2% of O_2 and I for Mixture with 0.02% of O_2

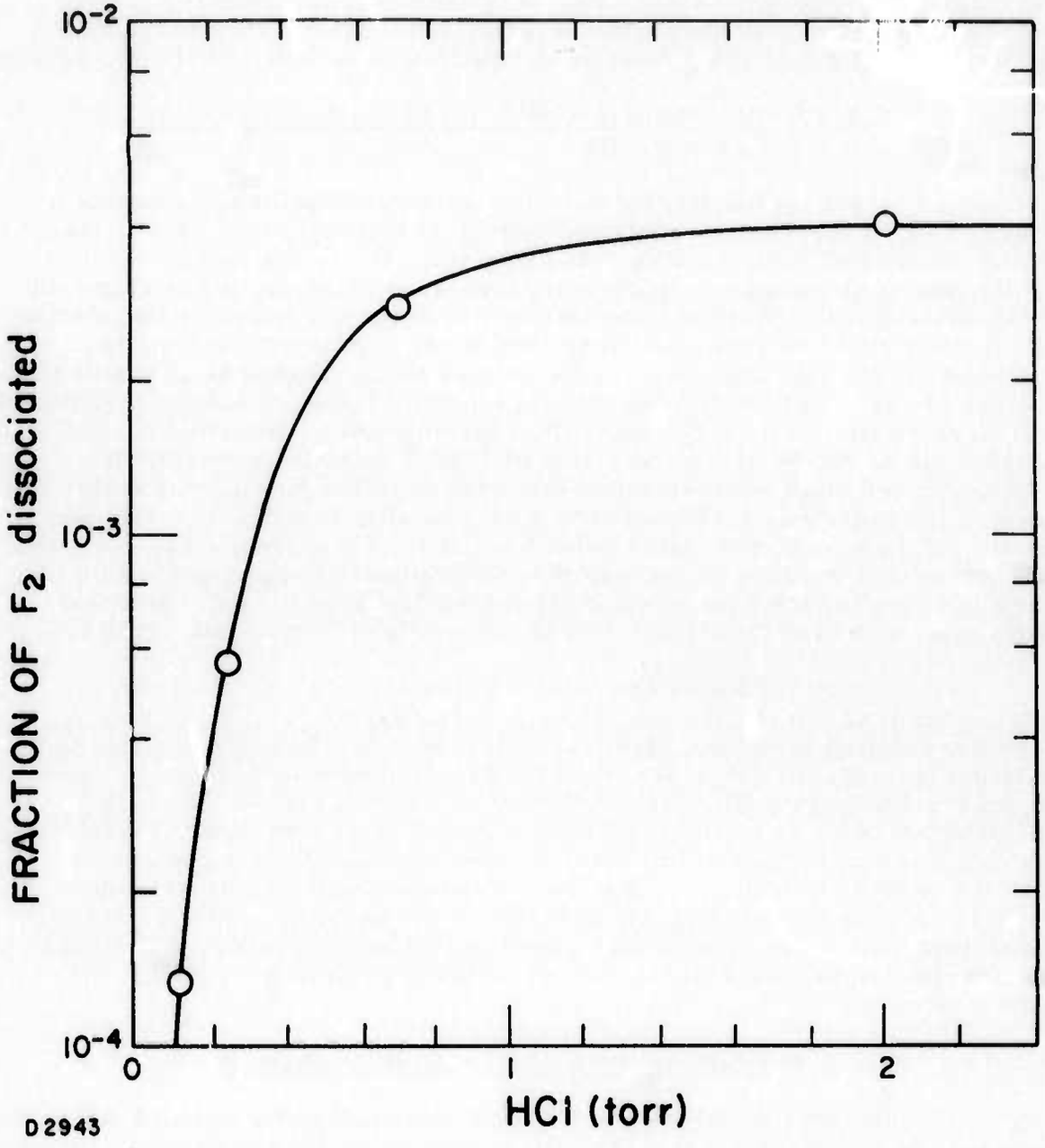

Fig. 29 The Measured F/F_2 Ratio as a Function of $HC\ell$ Pressure in Mixture

theoretical computations not using a chain branching mechanism. The calculated value using the chain branching Reaction (2) with $k_2 = 10^{-12}$ cm^3/sec is also plotted in Fig. 30. It is seen that the overall $H_2 + F_2$ reaction would proceed with a much faster speed than that observed experimentally if a fast chain branching reaction is included in the mechanism.

1.2.2.7 Determination of Beam Distortion Inside the Laser Cavity

Since (a) the H_2/F_2 reaction liberates significant amounts of energy (~35%) into the translational degree of freedom, and, (b) the rate of HF vibrational relaxation is extremely fast, the temperature of the cavity gas must increase rapidly with time after flash lamp initiation. It is possible that the photons traveling within the cavity between the window and mirror could be seriously scattered because of possible density gradients in the gas, and thus the beam may not be regenerated inside the optical cavity. To test this hypothesis a simple light scattering experiment was performed. Figure 31 shows the experimental arrangement. The beam from an He-Ne laser operating at 6328 Å was aligned within the cavity and reflected between the two windows. After two passes within the cavity, the beam was reflected onto a narrow slit, and the intensity was monitored by a photomultiplier behind the slit. The purpose of the experiment was to determine if serious density gradients could exist within the cavity gas during the time when laser action had been seen. The monochrometer was used before the PM to reduce flash lamp scattered light.

Figure 32 shows the temporal intensity variation of the reflected beam after the flash initiation of a standard H_2/F_2 mixture. A periodic oscillation of the beam was observed. By changing the gas composition from H_2/F_2/He to H_2/F_2/Ar, the oscillating period was found to be decreased roughly from 19 μsec/cycle to 36 μsec/cycle. Since the sound speed of He at 1 atm pressure is about 1 mm/μsec and the flash lamp diameter is about 17 mm, the value of 19 μsec/cycle seems comparable with the period of sound wave oscillation between walls of flash lamp. The observation that the oscillations are slower for the Ar mixture is also consistent with the reduced sound speed in that gas. Further discussion of the possible significance of this effect on laser performance will be presented later.

1.2.2.8 Examination of the Laser Burn Pattern

In order to determine (i) some information concerning the mode structure of this H_2/F_2 laser, and (ii) to determine if parasitic oscillations were involved in our laser system, the burn pattern of the laser output was taken and examined. Figure 33 shows the laser radiation intensity distribution, obtained at a distance of 40 cm from the output sapphire window. As one can clearly see, the burn mark is extremely bright at the center of the pattern. The diameter of this circular pattern is about 3 mm smaller than the inside diameter of our laser tube. Since our optical cavity is composed of an 8 m radius concave mirror and flat reflector, the Fresnel number, N for this semi-confocal resonator can be calculated as

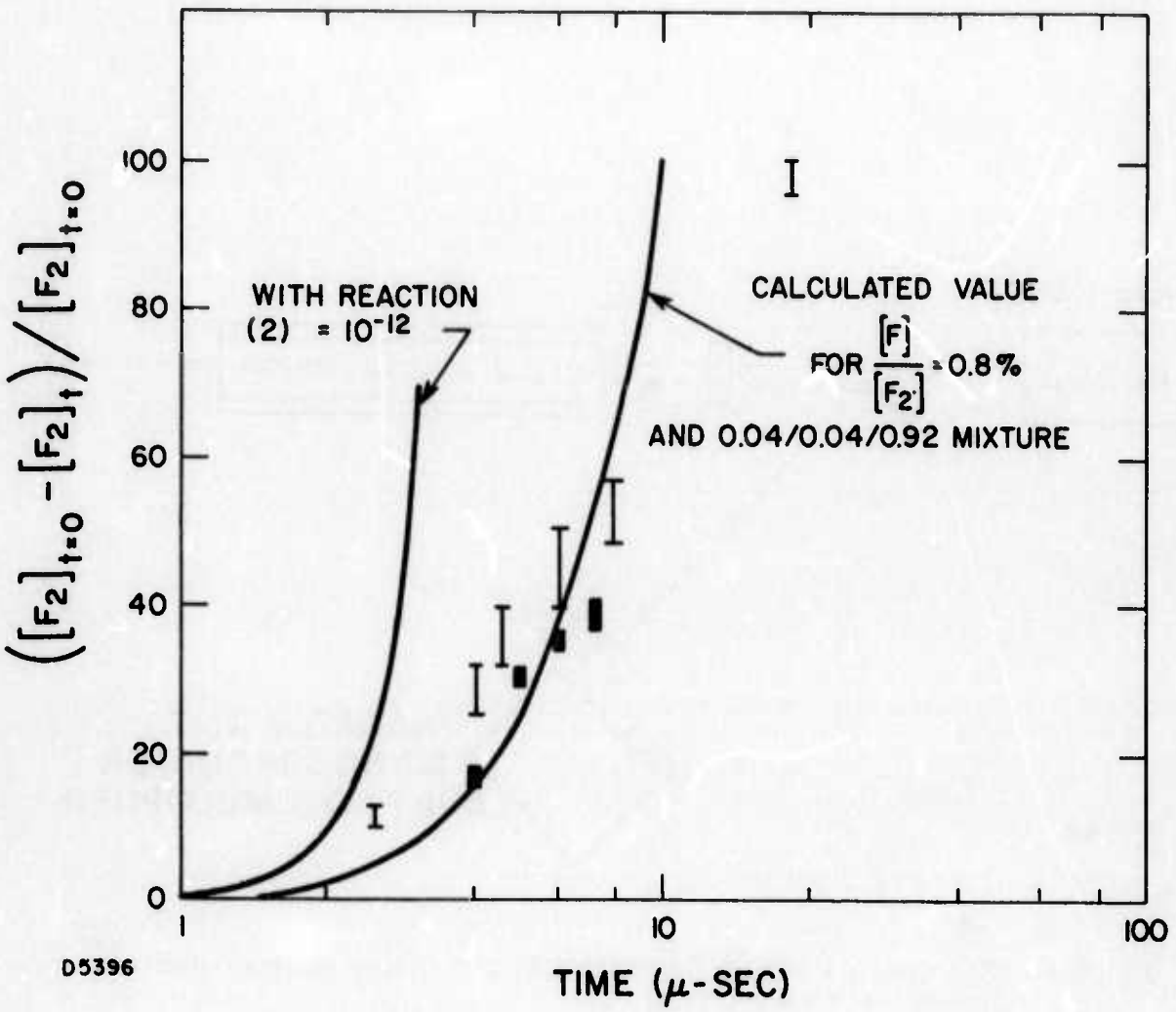

Fig. 30 The Transient Concentration of F_2 as a Function of Time after the Flash Initiation

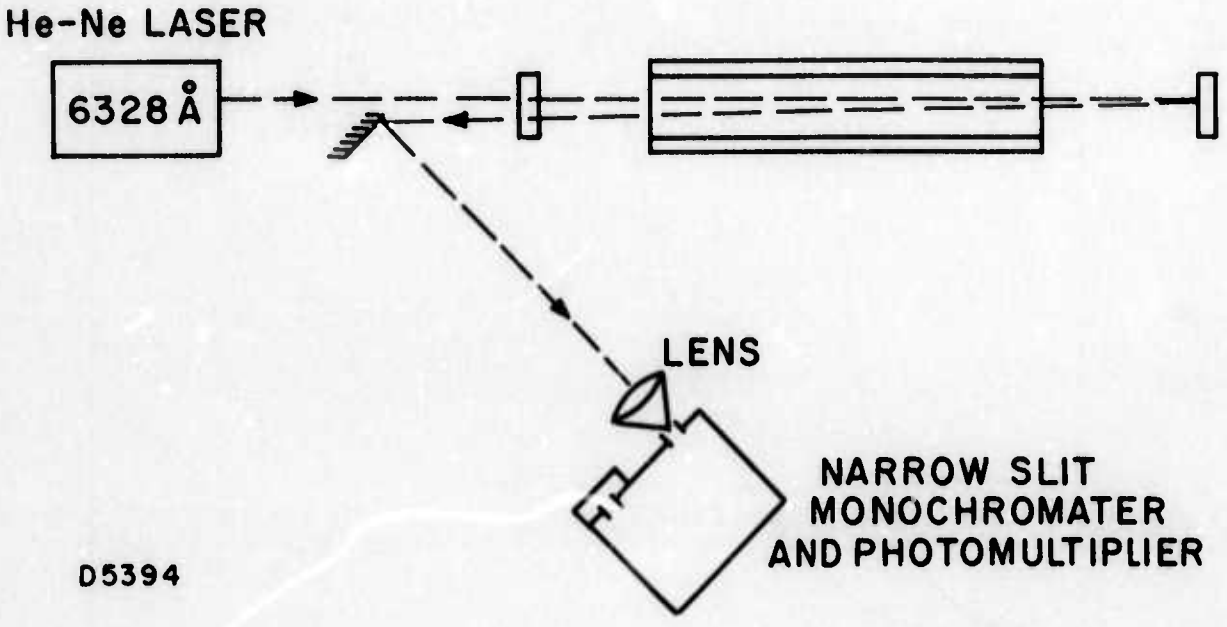

Fig. 31 The Optical Set Up Used for Determination of Beam Distortion Inside the Laser Cavity

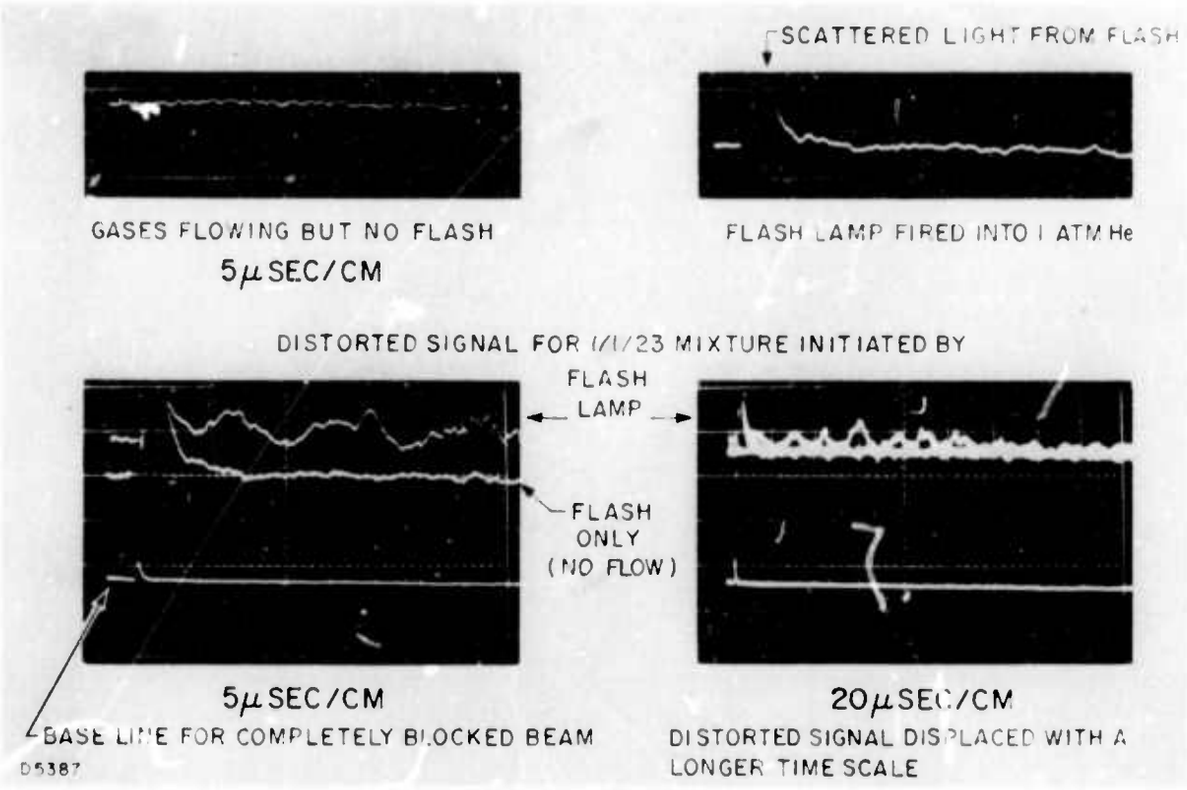

Fig. 32 The Temporal Intensity Variation of the Reflected Beam after the Flash Initiation of H_2/F_2 Mixture

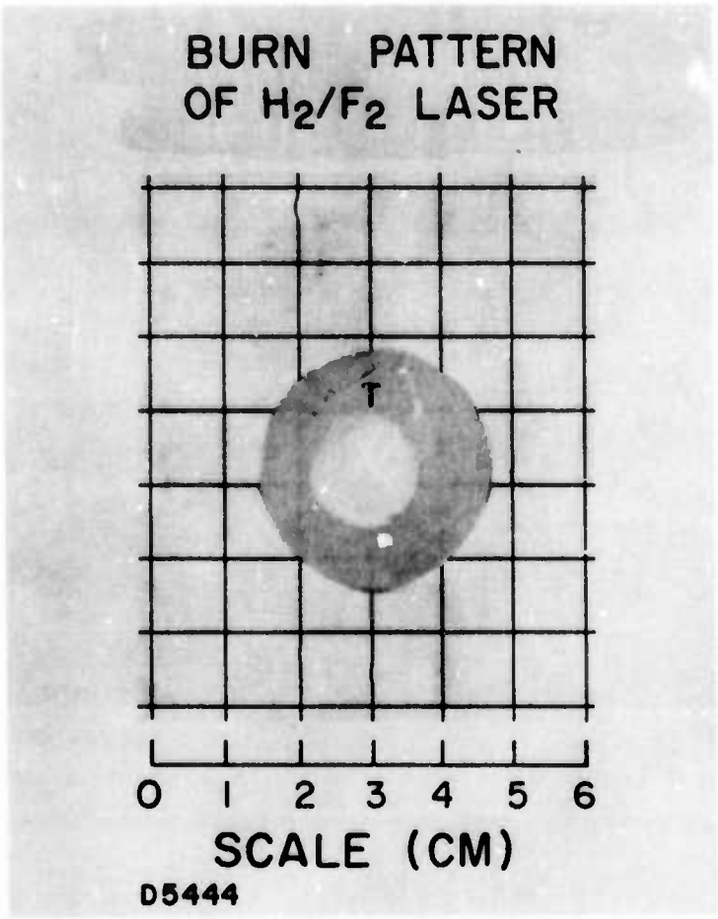

Fig. 33 The Burn Mark Observed at a Distance of 40 cm from the Output Sapphire Window

$$N = \frac{r^2}{L\lambda} = 31 \qquad (12)$$

where r is the radius of the mirror (2.5 cm) and L is the distance between reflectors (75 cm). The radius of the spot size can be estimated as

$$S_1 = \left[\left(\frac{\lambda}{\pi}\right)^2 \frac{b^2 L}{b-L}\right]^{1/4} = 1.5 \text{ mm} \qquad (13)$$

$$S_2 = \left[\left(\frac{\lambda}{\pi}\right)^2 L\,(b-L)\right]^{1/4} = 1.4 \text{ mm} \qquad (14)$$

where b is the radius of curvature of the concave mirror. S_1 and S_2 are the spot sizes on the two mirror surfaces. The diameter of a multimode laser spot should be about 17 - 1.5 = 15.5 mm which is precisely what we have found (see Fig. 33). If parasitic modes were dominating our laser system, the size and the diameter of the burn mark should be considerably larger due to beam divergence, which is clearly not what we have seen.

1.2.2.9 Estimate of the Rate of Rotational Relaxation of HF

In our last contract report[5] we had clearly pointed out that, during the duration of the HF vibration-rotational laser action, the rotational degree of freedom of the HF molecules may not have reached equilibrium with the translational mode. The fact that far-IR laser radiation was observed in our H_2/F_2 system as described in Section 1.2.2.4 strongly suggests that a measurement of the rate of rotational relaxation of HF is important to understand and model this laser system.

Figure 34 shows the experimental arrangement of a double-resonance absorption experiment that we assembled to attempt to measure rotational relaxation of HF. Two electric HF pulsed lasers utilizing the SF_6/H_2 reaction were used. Laser #1 puts out 5 mJ/cm^2 with 30% of this energy in the $v = 1 \rightarrow 0$ transitions (10% $1P_4$, 10% $1P_5$, 6% $1P_6$ and 4% $1P_7$). The $1P_7$ photons were chosen to excite the HF molecules in the cell. Laser #2, fired with a variable delayed time after Laser #1, was operated on the $2P_6$ transition, and was also positioned to pass through the same volume of gas that was excited by Laser #1. The amount of $2P_6$ absorption was monitored.

Unfortunately, due to the limitations of time and money, this measurement was not completed. Some delay between the $1P_7$ pump and $2P_6$ probe pulses were observed, but with the very low pressures of HF used (<0.1 torr) it was difficult to determine the absolute concentration of HF and hence deduce a rate. However, with our crude data, we can conclude that the relaxation of the HF (v = 1) state by processes like

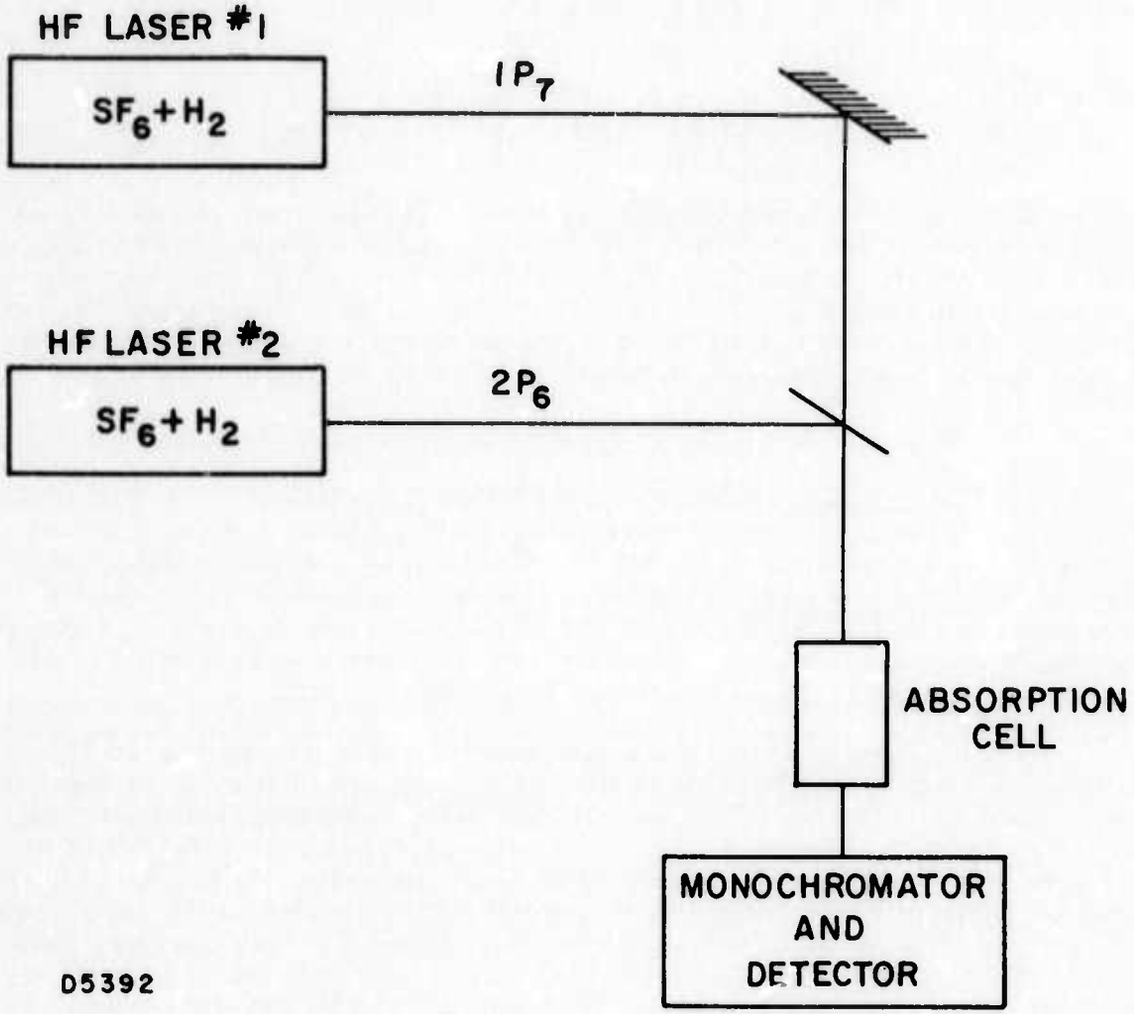

Fig. 34 The Experimental Arrangement of a Double Resonance Absorption Experiment Used for Measuring the Rotational Relaxation of HF

$$\text{HF } (v = 1,\ J = 7) + \text{HF } (v = 0,\ J = 2)$$
$$\rightarrow \text{HF } (v = 0,\ J = 7) + \text{HF } (v = 1,\ J = 2) \qquad (15)$$
$$+ \Delta E \approx 0$$

and

$$\text{HF } (v = 1,\ J = 1) + \text{HF } (v = 0,\ J = 2)$$
$$\rightarrow \text{HF } (v = 1,\ J = 6 \text{ or } 5) + \text{HF } (v = 0,\ J = 2,\ 3,\ \text{or } 4) \qquad (16)$$
$$+ \Delta E = \text{small but larger than zero}$$

can be extremely fast and takes only a few collisions or could even be as fast as gas kinetic. It should be informative to measure the relaxation time of the HF ($v = 0$, $J > 10$) states where the exact $v \rightarrow v$ energy transfer will not be present and only $R \rightarrow R$ or $R \rightarrow T$ could participate in the relaxation.

1.3 MODEL CALCULATION FOR THE PULSED HF CHEMICAL LASER

1.3.1. Basic Philosophy

Theoretical modeling of the pulsed H_2/F_2 laser was performed for the following reasons:

(i) To see if a direct comparison between the experimental results (such as pulse shape, output spectra and output energy), and predications from a simplified theoretical model could lead to sufficient understanding of laser performance so that the potentiality of a scaled-up laser system can be assessed without involving too much additional experimental effort.

(ii) Since this is one of the few laser systems in which the rates of a) stimulated emission, b) chemical reactions, c) rotational relaxation and d) vibrational relaxation can be comparable, a parametric or systematic study on their effects relative to the theoretical laser performance should be of crucial importance and value to the understanding of fundamental laser physics.

1.3.2. Reaction Kinetics

The major processes involved in H_2/F_2 laser reaction can be summarized as: (a) the photodissociation reaction used for initiation, (b) the chain reactions producing vibrationally excited HF molecules, (c) the various vibrational relaxation, rotational relaxation and energy transfer processes of the excited HF molecules and (d) the stimulated emission producing the laser actions. Table III lists these major reactions. The rate constants of most of the important reactions are known, but some critical rates are not known. Since a modeling calculation excluding these unknown but important reactions is already quite complicated, the computation was first performed without consideration of reactions (VIII) (IX) (X). Later on, these effects are separately tested.

1.3.3 Basic Assumptions

In order to simplify the calculations a few assumptions were made:

(i) For a given vibrational energy level, two extreme rotational distributions are compared;

a) A completely equilibrated Boltzmann distribution at the translational temperature which assumes that rotational relaxation is extremely fast.

b) A completely unrelaxed rotational distribution, assuming that rotational relaxation is very slow compared

TABLE III

REACTIONS INCLUDED IN KINETICS MODEL

(I)	Photodissociation	$F_2 + h\nu \rightarrow 2F$
(II)	Chemical Production	$F + H_2 \rightarrow HF^* (v) + H$ $H + F_2 \rightarrow HF^* v) + F$
(III)	Vibrational Relaxation	$HF (v) + M \rightarrow HF (v - 1) + M$ $M = HF, H_2, F_2, N_2, He, F, H.$ $H_2(v) + M \rightarrow H_2 (v - 1) + M$
(IV)	Vibrational Energy Transfer	$HF (v) + HF (v') \longleftrightarrow HF (v + 1) + HF (v' - 1)$ $HF (v) + H_2 (v') \longleftrightarrow HF (v + 1) + H_2 (v' - 1)$ $H_2 (1) + H_2 (1) \longleftrightarrow H_2 (2) + H_2 (0)$
(V)	Recombination	$H + F + M \rightarrow HF + M$ $F + F + M \rightarrow F_2 + M$ $H + H + M \rightarrow H_2 + M$
(VI)	Branching	$HF (v) + F_2 \rightarrow 2F + HF (0)$
(VII)	Stimulated Emission	$HF (v) + h\nu \rightarrow HF (v - 1) + 2h\nu$

RATES UNKNOWN BUT IMPORTANT

(VIII)	Effect of Vibrational Excitation upon the Rates of Vibrational Relaxation	$HF (v) + HF (v') \rightarrow HF (v - 1) + HF (v')$
(IX)	Rotational Relaxation	$HF (v, J) + M \rightarrow HF (v\ J') + M$
(X)	Vibration-to-Rotational Energy Transfer	$HF (v, J) + M \rightarrow HF (v-1, J') + M$

with the rate of stimulated emission and during the lasing period the molecules still maintain their original rotational distribution.

(ii) For each vibrational level only one rotational line (that with a maximum gain i.e. a P-branch transition) is capable of laser action at any one time. However, various vibrational levels may lase simultaneously.

(iii) A homogeneous photodissociation of F_2 molecules.

(iv) Both stimulated emission and vibrational relaxation are limited to single quantum transitions.

(v) It is assumed that the gain-equal-loss condition holds during laser oscillation.

(vi) It is further assumed that the line width of the laser transitions is mainly due to collisions with He, HF, H_2 molecules and hole burning within the Doppler line width is not considered.

Among all these assumptions, Nos. (iii) and (iv) are reasonably close to reality. Number (ii) is in obvious contradiction with the experimental results which show that often more than two vibration-rotation lines oscillate simultaneously. However, this approximation will not appreciably alter the total laser energy or laser duration. Assumption No. (i) is unavoidable because of the lack of knowledge of rotational relaxation rates in HF, but should provide limits by which to compare the experimental data. Number (v) is not a bad assumption for small gain lasers. However, for laser transitions with extremely high gain or superradiation, the results estimated under this condition can only be considered as a lower limit. Number (vi) may be correct, unless atoms like H or F have extremely large collisional broadening cross sections. For high pressure, viscous gas flow (which is the condition of our HF laser), hole burning should not be important at all.

1.3.4 Description of the Model

The theoretical model is basically that used by Airey[14] for the pulsed HCℓ laser but extended to many vibrational energy levels for the HF system. The model assumes that for a particular vibrational level only that P-branch transitions with the greatest gain can lase and that gain can not become greater than loss.

As in the experiments, the reaction is initiated by ultraviolet light which photodissociates some of the fluorine molecules present, i.e.

$$F_2 + h\nu \rightarrow 2F \qquad \text{(I)*}$$

Following which the reaction proceeds via the chain

$$\begin{aligned} F + H_2 &\rightarrow HF\ (v) + H \qquad -\Delta H = 32 \text{ kcal/mole} \\ H + F_2 &\rightarrow HF\ (v) + F \qquad -\Delta H = 98 \text{ kcal/mole} \end{aligned} \qquad \text{(II)}$$

The first reaction, called the "cold" reaction, has sufficient energy to populate vibrational levels of HF up to v = 3, and the second, or "hot" reaction may populate up to v = 8. Roughly half of the reaction energy appears as vibrational energy. This energy may be redistributed through (v-v) collisions, e. g.,

$$HF\ (v) + HF\ (v') \rightarrow HF\ (v+1) + HF\ (v' - 1) \qquad \text{(IV)}$$

or may be converted to translational energy (or more likely rotational energy) through collisions, e. g.,

$$HF\ (v) + M \rightarrow HF\ (v - 1) + M \qquad \text{(III)}$$

Obviously the vibrational energy may also be removed as laser energy.

For each vibrational level, the population is determined by integrating with respect to time an expression of the form

$$\frac{dN_v}{dt} = \underbrace{\sum_i k_i \left[X_i\right] \left[Y_i\right]}_{\text{production, vibrational relaxation}} - \underbrace{\left\{\frac{N_{v,J-1}}{2J-1} - \frac{N_{v-1,J}}{2J+1}\right\} J\rho_v^{v-1} B_v^{v-1}}_{\text{stimulated emission from v level}} \qquad \text{(17)}$$

$$+ \underbrace{\left\{\frac{N_{v+1,J'-1}}{2J'-1} - \frac{N_{v,J'}}{2J'+1}\right\} J'\rho_v^{v-1} B_v^{v-1}}_{\text{stimulated emission from level v + 1}}$$

where

N_v is the population of the v^{th} vibrational level

k_i represents rate constants of various reactions

*These Roman numerals relate to the reactions as listed in Table III

X_i and Y_i are molecules involved in reaction i

N_{vJ} is the population of the J^{th} rotational level of the v^{th} vibrational level

ρ_v^{v-1} is the radiation density from level v to v-1 (ergs-sec/cm^3)

B_v^{v-1} is that part of the Einstein coefficient which is J independent

The gain of a particular P-branch transition can be written as:

$$G(v,J) = \frac{A_v^{v-1}}{\Delta\nu_{v,J}(2\pi\omega_v^{v-1})^2} \; J\left\{\frac{N_{v,J-1}}{2J-1} - \frac{N_{v-1,J}}{2J+1}\right\} \qquad (18)$$

where

$\Delta\nu_{v,J}$ is the full line width at half maximum (sec^{-1})

ω_v^{v-1} is the wave number of the line center (cm^{-1})

A_v^{v-1} is the Einstein probability of spontaneous emission corresponding to the integrated band intensity

The Einstein constants B and A are correlated as

$$B_v^{v-1} = A_v^{v-1} \Big/ \left(8\pi h (\omega_v^{v-1})^3\right) \qquad (19)$$

During laser action, the gain is set equal to the cavity loss, i.e.

$$R(1 - L_c)\exp(2 G \ell) = 1 \qquad (20)$$

where

L_c is the output coupling fraction

R is the "effective" reflectivity (which includes all useless losses)

ℓ is the active length of the cavity.

The calculational procedure is simplified as follows:

(a) The quantities $I_{v,J}$ and M_v, defined as follows:

$$I_{v,J} = J\left\{\frac{N_{v,J-1}}{2J-1} - \frac{N_{v-1,J}}{2J+1}\right\} \qquad (21)$$

and

$$M_v = \ell n \left[\frac{1}{R\,(1 - L_c)}\right] \quad \frac{\Delta\nu\ (2\pi\omega_v^{v-1})^{\,2}}{2\ell\ A_v^{v-1}}$$

are calculated. The line width, $\Delta\nu$, is taken to be independent of quantum number.

(b) At any step in the calculation, the maximum value of the quantity $I_{v,J}$ is found for each vibrational level, i.e.,

$$I_v^m = \underset{J=1}{\overset{\infty}{\text{Max}}} \left\{I_{v,J}\right\} \tag{23}$$

It is assumed that lasing action from a particular vibrational state, v, is only possible if

$$I_v^m \geq M_v \tag{24}$$

Since the quantity loss per path is a constant value, the condition that gain may not become greater than loss leads to the derivation that wherever the above condition (Eq. (24)) is met;

$$\frac{dG(v,J)}{dt} = 0, \quad \text{or} \quad \frac{d\,I_v^m}{dt} = 0 \tag{25}$$

The expression of $\dfrac{dN_v}{dt}$ can be rewritten as

$$\frac{dN_v}{dt} = \left.\frac{dN_v}{dt}\right|_c + I_{v+1}^m\ \rho_{v+1}^v\ B_{v+1}^v - I_v^m\ \rho_v^{v-1}\ B_v^{v-1} \tag{26}$$

where

$$N_v = \sum_{J=o}^{\infty} N_{v,J} = N_v \sum_{J=o}^{\infty} f_v(J); \tag{27}$$

$$\left.\frac{dN_v}{dt}\right|_c$$

is the contribution to the rate of change of vibrational level v due to collisional processes and spontaneous emission.

(c) Combining Eqs. (25) and (26) with the assumption that $\rho_v^{v-1} = o$ gives a set of algebraic equations for ρ_v^{v-1} and dN_v/dt if condition (Eq. (24)) is not met. Solving these simultaneous equations give us ρ_v^{v-1}.

(i) For the case of the equilibrium distribution of rotational energy levels (assumption 1a), $f_v(J)$ of Eq. (27) can be written as:

$$f_v(J) = (2J + 1) \left\{ \exp\left(-J(J+1)/Q_{Rv}\right) \Big/ Q_{Rv} \right\} \quad (28)$$

where Q_{Rv} is the rotational partition function:

$$Q_{Rv} = \frac{kT}{hcB_v} \quad (29)$$

with B_v the rotational constant of vibrational state v. This gives the following expression for Eq. (25):

$$\frac{\partial I_v^m}{\partial N_v} \frac{dN_v}{dt} + \frac{\partial I_v^m}{\partial N_{v-1}} \frac{dN_{v-1}}{dt} + \frac{\partial I_v^m}{\partial T} \frac{dT}{dt} = 0 \quad (25a)$$

(ii) For the case of frozen rotation (assumption (ib)), the rotational distribution function can be determined by the detailed rate constants of the chemical production reactions:

$$\begin{aligned} F + H_2 &\xrightarrow{k_{1v(J)}} HF(v, J) + H \\ H + F_2 &\xrightarrow{k_{2v(J)}} HF(v, J) + F \end{aligned} \quad (II)$$

The production of a particular vibration-rotation level is

$$\frac{d[HF(v, J)]}{dt} = [F][H_2]\, k_{1v}(J) + [H][F_2]\, k_{2v}(J) \quad (30)$$

and the distribution function $f_v(J)$ of Eq. (27) is then assumed to be

$$f_v(J) = \frac{d[HF(v, J)]}{dt} \Big/ \sum_J \frac{d[HF(v, J)]}{dt} \quad (31)$$

$$= \frac{[F][H_2]\, k_{1v}(J) + [H][F_2]\, k_{2v}(J)}{\sum_J \left\{ [F][H_2]\, k_{1v}(J) + [H][F_2]\, k_{2v}(J) \right\}}$$

Since the characteristic time for removal of H atoms by the hot reaction (the slower of the two reactions) is $1/4\mu$ sec for the conditions of interest, and this time is less than the time for production of HF. (The production of HF is limited by the production of F-atoms by the flash lamp.) A steady state is set up between the two reactions such that

$$\frac{d[H]}{dt} = \sum_{v,J} [F][H_2]\ k_{1v}(J) - \sum_{v,J} [H][F_2]\ k_{2v}(J) \approx 0 \quad (32)$$

which leads to:

$$f_v(J) = \frac{k_{1v(J)}/k_{1T}}{k_{1v}/k_{1T}} \frac{+k_{2v}(J)/k_{2T}}{+k_{2v}/k_{2T}} \quad (33)$$

where

$$k_{1v} = \sum_J k_{1v}(J), \qquad k_{1T} = \sum_v k_{1v} \quad (34)$$

This distribution function is thus independent of time and temperature and the last term in Eq. (25a) drops out because

$$\frac{\partial\ {}_1V^m}{\partial T} = 0 \quad (35)$$

(d) Throughout the integration the gas temperature T is calculated by integrating

$$\frac{dT}{dt} = \frac{1}{C_v}\left[k_{1T}\ [F]\ [H_2]\ E_1 + k_{2T}\ [F_2]\ [H]\ E_2 + \frac{d[F]}{dt}\bigg|_{FLASH} E_A - \frac{d}{dt}\ E_{VIB}(T_v)\right] \quad (36)$$

In which C_v is the specific heat at constant volume; E_1 and E_2 are those portions of the reaction energies for the cold and hot reactions, respectively, which go directly into translation; k_{1T} and k_{2T} are the rate constants for the cold and hot reactions, respectively, E_A is the portion of the absorbed photon energy which appears as translational energy (photon energy minus dissociation energy); and the final term is the contribution due

to deactivation of vibrational energy. This translational temperature is used in calculating those rate constants which depend on temperature, and in calculating the gain.

(e) Finally, for converting the resulting values of ρ_v^{v-1} into the power output in watts/cm^3, a multipliative factor C_c is used, where

$$C_c = \frac{10^{-7} L_c \quad \Delta\nu \quad 3 \times 10^8}{2\ell} \tag{37}$$

The total energy output in joules/cm^3 is then

$$E = \int_0^t \sum_v C_c \quad \rho_v^{v-1} \quad dt \tag{38}$$

1.3.5 Major Rate Constants

Clearly the validity and usefulness of the computation depends heavily on the accuracy of the rates used. The values of the major rate constants listed in Table III are given below in units of cm^3/particle-sec.

(a) Production (II)

$$F + H_2 \xrightarrow{k_{1v}} HF(v) + H$$

$$k_{10}:k_{11}:k_{12}:k_{13}:k_{14} = 0:0.29:1.0:0.47:0:0:$$

$$\sum_v^4 k_{1v} = 2.6 \times 10^{-10} \exp(-800/T)$$

$$H + F_2 \xrightarrow{k_{2v}} HF(v) + F$$

$$k_{20}:k_{21}:k_{22}:\ldots\ldots k_{29} = 0:0.13:0.16:0.29:0.35:0.76:1.0:0.38:0.25:0$$

$$\sum_v^{10} k_{2v} = 2.2 \times 10^{-10} \exp(-1200/T)$$

$$H + HF(v) \xrightarrow{k_{3v}} F + H_2$$

$$k_{3v} = 0, \text{ for } v \leq 3$$

$$k_{3v} = 5 \times 10^{-12} \text{ for } v \geq 4$$

(b) Non-reactive processes

(i) Vibration to translational energy transfer rates (III)

$$HF(v) + F \rightarrow HF(v-1) + F \quad , \quad k_v = 2.5\times10^{-12}\, v^n$$

$$HF(v) + H \rightarrow HF(v-1) + H \quad , \quad k_v = 2.5\times10^{-12}\, v^n$$

$$HF(v) + F_2 \rightarrow HF(v-1) + F_2 \quad , \quad k_v = 2.5\times10^{-15}\, v^n$$

$$HF(v) + H_2 \rightarrow HF(v-1) + H_2 \quad , \quad k_v = 2.5\times10^{-15}\, v^n$$

$$HF(v) + HF \rightarrow HF(v-1) + HF \quad , \quad k_v = 8\times10^{-13} \exp(785(T^{-1/3} - .105)^2)\, v^n$$

where n = 1 or 2

(ii) Vibration-vibrational energy transfer rates (IV)

$$HF(v) + HF(v') \underset{k^-}{\overset{k^+}{\rightleftharpoons}} HF(v-1) + HF(v'+1) \quad \text{for } v > v'+1$$

Two sets of rate constants have been tried: 1) quantum number dependent rates and 2) energy discrepancy dependent rate constants:

1) $k^-(v, v') = 2.5 \times 10^{-12}\, v\,(v'+1)$

or

2) $$k^-(v, v') = \begin{cases} 2.5\times10^{-12}, & \Delta E \le 300 \text{ cm}^{-1} \\ 2.5\times10^{-13}, & 300 < \Delta E < 600 \text{ cm}^{-1} \\ 2.5\times10^{-14}, & 600 < \Delta E \end{cases}$$

and

$$k^+(v, v') = k^- \exp(-\Delta E/kT)$$

$$HF(v)+H_2(v') \underset{k^-}{\overset{k^+}{\rightleftharpoons}} HF(v+1)+H_2(v'-1)$$

$$k^+(v, v') = 6.9\times10^{-12}\, P_{vv}^{HF_1,\ H_2}$$

v	.0	1	2	3	4	5	6	7	8	9
P_{v1}	.25	.45	.75	1.0	.95	.8	.65	.45	.25	.13
P_{v2}	.4	1.0	1.5	2.0	3.0	2.8	2.1	1.8	1.3	.75

where $k^{-}(v, v') = k^{+}(v, v') \exp(-\Delta E/kT)$

(c) Other Rate Constants

The reactions described above are those considered to be the most important for the H_2/F_2 chain reaction. However, the other reactions photodissociation of F_2(I), recombination reactions of atoms (V), and chain branching reactions of HF by F_2(VI) are definitely involved and also important. The following rate constants for these other reactions have been adopted in the calculation:

$F_2 + h\nu \rightarrow 2F$

ϵ = absorption coefficient = 6 litre/mole-cm

$H + F + M \rightarrow HF\ (0) + M$, $\quad k = 7.2 \times 10^{-30}/T$

$F + F + M \rightarrow F_2 + M$, $\quad k = 3.0 \times 10^{-32}/T$

$H + H + M \rightarrow H_2 + M$, $\quad k = 6.6 \times 10^{-30}/T$

$HF(v) + F_2 \rightarrow 2F + HF\ (0)$.

$k(v \leq 4) = 10^{-17} T^{1/2} \exp(E_v - E)/RT$

$k(v > 4) = 10^{-17} T^{1/2}$

where E = 37 kcal/mole and E_v = vibrational energy level of v state

1.3.6 Systematic Studies on Various Parameters

1.3.6.1 Line Width

As one can clearly see from both the gain Eq. (18) and output power expression (38), the line width $\Delta\nu_{vJ}$ has direct influence on the calculated gain and laser output energy. Consequently, in the

computation, the value of $\Delta\nu_{vJ}$ has to be carefully chosen. Meredith et al[15] have recently published their calculated line widths for HF-HF collisions. At 400°K, a peak line width of 0.42 cm^{-1}/atm for J=2 was found. The value drops off sharply as J increases. For example, a value of 0.08 was found for J=8 state. For our standard gas mixture, with a maximum final HF pressure of 61 torr, the maximum broadening should be around 0.04 cm^{-1}. For reactions with 33% completion (the approximate end of laser action), the maximum HF pressure will be less than 20 torr, and the maximum line width broadened by HF=HF collisions will be less than 0.013 cm^{-1}.

Meredith et al have also calculated the line width values for collisions of HF-H_2, HF-N_2 and HF-He. It was found that γ (line width) values decreases only slowly with the rotational quantum number J. For HF-H_2 collisions a line broadening value of γ = 0.092 cm^{-1}/atm was found for J=1, γ=0.062 for J=4 and γ=0.05 for J=8. The J dependence for HF-N_2 is about the same but with γ 10% larger. The values for HF-He also have about the same J dependence, but with a maximum γ of about 0.02 to 0.03 cm^{-1}/atm for J=1. For higher J state transitions, the γ for HF-He value is probably about 0.01 to 0.02 cm^{-1}/atm.

Therefore, the total line width broadened by combined collisional effects of HF-HF, HF-H_2, HF-He, and HF-F_2 will probably be around 0.03 $\pm$ .01 cm^{-1} for low J state transitions and 0.015 $\pm$ .0005 cm^{-1} for high J transitions. Most of the broadening is due to HF-He collisions. As the temperature of the gases increase, the difference in γ between high and low J state transitions become smaller, and the average line width gets broader, which decreases the gain. Figure 35 shows the calculated output energy as a function of line width $\Delta\nu$. For simplicity a line width average over all J state transitions was used. It was found that for an averaged line width of 0.02 cm^{-1}, an output energy of 3.5 joule/100 cc was calculated for 90% output coupling for a 0.04/0.04/0.92 mixture which is in rough agreement to the experimental observations (see Fig. 16).

1.3.6.2 The Effect of Rotational Relaxation

As we have discussed earlier the assumption of a Boltzmann distribution among rotational energy levels is quite questionable. But with present lack of knowledge of rotational relaxation rates in HF, it is not possible to make a detailed calculation of its effects. Since the effect of rotational distribution on the laser performance is not obvious from the equations, we shall compare the calculated output energy and laser duration only. Figure 36 shows the calculated laser output power of both frozen rotational and equilibrated rotational distributions for the standard gas mixture of 0.04/0.04/0.92 and output coupling of 90%. It is clear that for the case of the frozen rotational distribution, the program predicts a much larger output energy and longer pulse duration than that of equilibrated rotational distributions. Since the program allows only one vibration-rotational lasing transition on each vibrational energy level, the frozen rotation case still maintains its

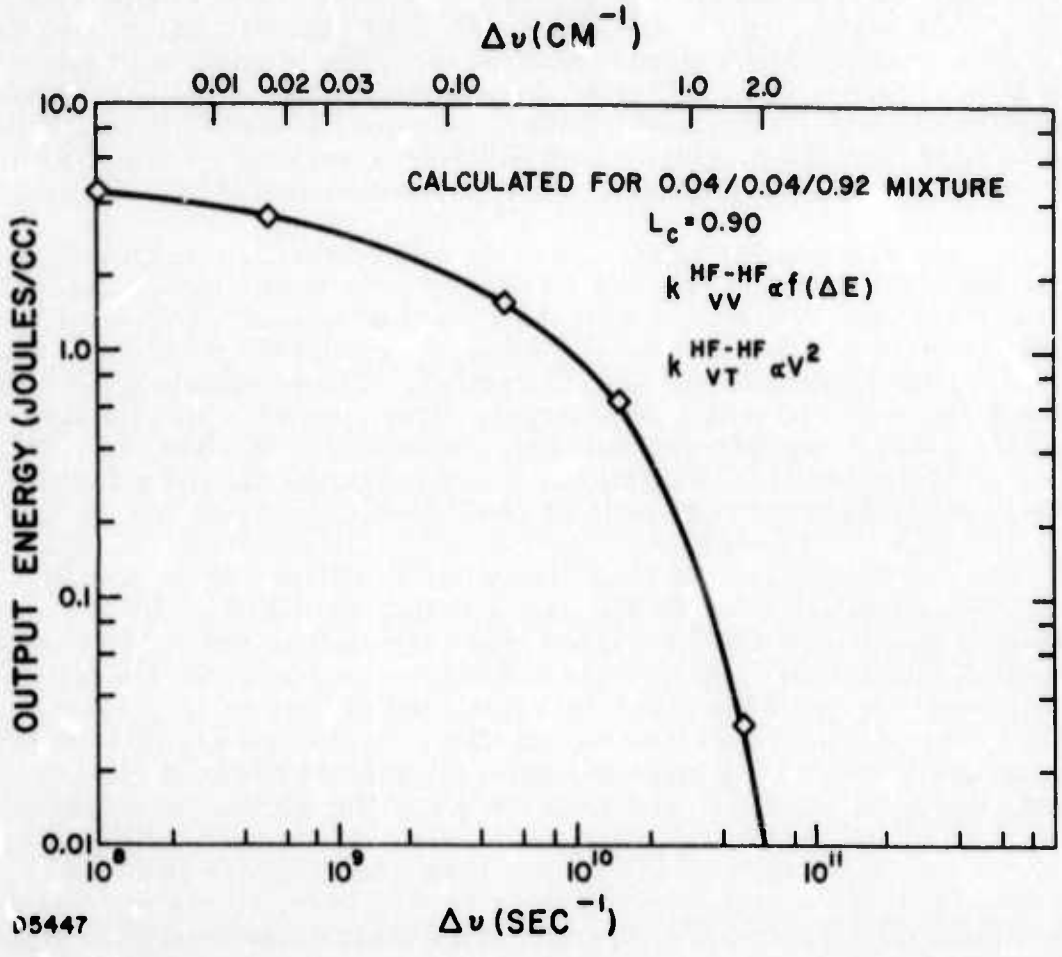

Fig. 35 The Calculated Output Energy Plotted as a Function of Line Width $\Delta\nu$

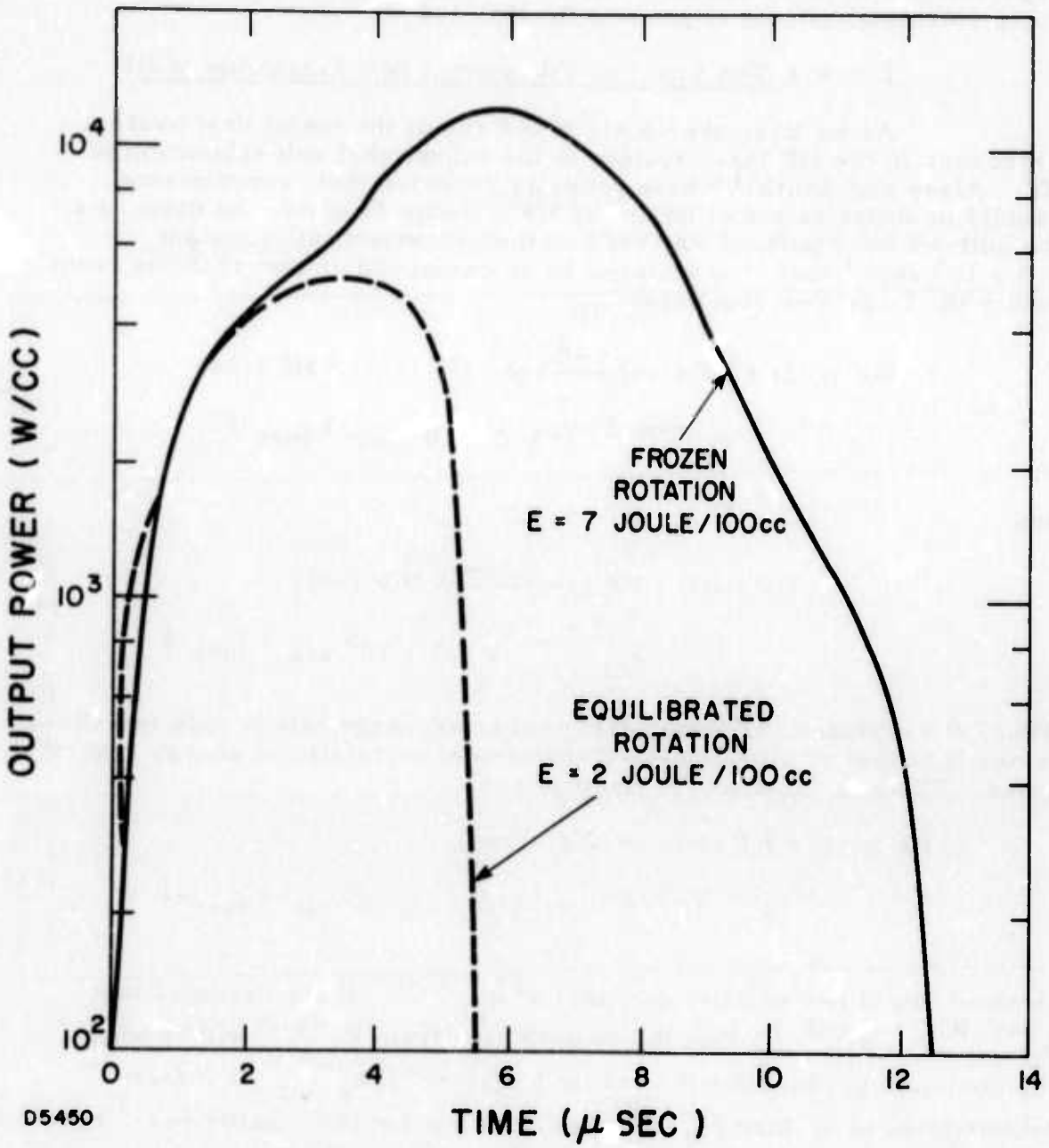

Fig. 36 The Calculated Laser Output Spectra for Both Frozen and Equilibrated Rotational Distributions in Mixture of $H_2/F_2/He$ = 0.04/0.04/0.92 and 90% Output Coupling

original rotational distribution, but the equilibrated rotation case gives a peak intensity spectra close to that of a Boltzmann distribution. The experimental observation falls right in between. Further discussions of these rotational effects is given in Section 1.4.2.

1.3.6.3 The Effect of Vibrational Self Relaxation of HF

As we have previously noted one of the major deactivation processes in the HF laser system is the vibrational self relaxation of HF. Airey and Smith[16] have recently reported their experimental results on deactivation of HF (v) by HF. Table IV shows the data. As the authors have pointed out, for v=2 the measured rate constant 5.5×10^5 sec^{-1} torr^{-1} is believed to be composed of contributions from both v→R.T and v→v reactions:

$$HF\ (v=2) + HF\ (v=o) \xrightarrow{v \to R.T} HF\ (v=1) + HF\ (v=o)$$

$$k_{21}^{v \to R.T} = 1.8 \times 10^5 \text{ sec}^{-1} \text{ torr}^{-1} \tag{39}$$

and

$$HF\ (v=2) + HF\ (v=o) \xrightarrow{v \to v} 2HF\ (v=1)$$

$$k_{21}^{v \to v} = 3.7 \times 10^5 \text{ sec}^{-1} \text{ torr}^{-1} \tag{40}$$

Thus, the vibration-to-vibrational energy exchange rate is only two times faster than that of vibration-to-translational or rotational energy transfer rates. The rate constant for the process:

$$HF\ (v=1) + HF\ (v=o) \rightarrow 2HF\ (v=o)$$

$$k_{10}^{v \to T.R} = 1.0 \pm 0.3 \times 10^5 \text{ sec}^{-1} \text{ torr}^{-1} \tag{41}$$

is about two times smaller than that of $k_{21}^{v \to T.R}$. If one assumes that $k_{n,n-1}^{v \to T.R} \propto \nu\, k_{10}^{v \to T.R}$, then the contribution from $k^{v \to T.R}$ will become the dominate process for the v=4 or 5 states. If $k_{n,n-1}^{v \to T.R}$ is indeed proportional to ν, then $k_{54}^{v \to T.R}$ should be $5 \times 1 \times 10^5 = 5 \times 10^5$ sec^{-1} torr^{-1} and $k_{43}^{v \to T.R}$ should be $4 \times 1 \times 10^5 = 4 \times 10^5$ sec^{-1} torr^{-1}, both of which are considerably smaller than the observed combined rate constants (see Table IV). However, if one assumes a ν^2 dependence, then $k_{54}^{v \to T.R} = 25 \times 1 \times 10^5 = 2.5 \times 10^6$ and $k_{43}^{v \to T.R} = 16 \times 1 \times 10^5 = 1.6 \times 10^6$, both values of which agree well with the data. Table V shows the effects of both v→v

TABLE IV

RATE COEFFICIENTS FOR DEACTIVATION OF HF (v) BY HF

v	$k^{HF, HF}_{v, v-1}$ (uncorr) ($torr^{-1}$. sec^{-1})	$Z^{HF, HF}_{v, v-1}$
1	9.4×10^4	70
2	5.5×10^5	12
3	6×10^5	11
4	$> 1.7 \times 10^6$	< 4
5	$> 2.6 \times 10^6$	< 3
6	?	?
7	?	?
8	?	?

and v→T.R rates on the calculated output energy and laser duration. It clearly indicates that the v→v rate does not have too much influence on the laser output energy but the v→T.R rate does. Computations using $k^{v\rightarrow T.R}_{n,n-1} \propto \nu$ predicts twice as much output energy as that using $k^{v\rightarrow T.R}_{n,n-1} \propto \nu^2$. The former rates also predict a larger laser duration than that using an n^2 dependence.

1.3.6.4 The Effect of Chain Branching Reactions

Russian authors [7] have claimed that chain branching occurs through the reaction

$$HF\ (v \geq 4) + F_2 \longrightarrow HF + 2F \qquad (VI)$$

If this indeed occurs in the H_2/F_2 laser system, the rate of the overall reaction will increase sharply (exponentially), and the duration of the laser pulse should also decrease sharply due to the rise in gas temperature. Unfortunately, the rate constants for the above reactions are not known with any degree of certainty. If one adopts rate constants of

$$k\ (v \leq 4) = 10^{-17}\ T^{1/2} \exp\ (E_v - E)/RT \qquad (42)$$

and

$$k\ (v > 4) = 10^{-17}\ T^{1/2} \qquad (43)$$

where E = 37 kcal/mole and E_v = vibrational energy of the v^{th} state as claimed by the Russian authors, the contribution of VI to the overall reaction becomes unimportant. However, if one assumes a rate constant of 10^{-12}, the program predicts an output energy twice as large and a pulse duration of about two times shorter than that using the slower rate. The calculation with the fast chain branching reaction does give a result (laser duration and output energy) in better agreement with the data (Table V), but cannot explain the variation of output energy with coupling.

1.3.6.5 The Assumption of Constant Cavity Loss and Gain-Equal-Loss Condition

As we have stated at the very beginning, the modeling calculation assumes that, during the laser action, gain equals loss and that the optical loss is a constant. From the light scattering experiment, we have clearly demonstrated that the beam can be seriously distorted inside the laser cavity. Therefore, the assumption of constant loss during the laser duration could be questioned. In order to test the effect of possible beam distortion on the performance of the HF laser, a qualitative analysis was made.

TABLE V

Calculation Output Energy for a Mixture of 1/1/23 with $F/F_2 = 0.01$, $R = 0.97$, $L = 50$cm, $\Delta\nu = 5 \times 10^8$ sec^{-1}, equilibrated rotational distribution and the parameters as listed.

Output Coupling L_c	$k_{n,n-1}^{v\rightarrow v}$	$k_{n,n-1}^{v\rightarrow T,R}$	k_{HF+F_2} Chain Branching	Output Energy (Joule/100cc)	Pulse Duration (μsec)
0.9	$\propto vv'$	$\propto v^1$	$\sim 10^{-15}$	3.5	8.0
	$\propto vv'$	$\propto v^2$	$\sim 10^{-15}$	2.0	5.5
	$\propto f(\Delta E)$	$\propto v^1$	$\sim 10^{-15}$	3.2	8.5
	$\propto f(\Delta E)$	$\propto v^2$	$\sim 10^{-15}$	2.0	5.0
	$\propto vv'$	$\propto v^2$	$\sim 10^{-12}$	3.8	2.5
Experimental observation (using Sapphire window)				$3.6 \pm .4$	3.5
0.5	$\propto vv'$	$\propto v^1$	$\sim 10^{-15}$	7.6	9.0
	$\propto vv'$	$\propto v^2$	$\sim 10^{-15}$	4.5	6.0
	$\propto f(\Delta E)$	$\propto v^1$	$\sim 10^{-15}$	7.5	9.5
	$\propto f(\Delta E)$	$\propto v^2$	$\sim 10^{-15}$	4.0	6.0
	$\propto vv'$	$\propto v^2$	$\sim 10^{-12}$	8.5	3.5
Experimental observation (using Silicone window)				$2.2 \pm .3$	4.0

For a simple two level system, Rigrod[17] has derived an expression for the radiation intensity from a cavity with one reflecting mirror and one transmitting mirror which can be expressed as:

$$\frac{I}{I_o} = \frac{L_c(1 + \ell n(1 - L_T)/2g_o\ell)}{L_c + \frac{L_T - L_c}{(1 - L_T)^{1/2}}} \tag{44}$$

where

g_o is the small signal gain,

L_T is the total losses ($L_T \equiv 1 - (1 - L_c)(1 - L_D)$),

I_o is the intensity in the limit $L_T \rightarrow L_c \rightarrow 0$,

L_c is the output coupling,

ℓ is the cavity length,

L_D (=1-R) is the dissipative losses or in our case possible losses caused by beam distortion.

Figure 37 shows I/I_o vs L_D for various values of small signal gain for two experimental values of output coupling. The fact that twice as much intensity is observed experimentally for the higher output coupling case indicates that $L_D > .4$ since I/I_o must certainly be less than one half for the lower coupling case. In any event, this analysis has clearly indicated that for high gain lasers, if the beam becomes distorted due to density variations within the cavity, the laser energy extracted from a high output coupling cavity is not necessarily smaller than that of smaller output coupling. This conclusion is consistent with our experimental observations, but does not prove that beam distortion (or a high value of L_D) is a dominant effect in our laser.

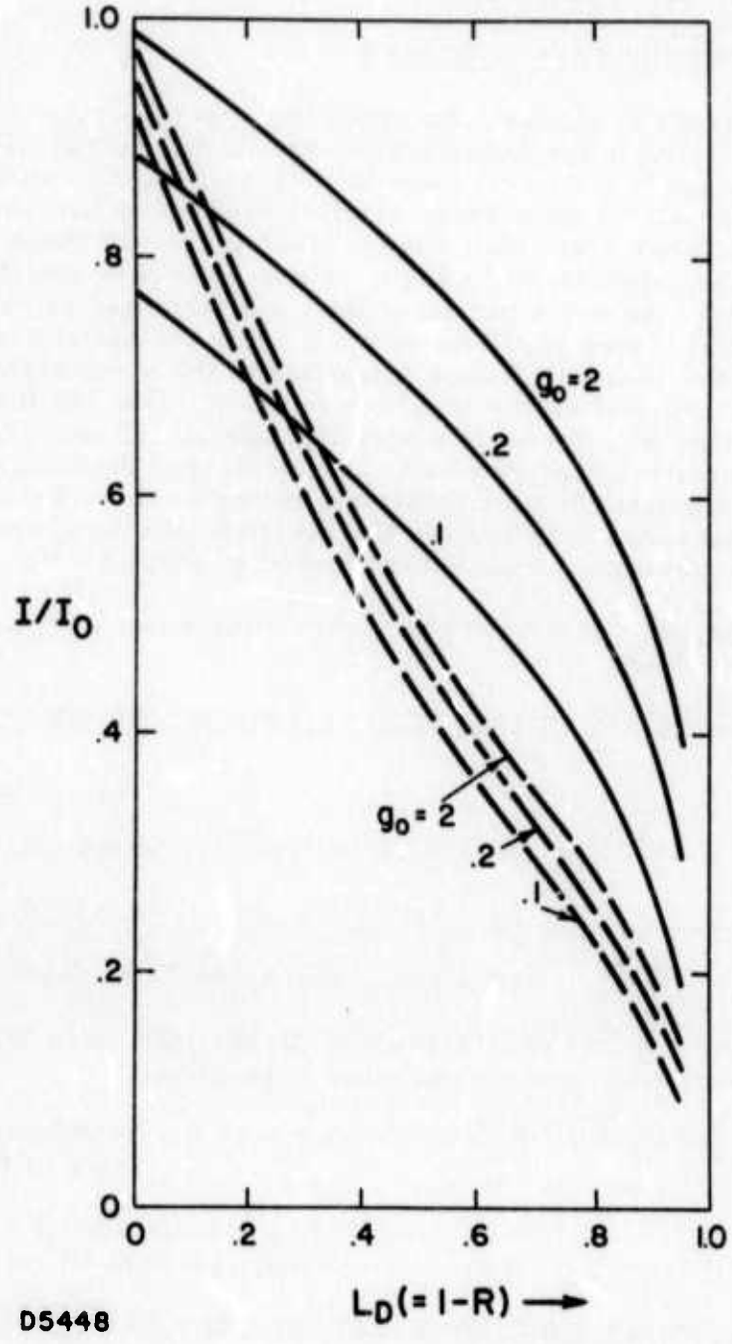

Fig. 37 The Plot of I/Io vs L_D for Small Signal Gain Derived from Rigrod's Expression Solid Lines for L_C = 0.9 and Dash L' .es for L_C = 0.5 ℓ = 50 cm

1.4 SUMMARY ON THE PERFORMANCE OF FLASH LAMP INITIATED, PULSED HF CHEMICAL LASER

1.4.1 On the Chemical Efficiency

In order to evaluate an upper limit on the amount of chemical energy that is available for laser action, the initial energy distributions of both the F + H_2 and H + F_2 reactions have to be carefully studied. Recently Polanyi et al [3] have given detailed reports on the experimentally measured vibrational/rotational energy distributions of these two reactions. Their results are reproduced in Figs. 38 and 39. They found that the cold reaction (F + H_2) favors formation of the v = 2 state and is capable of producing vibrational states of HF up to v = 3. For the hot reaction, (H + F_2) they found that the reaction favors formation of the v = 6 state and is capable of producing vibrational states of HF up to v = 8. Besides the formation of vibrational excited HF, these data also indicate significant rotational non-Boltzmann distributions as well. Particularly, the cold reaction preferentially populates higher rotational states as the vibrational state population decreases, while for the hot reaction all vibrational states have about the same rotational distribution peaked at about J = 8.

Using this data, the chemical efficiency of our laser system can be analyzed as follows:

TOTAL CHEMICAL ENERGY LIBERATED FROM THE REACTION OF

		f_V	f_R	f_T
F + H_2 → HF + H	- ΔH = 31.5 kcal/mole	0.66	0.08	0.26
H + F_2 → HF + F	- ΔH = 102 kcal/mole	0.53	0.03	0.44
H_2 + F_2 → 2HF	- ΔH = 133.5 kcal or 66.75 kcal/mole of HF formation			

where f_V, f_R, and f_T are the fraction of ΔH that end up in the HF vibrational, rotational, or translational mode respectively.

TOTAL ENERGY INTO VIBRATION = 20.8 + 54.0 = 74.8 kcal or 37.4 kcal/mole of HF formation

= 1290 joule/100 CC of H_2 + F_2 at 1 atm or 645 joule/100 CC of HF formation

TOTAL VIBRATIONAL ENERGY AVAILABLE IN 100 CC MIXTURE OF $H_2/F_2/He$ = 0.04/0.04/0.92

= 1290 x 0.04 = 51.6 joule/100 CC of standard H_2/F_2/He mixture at 1 atm or 51.6 joule/8 CC of HF formation at 1 atm.

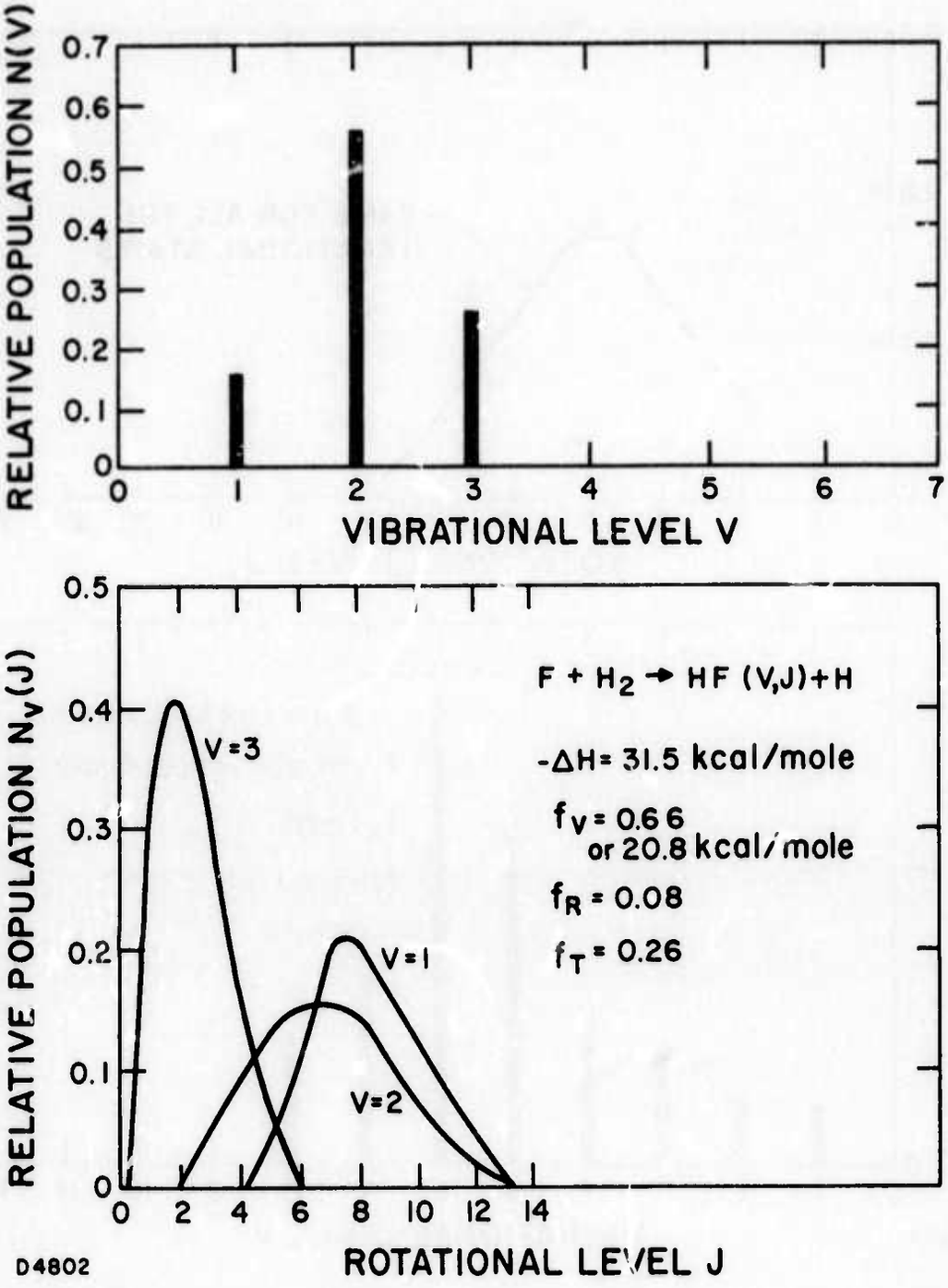

Fig. 38 Polanyi's Result on the Vibration/Rotational Energy Distribution of $F + H_2 \rightarrow HF + H$ Reaction

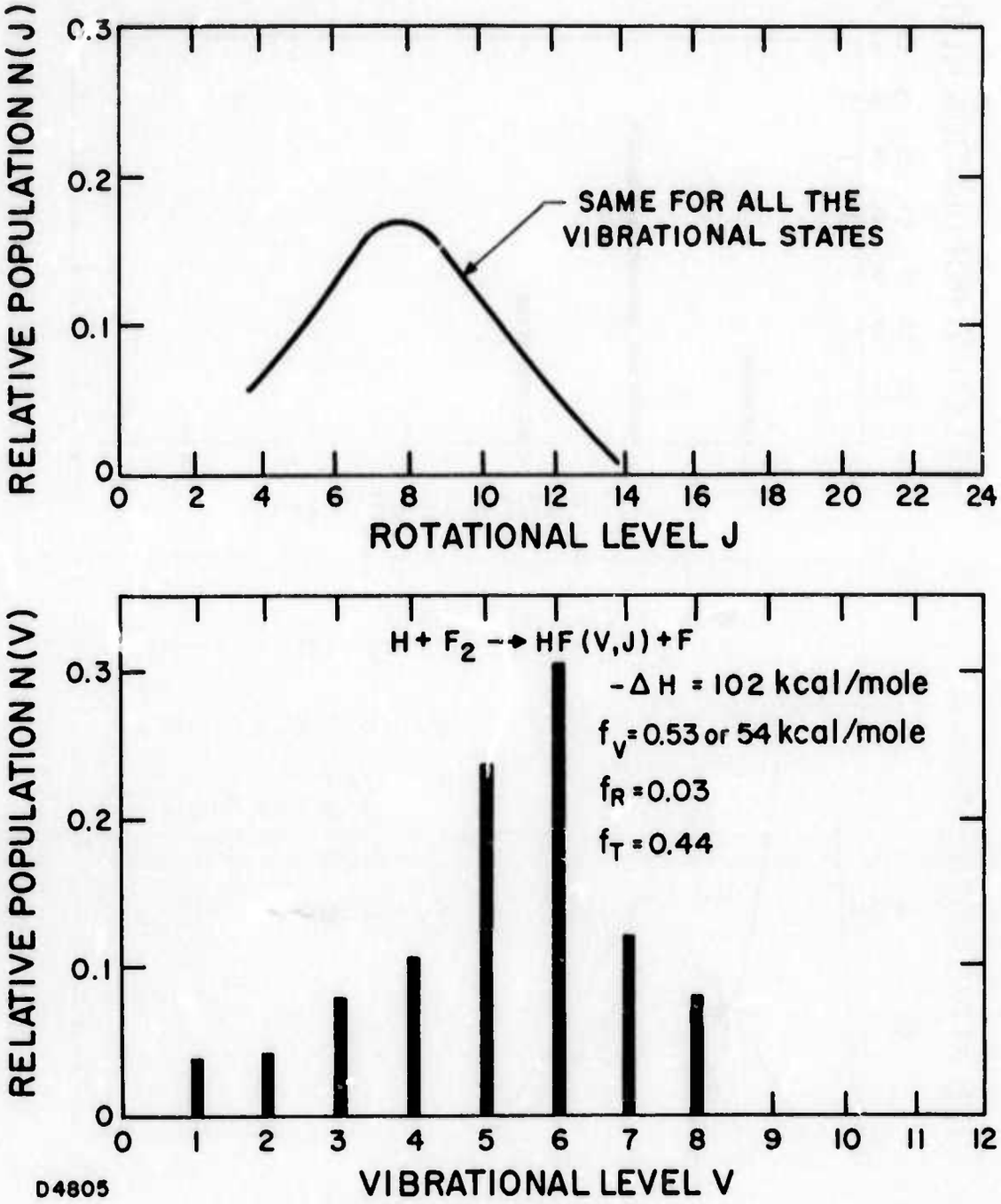

Fig. 39 Polanyi's Result on the Vibration/Rotational Energy Distributic of $H + F_2 \rightarrow HF + F$ Reaction

TOTAL LASER ENERGY OBSERVED = 4 JOULE IN 3 μSEC

(LASER ENERGY)/(AVAILABLE VIBRATIONAL ENERGY) ≈ 8%

EXTENT OF CHEMICAL REACTION ESTIMATED WITH $F/F_2 = 0.01$

FOR 3 μSEC PERIOD ≈ 30%

TOTAL CHEMICAL ENERGY LIBERATED INTO VIBRATION WITHIN

3 μSEC DURATION = 15 JOULES

PERCENT OF VIBRATIONAL ENERGY CONVERTED INTO LASER

ENERGY DURING THE 3 μSEC PERIOD = 4/15 ≈ 30%

THE MAXIMUM POSSIBLE CHEMICAL EFFICIENCY = 59%

CHEMICAL EFFICIENCY = LASER ENERGY/TOTAL CHEMICAL ENERGY

RELEASED ≈ 4%

Therefore, the chemical efficiency of our system for 0.04/0.04/0.92 mixture is 4%. The chemical efficiency for the 0.04/0.02/0.94 mixture and the 0.16/0.08/0.76 mixture are also 4%. A substantial fraction of the available energy of the reaction that goes into vibration has been recovered as laser energy. The major reason for the termination of laser action is probably the heating of the gas mixture as the reaction proceeds with subsequent loss of gain.

The overall electric-to-laser energy efficiency obtained from a mixture of 0.16/0.08/0.76 was calculated to be about 1.3% which is about twice as much as that reported in our previous contract report.(5) Since the active volume of our laser device is only 0.1 liter at a pressure of 1.1 atm, the final laser energy density in units of joules/liter-atm is 80 joule/liter-atm with a composition of 16%, H_2, 8% F_2 and 76% He. For higher concentrations of F_2 and H_2 in He, the output energy would be expected to increase proportionately.

1.4.2 On the Assumption of Equilibration of Rotational Energy Levels

Among almost all the known vibration-rotational laser systems reported in the literature, the equilibration of the rotational energy levels has always been assumed to have been established before the laser transitions. This assumption is probably true for lasing molecules having small rotational energy level spacing and hence faster rates of rotational relaxations than HF. Since the molecule HF has a rotational constant $B = 20\ cm^{-1}$, the spacing between J = 10 and J = 9 levels is $2BJ = 400\ cm^{-1}$ which is about twice kT at room temperature. The time for the rotational relaxation of HF (J = 10) state could be very long and take many collisions to reach equilibration. Polanyi et al (18) have also made an experimental estimate of the probability of rotational relaxation of HCl. The results are replotted in Fig. 40 as the probability per collision of a rotational transition as a function of ΔE, the energy spacing between rotational states. It was found that for low J states $\Delta J = \pm 2$ and $\Delta J = \pm 1$ transitions are all probable. But for high J levels, the $\Delta J = \pm 1$ transitions dominate. If one assumes that

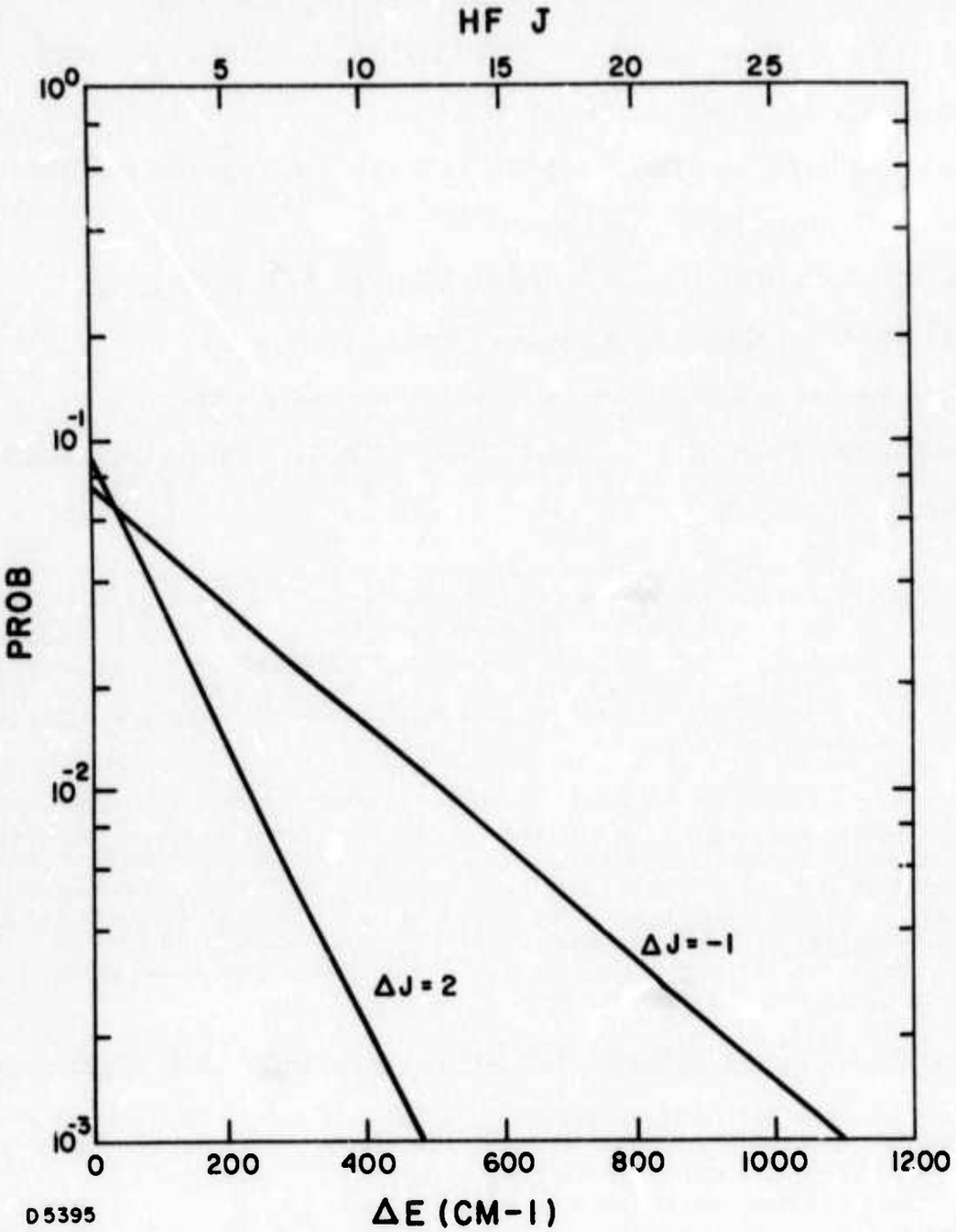

Fig. 40 Estimated Rates of Rotational Relaxation of HF from Polanyi's Data on HCl

HF rotational energy levels relax with a similar energy dependence ($E_J - E_{J'}$) as HCl and therefore the probability depends only on the rotational energy spacing, then the relaxation of the J = 10 state should require 100 collisions. The particular J state of HF corresponding to ΔE has been indicated at the top of Fig. 40. It is evident that 100 collisions is quite slow in comparison with the rate of stimulated emission and even slower than the rate of vibrational relaxation of HF.

Thus the assumption of a Boltzmann distribution among all the rotational energy levels before the lasing action is indeed questionable. The fact that (i) far-IR laser emission was observed in our H_2/F_2 system and (ii) two distinctive pulses within each individual vibrational-rotational transition are observed for high J states, strongly supports the argument that, at the beginning of HF laser action, the rotational energy equilibration must have not been established. Unfortunately, the double resonance absorption experiment to measure the HF rotational relaxation rate was not finished and was inconclusive. With the existing data we can only state that the rates of rotational relaxation of low J states are relatively fast. For a detailed knowledge of the mechanism and rate, more experimental work is needed.

Again, it is not clear what effect the rotational energy non-equilibration has on extracting IR laser photons. For one thing, it helps in building up population inversion among certain levels. It also decreases the tendency of losing laser gain through the process of rotational relaxation. The fact that (i) for the same gas mixture, different output coupling windows (with the same optical property at 2.7 μ but considerably different behavior in the far IR region) extract different amounts of IR laser energy, and (ii) adding SF_6 to the H_2/F_2 mixture significantly decreases the amount of IR laser output energy, also supports the contention that the rotational energy distribution is playing an important part in the process of HF IR laser action.

1.4.3 On the Possibility of Parasitic Oscillation

Scientists at the Aerospace Corporation [19] have claimed that parasitic oscillation may be playing an important role in their HF laser. Such oscillations, if consisting of modes that bounce off the walls of the laser tube, could result in the output laser beam appearing at larger angles to the axis, and thereby possessing poor optical quality. In some respects our laser performance is consistent with their arguments. For example, we get only half as much energy out by using a 50% output coupling (Si) window compared to a 90% output coupling (Sapphire). However, this phenomenon could also be attributed to the differences in optical properties of these two output window materials. However, the output energy observed by using a NaCl window is roughly the same as that obtained by using Si flat although these materials have different % transmission. Furthermore, the output energy obtained from KBr output coupling window is less than that of NaCl flat although these materials have almost identical transmissivity. Therefore, the parasitic argument is far from conclusive. Nevertheless, the close agreement between the burn pattern and the rough

calculation of spot size and multimode pattern strongly indicates that parasitic oscillations are not dominating in our HF laser. Of course, parasitic oscillations are still an important consideration in a intrinsically high gain laser such as this H_2/F_2 system.

1.4.4 On the Validity of Model Calculations

The rough agreement between the experimental observations (such as output energy and pulse duration) and predictions (Table V) resulting from the theoretical calculation have indicated that the model used is a reasonable one. At least, the model is capable of giving a qualitative picture of the performance of the HF laser studied. However, there are a few fundamental drawbacks to the model that could be the basis for further research:

(a) The model is constructed based on the assumption that a constant cavity loss is maintained during the laser action, which may not be true.

(b) The model does not take care of the effect of rotational relaxation and the possibility of vibration-to-rotational energy transfer which could seriously change the output spectra and energy.

(c) There is a contraction in logic between the constant gain assumption and the rapidity of relaxation rates. Since the constant gain assumption is constructed on the basis that any of the relaxation times should be long compared with the transient time of photons inside the cavity, it clearly requires that any kind of relaxation process must be slow and take a long time to reach equilibrium if it is not produced with an equilibrated distribution. The results from Polanyi's experiments have shown that the initial rotational distribution is highly non-Boltzmann. Thus, if one uses a Boltzmann distribution of rotational energy levels, one must assume that the rate of rotation relaxation is much faster than the transient time of photons in the cavity. Thus, from a logical point-of-view, the usefulness of constant gain assumption is quite questionable for this type of laser.

(d) For the gain-equals-loss condition to be true, the beam inside cavity must be regenerative, which may not be true in our HF experiments. However, little work was done under this program to try to improve the fluid mixing and uniformity. This problem appears to be solvable experimentally and, hence, need not be a fundamental limitation.

1.5 THEORETICAL CALCULATION ON THE VIBRATIONAL ENERGY TRANSFER RATE CONSTANTS

1.5.1 Introduction

It has been a long goal of this program to develop fast yet accurate computer programs which contain the essential physics for the calculation of the vibration-relaxation cross section in an atom-molecule collision. These programs in a simplified version have previously been applied to the V-R relaxation of OH by argon. A more realistic version of these programs is being developed and described in the following section (1.5.2). It is planned that such theory will be applied to problems of interest in the HF laser in the immediate future.

1.5.2 Cross-Section Theory

The number of collisional transitions per second or the transition probability P_{if}^{B} from state i to state f in the Born approximation is given by

$$P_{if}^{B} = \frac{2\pi}{\hbar} \int d\underline{k}'_A \int d\underline{k}'_B \left| \langle f \mid V \mid i \rangle \right|^2 \delta (E_f - E_i) \qquad (45)$$

where V is the interaction potential between collision partners A and B; E_i and E_f are initial and final energies; $E_i = E_A^t + E_B^t + E_A^i + E_B^i$, t and i denote the translational and internal energies and the integration is over final wave vectors of translational motion. We express initial and final wave functions as

$$i \equiv (2\pi)^{-3} \, e^{i(\underline{k}_A \cdot \underline{r}_A)} \, e^{i(\underline{k}_B \cdot \underline{r}_B)} \, \chi'_A \, \chi'_B \qquad (46)$$

and

$$i = (2\pi)^{-3} e^{i(\underline{k}'_A \cdot \underline{r}_A)} e^{i(\underline{k}'_B \cdot \underline{r}_B)} \chi'_A \chi'_B \tag{47}$$

where χ are the wave functions of the internal motion, $\underline{r}_A$ and $\underline{r}_B$ are the center of mass coordinates of A and B, and the final state is denoted by primes. We now assume that the interaction potential between A and B is the sum of the interaction potential of the constituent atoms, i.e.

$$V = \sum_{\mu,\nu} V(r_{\mu\nu}) \tag{48}$$

where the summation is over all atoms μ constituting A and all atoms ν constituting B and we take the potential between the constituent species to be a central one. In addition we assume that matrix element in Eq. (45) is the algebraic sum of such elements from individual scattering centers. This enables us to write

$$\langle f | V | i \rangle = \sum_{\mu,\nu} \langle f | V | (r_{\mu\nu}) \; i \rangle \tag{48a}$$

Now we introduce the Fourier transform of the wave functions for A and B

$$(2\pi)^{-3/2} \chi_i \exp[i\underline{k}_i \cdot \underline{r}_1] \equiv \Psi_i = (2\pi)^{-3/2} \int d\underline{k}_\nu \exp[i\underline{k}_\nu \cdot \underline{r}_\nu]$$

$$\times \phi(\underline{r}_1, \cdots \underline{r}_{\nu-1}, \underline{k}_\nu, \cdots) \tag{49}$$

where i = A, B. Clearly $\phi_i(\underline{r}_1, \cdots \underline{r}_{\nu-1}, \underline{k}_{\nu-1}, \underline{r}_{\nu-1} \cdots)$ is the amplitude that atom ν has momentum $\underline{k}_\nu$ simultaneous with other atoms being at $\underline{r}_1$, $\cdots$, $\underline{r}_{\nu-1}$, $\underline{r}_{\nu+1}$, $\cdots$.

The matrix elements $< f \left| V (r_{\mu\nu}) \right| i >$ needed to evaluate P_{if}^{B} can be written as

$$< f \left| V (r_{\mu\nu}) \right| i > = (2\pi)^{-6} \int d\tau_A \, d\tau_B \, d\underline{k}_\mu \, d\underline{k}'_\nu \, d\underline{k}'_\mu \, d\underline{k}'_\nu$$

$$\times \phi^{*'}_B (\underline{r}_1, \cdots \underline{r}_{\nu-1}, \underline{k}'_\nu, \underline{r}_{\nu+1} \cdots)$$

$$\phi^{*'}_A (\underline{r}_1, \cdots \underline{r}_{\nu-1}, \underline{k}'_\nu, \underline{r}_{\nu+1} \cdots)$$

$$\times \phi_B (\underline{r}_1, \cdots \underline{r}_{\nu-1}, \underline{k}_\nu, \cdots) \phi_A (\underline{r}_1, \cdots \underline{r}_{\mu-1}, \underline{k}_\mu, \underline{r}_{\mu+1} \cdots)$$

$$\times \exp [- i (\underline{k}'_\mu \cdot \underline{r}_\mu + \underline{k}'_\nu \cdot \underline{r}_\nu)]$$

$$V (r_{\mu\nu}) \exp [i (\underline{k}_\mu \cdot \underline{r}_\mu + \underline{k}_\nu \cdot \underline{r}_\nu)] \tag{50}$$

where $d\tau_A = \prod_\mu d\underline{r}_\mu$ and $d\tau_B = \prod_\nu d\underline{r}_\nu$.

Now we introduce center of mass and relative position and wave vectors for atoms μ and ν by the relations

$$\underline{R}_{\mu\nu} = \frac{m_\mu \underline{r}_\mu + m_\nu \underline{r}_\nu}{m_\mu + m_\nu} \tag{51}$$

$$\underline{r}_{\mu\nu} = \underline{r}_\mu - \underline{r}_\nu \tag{52a}$$

$$\underline{K}_{\mu\nu} = \underline{k}_\mu + \underline{k}_\nu \tag{52b}$$

$$\underline{k}_{\mu\nu} = \frac{m_\nu \underline{k}_\mu - m_\mu \underline{k}_\nu}{m_\mu + m_\nu} \tag{52c}$$

This enables us to write

$$\begin{aligned} \langle f | V(r_{\mu\nu}) | i \rangle = (2\pi)^{-3} \int & d\tau'_A \, d\tau'_B \, d\underline{K}_{\mu\nu} \, d\underline{k}_\mu \, d\underline{k}'_\mu \\ & \times \phi^{*'}_A (\underline{r}_1, \ldots, k'_\mu, \underline{r}_{\mu+1}, \ldots) \, \phi^{*'}_B (\underline{r}_1, \ldots, \underline{K}_{\mu\nu} - \underline{k}'_\mu, \ldots) \\ & \times \phi_A (\underline{r}_1, \ldots, \underline{k}_\mu, \underline{r}_{\mu+1}, \ldots) \, \phi_B (\underline{r}_1, \ldots, \underline{K}_{\mu\nu} - \underline{k}_\mu \ldots) \\ & \times \int \exp \left[- i \left(\underline{k}'_\mu - \frac{m_\mu}{m_\mu + m_\nu} \underline{K}_{\mu\nu} \right) \right] V(r_{\mu\nu}) \\ & \exp \left[i \left(\underline{k}_\mu - \frac{m_\mu}{m_\mu + m_\nu} \underline{K}_{\mu\nu} \right) \right] dr_{\mu\nu} \end{aligned} \tag{53}$$

where prime in $d\tau'_A$ means exclusion of $d\underline{r}_\mu$ from the volume element.

At this point we restrict our considerations to the case where A is an atom. In keeping with the spirit of our study we take the atom to be a structureless point particle. For this (from Eq. (49)) case $\chi_A = 1$ and

$$\phi_A = \delta (\underline{k}_A - \underline{k}_\mu) \tag{54a}$$

and

$$\phi'_A = \delta (\underline{k}'_A - \underline{k}'_\mu). \tag{54b}$$

Substituting Eqs. (54) in (53) we get

$$< f \mid V (r_{a\nu}) \mid i > = (2\pi)^{-3} \int d\tau'_B \, d\underline{K}_{a\nu} \, \phi^{*'}_B (\underline{r}_1, \ldots, \underline{K}_{a\nu} - \underline{k}'_a,)$$

$$\phi_B (\underline{r}_1, \ldots, \underline{K}_{a\nu} - \underline{k}_a, \ldots) \times \int \exp \left[-i \left(\underline{k}'_a - \frac{m_a}{m_a + m_\nu} K_{a\nu} \right) \right]$$

$$\times V_{a\nu} \exp \left[i \left(\underline{k}_a - \frac{m_a}{m_a + m} K_{a\nu} \right) \right] d\underline{r}_{a\nu} \qquad (55)$$

Assume that the integral

$$\int \exp \left[-i \left(\underline{k}'_a - \frac{m_a}{m_a + m_\nu} K_{a\nu} \right) \right] V (r_{a\nu}) \exp \left[i \left(\underline{k}_a - \frac{m_a}{m_a + m_\nu} K_{a\nu} \right) \right] \qquad (56)$$

is slowly varying function of $K_{a\nu}$ and using the relation

$$\int d\tau'_B \, d\underline{K}_{a\nu} \, \phi^{*}_B (\underline{r}_1, \ldots, \underline{K}_{a\nu} - \underline{k}'_a) \, \phi_B (\underline{r}_1, \ldots, \underline{K}_{a\nu} - \underline{k}_a, \ldots)$$

$$= \int d\tau_B \, \psi_B \, \psi^{*'}_B \, e^{-i\underline{q} \cdot \underline{r}_\nu} \qquad (57)$$

where $q \equiv \underline{k}'_a - \underline{k}_a$ is the momentum gained by the incident atom. Writing

$$\underline{r}_\nu = \underline{r}_B + \underline{r}_{\nu c} \qquad (58)$$

where $\underline{r}_B$ is the distance of CM of B from our space fixed coordinate system and $\underline{r}_{\nu c}$ is the distance of atom ν from CM of B, we get

$$\int d\tau_B \psi_B \psi_B^{*'} e^{-i\underline{q} \cdot \underline{r}_\nu} = \delta (\underline{k}'_B + \underline{q} - \underline{k}_B) < \chi'_B \left| e^{-i\underline{q} \cdot \underline{r}_{\nu c}} \right| \chi_B > \qquad (59)$$

The delta function in Eq. (59) is simply the result of conservation of linear momentum. Equation (55) can now be rewritten as

$$< f \left| V (r_{a\nu}) \right| i > = (2\pi)^{-3} \delta (\underline{k}'_B + \underline{k}'_A - \underline{k}_B - \underline{k}_A)$$

$$\times < \chi'_B \left| e^{-i\underline{q} \cdot \underline{r}_{\nu c}} \right| \chi_B >$$

$$\times \int \exp \left[-i \left(\underline{k}'_a - \frac{m_a}{m_a + m_\nu} \underline{K}_{a\nu} \right) \right]$$

$$V (r_{a\nu}) \exp \left[i \left(\underline{k}_a - \frac{m_a}{m_a + m_\nu} \underline{K}_{a\nu} \right) \right] d\underline{r}_{a\nu} \qquad (60)$$

Substitution of this result in Eq. (45) gives

$$P_{if}^B = \frac{2\pi}{\hbar} \int \frac{d\underline{k}'_A}{(2\pi)^3} \int \frac{d\underline{k}'_B}{(2\pi)^3} \left| \sum_\nu < \chi_B \left| e^{i\underline{q} \cdot \underline{r}_{\nu c}} \right| \chi_B > \right.$$

$$\times \int \exp \left[-i \left(\underline{k}'_a - \frac{m_a}{m_a + m_\nu} \underline{K}_{a\nu} \right] \right.$$

$$\left. V (r_{a\nu}) \exp \left[i \left(\underline{k}_a - \frac{m_a}{m_a + m_\nu} \underline{K}_{a\nu} \right) \right] \right|^2$$

$$\times \delta (\underline{k}'_A + k'_B - \underline{k}_A - \underline{k}_B) \delta (E_f - E_i) \qquad 61)$$

Changing the variables $d\underset{\sim}{k}'_A\, d\underset{\sim}{k}'_B$ to $d\underset{\sim}{K}\, d\underset{\sim}{k}'$ where $K = \underset{\sim}{k}_A + \underset{\sim}{k}_B = \underset{\sim}{k}'_A + \underset{\sim}{k}_B$ is the total momentum of CM of A and B and $\underset{\sim}{k}' = m_B \underset{\sim}{k}'_A - m_a \underset{\sim}{k}'_B / m_A + m_B$ is the relative momentum of A and B, we can write

$$P_{if}^B = \frac{\mu_t k'}{(2\pi)^2 \hbar^3} \int d\underset{\sim}{\Omega}_{k'} \left| \sum_\nu < \chi'_B \left| e^{i\underset{\sim}{q} \cdot \underset{\sim}{r}_{\nu c}} \right| \chi_B > \right.$$

$$\times \int \exp \left[-i \left(\underset{\sim}{k}'_a - \frac{m_a}{m_a + m_\nu} \underset{\sim}{K}_{a\nu} \right) \right] V(r_{a\nu})$$

$$\left. \exp \left[i \left(\underset{\sim}{k}_a - \frac{m_a}{m_a + m_\nu} \underset{\sim}{K}_{a\nu} \right) \right] \right|^2 \qquad (62)$$

where $\mu_t \equiv \frac{m_a m_B}{(m_a + m_B)}$ is the reduced mass of A and B.

Writing

$$\sigma_{if}^B = \frac{P_{if}^B \mu_t}{\hbar k} \qquad (63)$$

we get

$$\sigma_{if}^B = \left(\frac{\mu_t}{2\pi\hbar^2} \right)^2 \frac{k'}{k} \int d\underset{\sim}{\Omega}_{k'} \left| \sum_\nu < \chi'_B \left| e^{-i\underset{\sim}{q} \cdot \underset{\sim}{r}_c} \right| \chi_B > \right.$$

$$\times \int d\underset{\sim}{r}_{a\nu} \left[-i \left(\underset{\sim}{k}'_a - \frac{m_a}{m_a + m_\nu} \underset{\sim}{K}_{a\nu} \right) \right]$$

$$\left. V(r_{a\nu}) \exp \left[i \left(\underset{\sim}{k}_a - \frac{m_a}{m_a + m_\nu} \underset{\sim}{K}_{a\nu} \right) \right] \right|^2 \qquad (64)$$

We will evaluate Eq. (64) under the approximation

$$\underline{K}_{a\nu} = \underline{k}_a + \underline{k}_\nu \simeq \underline{k}_a + \underline{k}_B, \tag{65}$$

i.e., internal degrees of freedom make no contribution to $\underline{K}_{a\nu}$. We can then write

$$\underline{k}_a - \frac{m_a}{m_a + m_\nu}\ \underline{K}_{a\nu} \simeq \underline{k}_a - \frac{m_a}{m_a + m_\nu}\ \underline{K}$$

$$= \underline{k} - m_a \underline{K} \left(\frac{1}{m_a + m_\nu} - \frac{1}{m_a + m_B} \right) \tag{66}$$

where k is the initial relative momentum and $\underline{K}$ is the momentum of center of mass of atom and molecule. The approximation introduced in Eq. (65) is not fundamental to the formulation presented here. To simplify the calculations further we approximate the left-hand side of Eq. (66) by $\underline{k}$, i.e.,

$$\underline{k} - m_a \underline{K} \left(\frac{1}{m_a + m_\nu} - \frac{1}{m_a + m_B} \right) \approx \underline{k} \tag{67}$$

In addition using the relation

$$d\underset{\sim}{\Omega}_{k'} = - 2\pi \frac{qdq}{kk'} \tag{68}$$

we get

$$\sigma_{if}^{B} = \left(\frac{\mu_t}{2\pi\hbar^2} \right)^2 \frac{2\pi}{k^2} \int_{q_-}^{q_+} qdq \left| \sum_\nu < \chi'_B \left| e^{-i\underline{q} \cdot \underline{r}_{\nu c}} \right| \chi_B > \right. \tag{69}$$

$$\times 4\pi \sum_\ell \hat{\ell}\, P_\ell \left(\frac{k'^2 + k^2 - q^2}{2\, kk'} \right) \int_0^\infty j_\ell (kr_{a\nu})\, j_\ell (k' r_{a\nu}) \tag{69}$$

$$\left. V (r_{a\nu})\, r_{a\nu}^2\, dr_{a\nu} \right|^2$$

where $q_{\pm} = k' \pm k$, $\hat{\ell} \equiv (2\ell + 1)$, P_ℓ is Legendre Polynomial and j_ℓ is the spherical Bessel function. Equation (69) uses a straight line trajectory during a collision. Now we switch to distorted wave approximation and replace $j_\ell (kr_{a\nu})$ by $(kr_{a\nu})^{-1} R_\ell (kr_{a\nu}) e^{i\delta_\ell(k)}$ where R_ℓ is the solution of the equation

$$\frac{dR_\ell (kr_{a\nu})}{dr_{a\nu}^2} + \left[k^2 - \frac{\ell(\ell+1)}{r^2} - \frac{2 m_a m_\nu}{(m_a + m_\nu)\hbar^2} V(r_{a\nu}) \right] R_\ell (kr_{a\nu}) = 0 \quad (70)$$

and $\delta_\ell (k)$ is the asymptotic phase shift for partial wave ℓ and energy k in potential V(r). Appendix I discusses a method for fast numerical evaluation of the integral $\int_0^\infty R_\ell (kr)\, R_\ell (k'r)\, V(r)\, dr$ for the case when V(r) is Morse potential, i.e.,

$$V(r) = D \left[e^{-2\beta (r - R_0)} - 2e^{-\beta (r - R_0)} \right] \quad (71)$$

where D is the well-depth at R_0 and β is the range parameter.

Using the expression for $< \chi'_B \left| e^{-i\underline{q} \cdot \underline{r}_{\nu c}} \right| \chi_B >$ derived in Appendix II, we get the distorted wave cross section σ_{if}^D

$$\sigma_{if}^D = \frac{\mu_t^2}{\hbar^4 k^4 k'^2} 2\pi^2 \sum_\ell \frac{C^2 (j_i\, \ell\, j_f;\, 00)}{(2\ell + 1)} \int_{q_-}^{q_+} q\, dq$$

$$\times \left| \sum_{\ell_1, \ell_2} (-i)^{\ell_1 + \ell_2} \hat{\ell}_1 \hat{\ell}_2 \left(1 + (-)^{i+f+\ell_1} \right) C^2 (\ell_1\, \ell_2\, \ell;\, 00) \right.$$

$$\times \left[(i!)(f!)\, 2^{i+f} \right]^{1/2} \left[\Gamma \left(\ell_1 + \frac{3}{2} \right) \right]^{-1} \sum_{m=0}^{\left[\frac{i}{2}\right]} \sum_{n=0}^{\left[\frac{f}{2}\right]} \left(\frac{-1}{4} \right)^{m+n}$$

$$\left[m!\, (i-2m)!\, n!\, (f-2n)! \right]^{-1}$$

$$\times \Gamma\left(\frac{i + f - 2m - 2n + \ell_1 + 1}{2}\right) \left[e^{-a_1^2/4} \left(\frac{a_1}{2}\right)^{\ell_1} j_{\ell_2}\left(\frac{m_2}{M}\, bq\right) \right.$$

$$\times {}_1F_1\left(\frac{\ell_1 - i - f + 2m + 2n + 2}{2}; \ell_1 + \frac{3}{2}; \frac{a_1^2}{4}\right) G_1(k, k', q)$$

$$+ (-)^{\ell_1 + \ell_2} e^{-a_2^2/4} \left(\frac{a_2}{2}\right)^{\ell_1} j_{\ell_2}\left(\frac{m_1}{M}\, bq\right)$$

$$\left. \times {}_1F_1\left(\frac{\ell_1 - i - f + 2m + 2n + 2}{2}; \ell_1 + \frac{3}{2}; \frac{a_2^2}{4}\right) G_2(k, k', q) \right]^2 \qquad (72)$$

where

$$G_\nu(k, k', q) = \sum_L (2L + 1)\, P_L\left(\frac{k'^2 + k^2 - q^2}{2kk'}\right) \exp\left[i\left(\delta_\ell(k) + \delta_\ell(k')\right)\right]$$

$$\int_0 R_\ell(kr_{a\nu})\, R_\ell(k'r_{a\nu})\, V(r_{a\nu})\, dr_{a\nu} \qquad (73)$$

The computation of cross section using Eq. (70) is being carried out first for atom molecule situation and it is later proposed to extend these computations to molecule-molecule situations.

1.5.3 Conclusion

At present the theory is still at the developing stage. The research will be continued under the support of ARPA and AMICOM in Contract No. DAH01-72-C-0995.

In the future the cross sections for inelastic non-reactive scattering processes will be calculated. The theory will eventually be applied to reactions between HF molecules. Reactions like:

$$HF\ (v = n) + HF\ (v = o) \rightleftarrows HF\ (v = n - 1) + HF\ (v = 1)$$

and

$$HF\ (v = n) + HF\ (v = o) \rightarrow HF\ (v = n - 1) + HF\ (v = o)$$

will be investigated. It is hoped that this work will determine which are the most important deactivation processes in the HF laser. Since (1) these types of reactions have been found to be the most important relaxation processes involved in HF laser system and (2) the measurements on these types of rate constants involving higher vibrational levels are quite difficult, the theory of this kind should be of extreme value in furthering our understanding of the HF laser.

1.6 PULSED HF CHEMICAL LASER GENERATED BY OTHER CHEMICAL REACTION AND/OR INITIATION TECHNIQUES

1.6.1 Motivation

Our theoretical and experimental studies on the performance of the HF laser generated by the flash initiated H_2/F_2 reaction have clearly demonstrated that the HF chemical laser may offer considerable potential for future high power military applications. The laser energy obtained in the H_2/F_2/He mixture; 80 joule/ℓ-atm indeed represents the current state-of-art among all the chemical laser systems known to date. However, here are a few drawbacks that are worth noting:

(1) Due to the reactivity of the H_2/F_2 mixture, the gases cannot be premixed and stored in room temperature containers.

(2) The overall electrical efficiency is seriously limited by the ineffectiveness of converting electrical energy into useful ultraviolet photons for dissociating F_2 to initiate the reaction.

In order to overcome these two problems, two separate approaches were taken:

(1) Other energetic chemical reactions (besides H_2/F_2 or D_2/F_2) were studied. These other reagents are in most cases quite stable and easier to handle or to premix compared to H_2/F_2.

(2) Other techniques that might directly dissociate F_2 molecules without going through the route of generating ultraviolet photons were investigated, namely direct electric discharges or high energy electron beam initiation.

1.6.2 New Possible Chain-Branching Chemical Laser Systems

1.6.2.1 Introduction

Many Soviet laser chemists have proposed "chain-branching" chemical lasers[6] and have claimed successful operation of these lasers.[6] However, only minor efforts have been made by scientists in the United States. Krogh and Pimentel[20] recently reported a study on possible chain-branching (C-B) laser action originating from chemical reactions in a $ClF_3/H_2/Ar$ mixture. Gensel, Kompa and Wanner[21] have also observed C-B laser action from a mixture of IF_5 and H_2. Thus, it is reasonable to reinvestigate these systems and other similar reactions that might lead to the generation of efficient C-B chemical lasers.

From the chemical kinetics point of view, there are several advantages in the performance of a C-B chemical laser:

(1) In the C-B system, the population inversion maximum is only weakly dependent on the initiation energy.

(2) The reaction rate grows exponentially with time.

Advantage (1) would indicate a possible characteristic of high efficiency and advantage (2) would shorten the laser pulse and raise the laser power. For most chemical laser systems studied, the most competitive process reducing laser emission is the relaxation process. A faster chemical reaction would definitely favor a higher percentage of chemical energy converted into laser photons.

In the following section the performance of chemical lasers generated from the reactions between hydrogen and halogen fluorides (such as ClF_3, BrF_5, IF_5, and ClF) are presented. This type of reaction is of extreme interest for many reasons:

(1) It is one of the few systems that might proceed by either a chain or chain-branching (C-B) reaction, which enhances the potentiality of future development as a possible high-power, repetitively pulsed chemical laser.

(2) The overall reaction is very exothermic (as compared with $H_2 + F_2$ system) and capable of producing both vibrationally and rotationally excited species which is desirable as far as the production of the population inversion is concerned.

(3) Despite (1) and (2) described above, the reagents are quite stable as compared to mixtures of H_2/F_2. Although the chemicals will react slowly when mixed the reaction rates are slow enough for a complete mixing in a regular slow flow system. By adding a small amount of inhibitor like O_2, the stability has been further improved.

(4) Being produced by chain or C-B reactions, the output laser energy should not be very sensitive to the initiation energy, which suggests that in principle only a relatively small triggering energy is required for the laser ignition.

Table VI lists the important thermodynamic data, physical and chemical properties of the halogen fluorides that we have studied. Note that all of the chemicals are commercially available and can be stored at room temperature.

TABLE VI

IMPORTANT CHEMICAL AND PHYSICAL PROPERTIES OF XF_n*

Property	ClF_3	BrF_5	IF_5	SF_6	N_2F_4
Melting Point	-76.32°C	-60.5°	9.43°	-50.5°	----
Boiling Point	11.75°	41.30°	100.5°	-63.8°	-73°
Vapor pressure at room temp.	1.65 atm	0.53 atm	10 Torr	20 atm	8 atm
Corrosion on Copper or Steel	very slightly	very slightly	no	no	no
Etching Pyrex or Quartz	no	no	no	no	no
Automatic ignition in H_2 or hydrocarbons	yes	no, but will ignite by a flame	no	no	no

*Information obtained from Halogen Chemistry, Edited by V. Gutmann, Academic Press, 1967.

1.6.2.2 Reaction Scheme

Following the flash photolysis, the possible reactions involved in the mixture of H_2 and ClF_3 can be postulated as:

$$ClF_3 + h\nu \rightarrow ClF_2 + F \qquad \Delta H = 60 \text{ kcal/mole} \qquad (74a)$$

$$\rightarrow ClF + 2F \qquad \Delta H = 64 \qquad (74b)$$

$$\rightarrow ClF + F_2 \qquad \Delta H = 26 \qquad (74c)$$

$$\rightarrow F_2 + Cl + F \qquad \Delta H = 85 \qquad (74d)$$

ClF_3 absorbs strongly at wavelengths beyond 2600 Å, and quanta of this wavelength carry 110 kcal/mole of energy; thus dissociation of ClF_3 could proceed by any of the above mentioned reactions. The fact that HF laser action was observed indicates that reaction (74c) is not important. Besides reaction (74c), all the other reactions lead to the production of one or two F-atoms. Subsequent photolysis of ClF, of ClF_2 and of F_2 is also possible.

The fluorine atoms will initiate the pumping reactions, which produce H-atoms and introduce the reaction chain sequence:

$$F + H_2 \rightarrow HF + H \qquad \Delta H = -31.6 \text{ kcal/mole} \qquad (75)$$

$$H + ClF_3 \rightarrow HF + ClF_2 \qquad \Delta H = -76 \qquad (76a)$$

$$\rightarrow HF + ClF + F \qquad \Delta H = -72 \qquad (76b)$$

$$\rightarrow HF + Cl + 2F \qquad \Delta H = -12 \qquad (76c)$$

$$\rightarrow HF + Cl + F_2 \qquad \Delta H = -50 \qquad (76d)$$

$$\rightarrow HCl + F_2 + F \qquad \Delta H = -17 \qquad (76e)$$

$$\rightarrow HCl + 3F \qquad \Delta H = +20 \qquad (76f)$$

Except for reactions (76e) and (76f), which generate only new F-atoms, all the other reactions (76) proceed by generating both vibrationally excited HF molecules and new F-atoms, Cl-atoms, and radicals. Atoms will continue their reaction with H_2 by either (75) or

$$ClF_2 + H_2 \rightarrow HCl + H \qquad \Delta H = +1 \text{ kcal/mole} \qquad (77)$$

Although reaction (77) is thermoneutral, it will produce an additional H-atom for reaction (76)'s. The ClF_2 radical will probably react with H_2 by

$$ClF_2 + H_2 \rightarrow HF + ClF + H \qquad \Delta H = -28 \text{ kcal/mole} \qquad (78a)$$

$$\rightarrow 2\,HF + Cl \qquad \Delta H = -66 \qquad (78b)$$

$$\rightarrow HF + HCl + F \qquad \Delta H = -32 \qquad (78c)$$

Again, in either reaction (78) both vibrationally excited HF molecules and new atoms will be generated and recycled. The reaction between ClF_2 radical and H would add more F-atoms by processes;

$$H + ClF_2 \rightarrow HF + ClF \qquad \Delta H = -132 \text{ kcal/mole} \qquad (79a)$$

$$\rightarrow HF + Cl + F \qquad \Delta H = -72 \qquad (79b)$$

$$\rightarrow HCl + F_2 \qquad \Delta H = -77 \qquad (79c)$$

$$\rightarrow HCl + 2F \qquad \Delta H = -39 \qquad (79d)$$

Of course, ClF would also react with H by

$$H + ClF \rightarrow HF + Cl \qquad \Delta H = -43.4 \text{ kcal/mole} \qquad (80a)$$

$$\rightarrow HCl + F \qquad \Delta H = -75.9 \qquad (80b)$$

and liberate new atoms.

As one can clearly see, the production of vibrationally excited HF and HCl molecules can be very efficient and chain propagation may occur much faster than that of the H_2/F_2 system if reactions (76) proceed with a reasonable rate (as compared with reaction (75), which we know is fast). And as Professor Pimentel pointed out, insofar as reactions (76), (78) or (79) are concerned, they contribute constructive chain-branching.

1.6.2.3 Experiment and Results

The same apparatus (see Fig. 1) and operational procedures identical to that used in H_2/F_2 system were employed. The halogen fluorides, ClF_3, BrF_5, IF_5, or ClF were used in place of F_2. Measurements of the laser output energy were made with the Avco calorimeter and the laser duration or pulse shapes were monitored with an InSb PEM detector viewing scattered radiation from the calorimeter surface. Figure 41 shows a typical oscillogram of a laser pulse observed in a H_2/ClF_3 mixture. The total gas pressure was 1.1 atmospheres with 4% H_2, 4% ClF_3 and 92% He. The laser pulse duration is about 1μsec and the output energy is over 1 joule. The mixture of H_2/IF_7 was found to be extremely stable. It could be premixed and flashed many times to get laser pulses. Figure 42 shows the laser pulse observed in a H_2/ClF mixture. The total gas pressure is also 1.1 atmospheres with 4% H_2, 4% ClF and 92% He. The laser duration is about 10μsec and the output energy is over .7 joule. Table VII lists the output

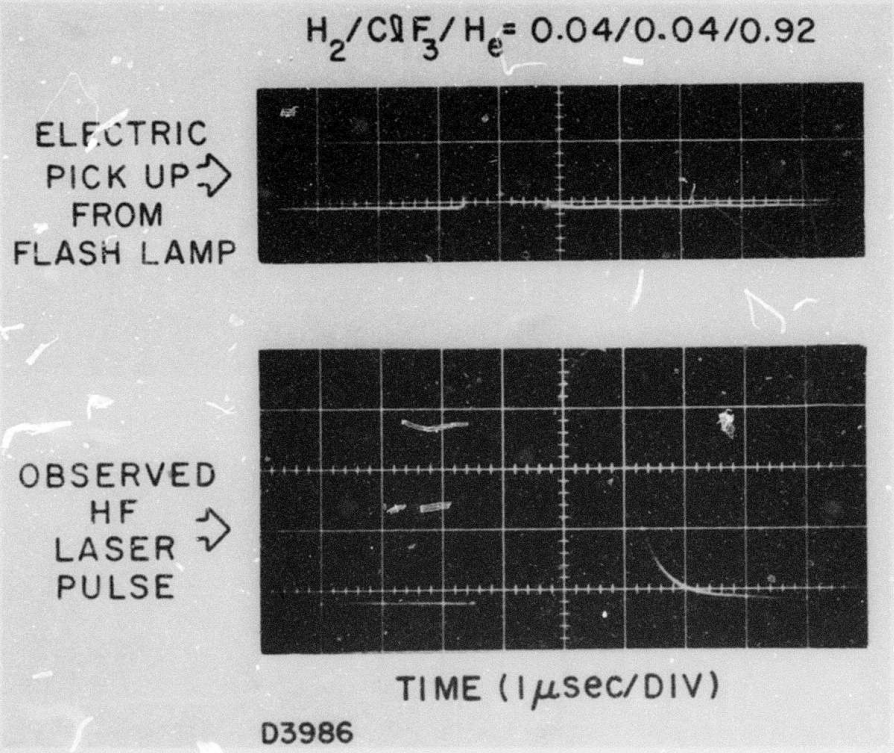

Fig. 41 Oscillogram of the Laser Pulse Observed in $H_2/Cl F_3$ Mixture

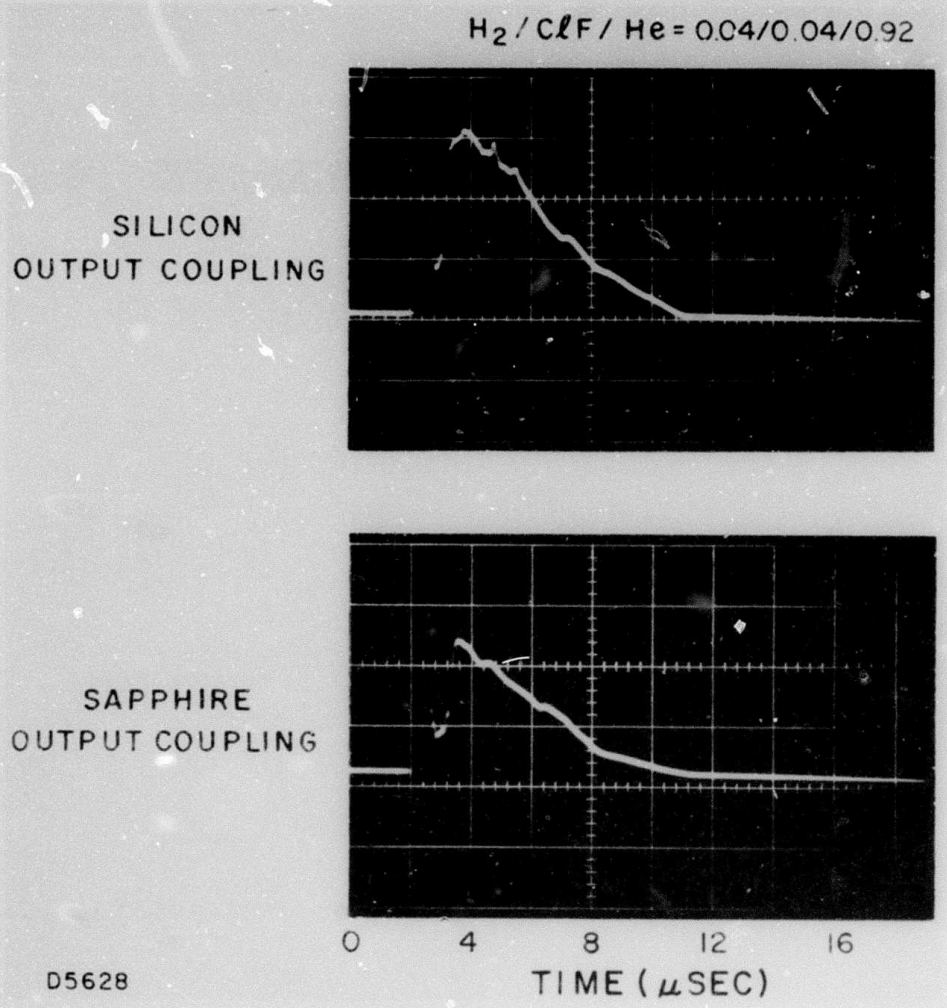

Fig. 42 Oscillogram of the Laser Pulse Observed in H_2/Cl F Mixture

TABLE VII

HF CHEMICAL LASERS GENERATED BY REACTIONS OTHER THAN THE $H_2 + F_2$ SYSTEM

	Output Energy	Duration
1) $H_2 + ClF_3$	1 joule	~ 1 μsec
2) $H_2 + BrF_3$	0.3 joule	~ 1 μsec
3) $H_2 + ClF$	0.7 joule (both HCl and HF lase)	~ 10 μsec
4) $H_2 + BrF_5$	0.5 joule	~ 1 μsec
5) $H_2 + IF_5$	0.5 joule	~ 1 μsec

energies and pulse durations observed in various H_2/halogen fluoride/He mixtures studied. These results compare favorably with our early experiments on the H_2/F_2 system, and the relatively high energy obtained also suggests that these reactions may operate on a chain mechanism. Future HF laser development based on these reactions is potentially feasible.

1.6.3 Pulsed HF Chemical Laser Initiated by an Electric Discharge

1.6.3.1 Introduction

Although the electron-pin discharge technique could not be used to volumetrically initiate chemical reactions, it is relatively simple and easy to construct. The object of this experiment was to evaluate the efficiency of electrical initiation of H_2/F_2 mixtures to produce laser action. It was hoped that enough information could be obtained so that the overall electrical efficiency can be derived.

1.6.3.2 Experimental

The gas mixing technique and optical cavity used is identical with that used in the flash-lamp-initiated H_2/F_2 laser experiment. The two Xe flash lamps were replaced by two pin-discharge teflon cavities. Each cavity contains 90 1 kV resistors located within a 15 mm x 250 mm rectangular cross section. An 8 mm diameter brass bar was used as an anode. The high voltage power supply and pulsing unit originally used for Avco N_2 laser (which puts out 100 nsec pulses) were used to drive and trigger the electric discharge. Single 0.012μf capacitors or a pair of 0.012μf capacitors coupled in series were used for varying the discharge energy. The laser output energies were measured with an Avco energy meter, and the pulse shape was monitored by an InSb PEM detector.

1.6.3.3 Results

Measurement of both laser output energy and pulse shape on various H_2/F_2/He mixtures were performed under two experimental conditions:

(1) The electric input energies were varied by changing the discharge voltage across the capacitor.

(2) The electric input energies were varied by changing the capacitance at a fixed charging voltage.

Figure 43 shows a plot of the laser output energy versus capacitor charging voltage observed in a 0.08/0.08/0.84 He mixture. It is clearly demonstrated that the relation between the electric input energy and laser output energy is not linear. By decreasing the capacitance from 0.012μf to 0.006μf, at a charging voltage of 10 kV, the laser output energy was found to drop only slightly as indicated in the figure. Figure 44 shows a typical HF laser pulse observed in the mixture of H_2/F_2/He = 0.04/0.04/0.92. The charging voltage was 17.5 kV and capacitance was 0.012μf. An output energy of 0.13 joule was observed.

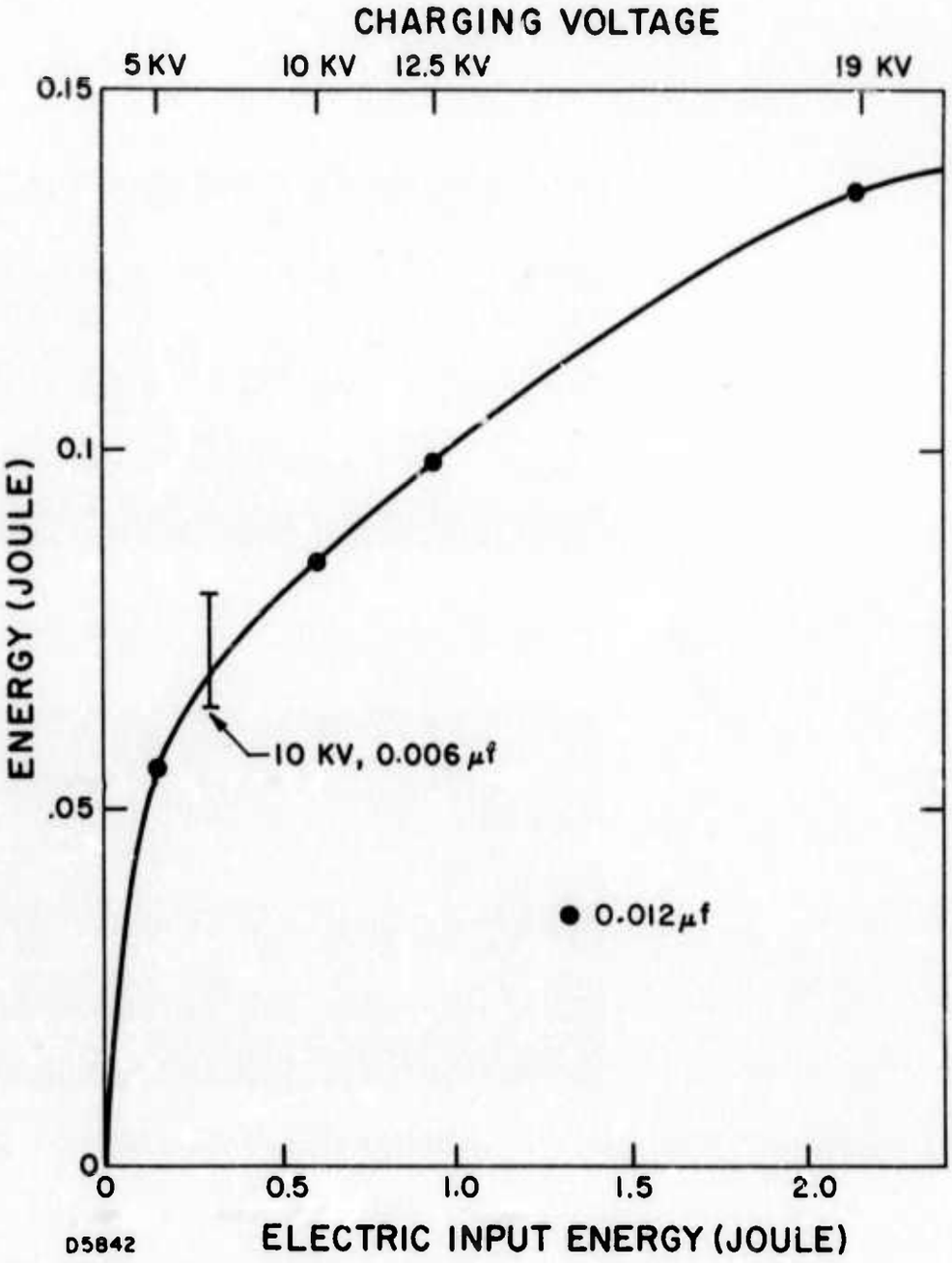

Fig. 43 The Measured Laser Output Energy Versus Capacitor Voltage Observed in the $H_2/F_2/He$ = 0.08/0.08/0.94 Mixture

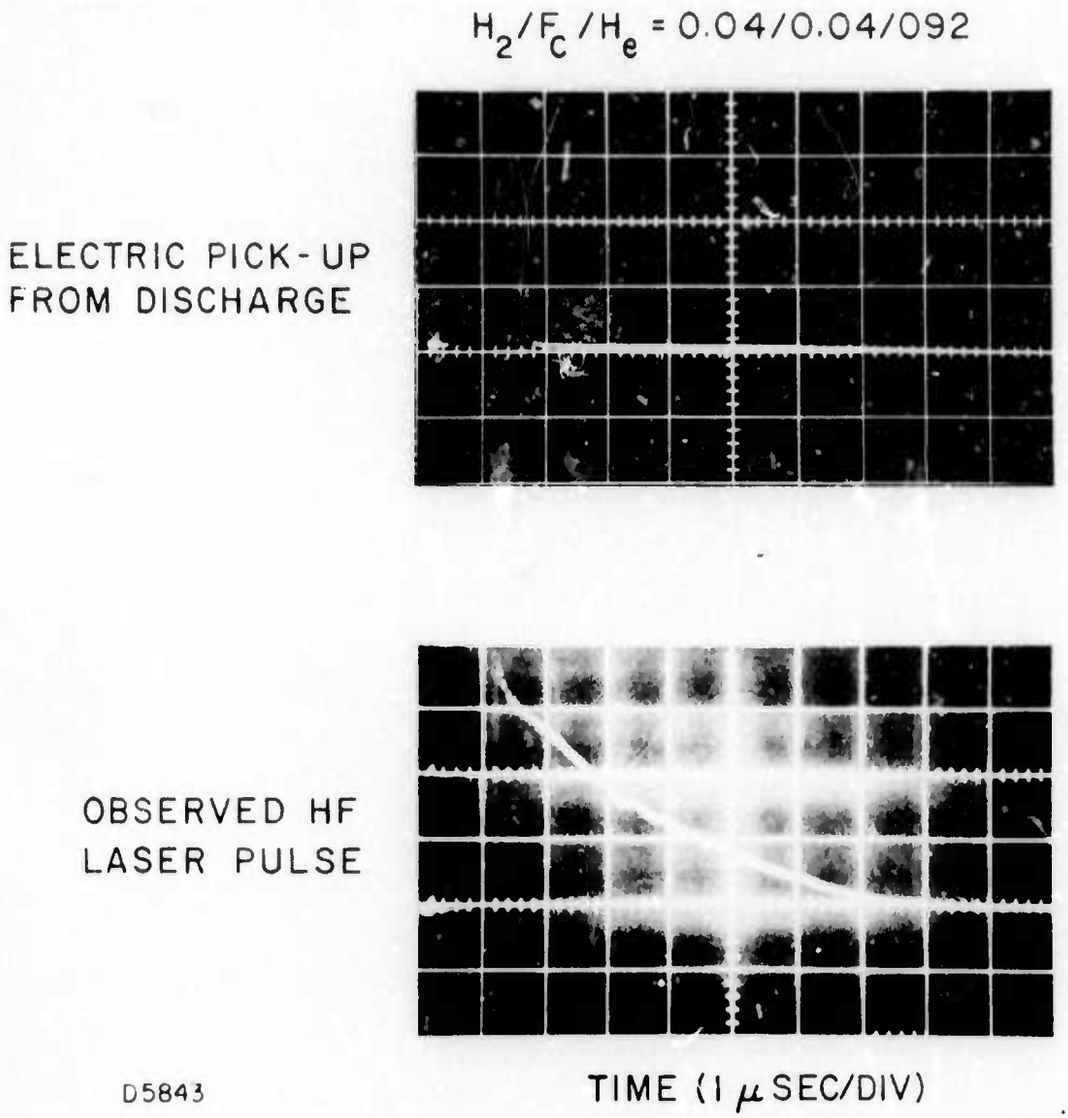

Fig. 44 Oscillogram of the HF Laser Pulse Observed in the H_2/F_2/He Mixture Initiated by the Electric Discharge

1.6.3.4 On the Overall Electrical Efficiency

In order to evaluate the total electronic-to-laser energy efficiency, the exact amount of electric energy that was deposited into the gas mixture has to be carefully calculated. Let R_t = total resistance, R_g = resistance across the gas mixture, R_r = resistance across resistor, C = capacitance, V = charging voltage, E_{input} = total electric input energy, E_r = total energy deposited in resistors, E_{gas} = total energy deposited in gas and I (t) = transient current. Then

$$R_r = \frac{10^3}{180} = 5.56 \text{ ohm} \tag{81}$$

$$R_t = R_r + R_g(t) \tag{82}$$

$$E_r = \int_o^t [I(t)]^2 R_r \, dt \tag{83}$$

where transient current is assumed to be $I(t) = I_o \exp(-t/R_tC)$.

$$E_r = I_o^2 R_r \int_o^\infty \exp(-2t/R_tC) \, dt \tag{84}$$

Since R_t is also a function of t and it is not clear what is the formulation of R_g, the exact integration is difficult. However, if $R_r \gg R_g$, one can approximate $R_t \approx R_r$ then

$$E_r = I_o^2 R_r \frac{R_tC}{2} \tag{85}$$

$$= \frac{1}{2} CV^2 \left(\frac{R_r}{R_t}\right) \tag{86}$$

$$= E_{input} \frac{1}{1 + (R_g/R_r)} \tag{87}$$

If $R_g \ll R_r$, $E_r \approx E_{input}$.

Unfortunately, due to the shortage of time, the exact value of R_t or R_g was not accurately measured. If one assumes that $R_g \ll R_r$, the lower limit on the overall electrical efficiency for a 5 kV discharge is

$$\frac{\text{Laser output energy}}{\text{Electrical input energy}} = \frac{56 \text{ mjoule}}{150 \text{ mjoule}} = 40\%$$

where most of the electrical energy was deposited in the resistors and not the gas.

If one assumes that $R_g \approx R_r$, the ratio of

$$\frac{\text{Laser output energy}}{\text{Energy deposited in gas}} = \frac{\text{Laser output energy}}{E_{input}/2} = 80\%$$

Another emperical factor that is important but cannot be accurately measured is the active discharging volume of gas. If one assumes that the discharge does not disperse too far in a 2 cm distance, an active excitation volume of 3 cm^3 is obtained. Thus the output energy is 0.14 joule/3 cm^3 $\approx$50 joules/ℓ in the mixtures of $H_2/F_2/He$ = 8%/8%/84%. The technique of electric discharge does look more efficient than flash lamp initiation of HF chemical lasers.

1.6.4 Monoenergetic Electron Beam Dissociation of Fluorine

1.6.4.1 Introduction

Initiation of chemical laser action by a electron beam has been reported by Gregg, et al.[22] Since no values of laser pulse energy were quoted by these workers, it is impossible to estimate how efficient the electron beam is as an initiation source, other than qualitatively it appeared better than flash lamp initiation. Gregg, et al., used fluorine containing compounds (N_2F_4, NF_3) as their source of fluorine atoms, and it is not known whether a chain or single step reaction resulted from the initiation. Mixtures of fluorine and hydrogen do combine to form HF in a chain reaction and, therefore, require less initiation energy to go to completion than a simple, one step reaction. Laser action from F_2/H_2 mixtures has been previously demonstrated.[23]

In this study, a high energy electron beam was injected into a gaseous mixture of F_2, He, CO_2, and HCl. Particular attention was focused on the determination of the number of fluorine atoms produced by means of a chemical titration. The measurement of the fluorine atom concentration was preferred to a measurement of laser pulse energy, simply due to the fact that the latter depends on cavity coupling and mode volume as well as the reaction rate of the atoms produced, and, therefore, is less direct. Previous detailed studies on the efficiency and mechanism of HF and HCl chemical lasers[24, 25] have been frequently hampered by the uncertainty of

the atom concentration involved in the initiation step. The quantitative measurement of fluorine atom concentration produced by high energy electrons reported here should be important to the further development of laser science and technology.

1.6.4.2 Experimental

The goal of this experiment was to use a high energy electron beam to dissociate F_2 and then to quantitatively measure the F-atoms produced. From a knowledge of the energy deposition of the electron beam in the gas, the energy necessary to produce an F-atom can then be determined. Since the amount of F_2 dissociation produced was expected to be small, e.g., of the order of a percent or so, a sensitive and direct measurement of the F-atom concentration was desired. It was decided to use a chemical titration technique based on the known fast reaction

$$F + HCl \rightarrow HF + Cl \qquad (88)$$

The product HF produced in this reaction could be quantitatively measured in absorption via a probe HF laser. However, since F_2 and HCl react spontaneously, but slowly, a flow system to mix the reagents and flow them rapidly into the reaction chamber must be employed. Such a flow system,[26] constructed for experiments involving mixtures of H_2 and F_2 to investigate laser action, was already available at AERL. It was decided to employ this mixing system and couple it to an existing electron beam device available from Simulation Physics, Inc. (SPI). This particular electron gun had several advantages: (1) it was available and easily transportable to the experiment since it employs a dry dielectric energy storage system; (2) the size and dimensions of the emitting surface were reasonably compatible with the flow system geometry; (3) the gun was of the plasma diode type, producing a high current density to maximize the dissociation of F-atoms; and (4) SPI had suitable calibration techniques and calculation procedures available to determine the energy deposition of the electron beam in the gas. Although this combination of existing flow system and electron gun seemed the most expeditious and feasible approach and did result in experimental data, it will be obvious that a more optimum mating of E-beam and gas mixture could have been achieved.

A schematic of the experimental apparatus is shown in Fig. 45. The fluorine and hydrogen chloride are premixed with He diluent in separate storage tanks. Both storage tanks are pressurized well above one atmosphere. The remainder of the flow system is pressurized to about 1 atm with the diluent. During a run, fast acting valves open to admit the gases to a mixing manifold which distributes the gases in alternate sheets of F_2 and HCl about 2 mm thick. The gases mix as they flow through the mixing region, the residence time being typically 20 milliseconds. The mixed gases then pass into the interaction chamber, where the electron beam is fired transverse to the direction of the gas flow. The spent gas exhausts through traps for removing the HF. The probe HF laser enters the interaction chamber transverse to

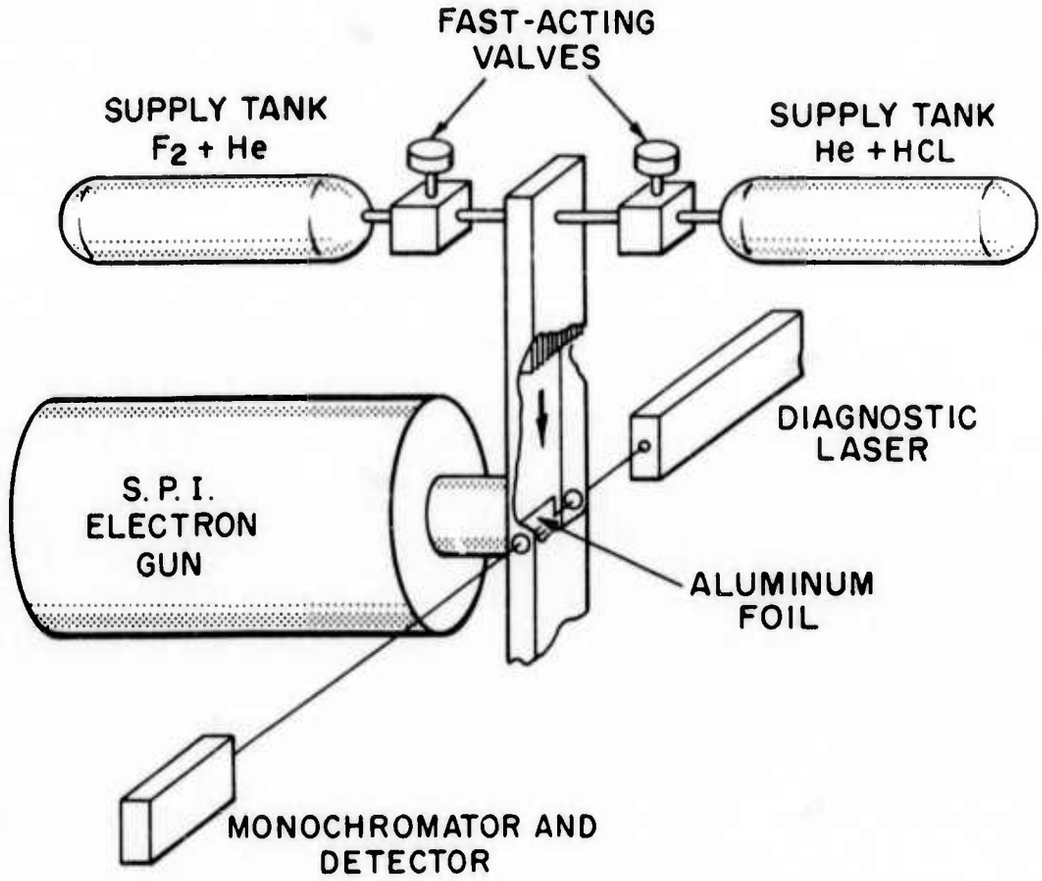

D3480

Fig. 45 Schematic of Fluorine Dissociation Experiment.

both the direction of the electron beam and the gas flow. A particular vibration/rotation transition of HF is selected by a monochromator and measured with an infrared detector.

The electrons were produced by a SPI electron beam generator, capable of producing electrons with a beam energy ranging from 20 to 140 keV, and a current density at the anode from 100 to 600 amperes/cm^2. Pulse widths of the electron beam were typically 250 nanoseconds. Figure 46 shows an actual photograph of the SPI-PULSE 2500 electron beam generator used in this experiment. Figure 47 shows the details of the working section of the gun and its mating to the interaction chamber. The electron gun consists of a DC charged, low impedance, coaxial structure which is switched into a field/plasma emission tube via a triggered gas gap. The 1 ohm, 15,000 pf coaxial energy storage has a characteristic transit time of 30 nanoseconds. Charged to 250 kilovolts by an electrostatic generator, the system stores approximately 450 joules. After about one minute charging, a command pulse initiates the discharge of the line into the field emission tube. Electrons emitted from the cathode fall through the instantaneous cathode-anode potential difference, strike and pass through the transmission anode, composed of a 0.0005" thick aluminum foil and tungsten wire supporting screen, and into the experimental chamber. The diode operates at a pressure of 10^{-5} torr while the gas channel contains the gas mixture at 760 torr. After passing through the aluminum foil window, the electron beam drifted through a 4 cm long × 1 cm wide "neck" into the 5 cm wide interaction chamber. The dimensions of the emitter, the transmission anode, and "neck" were all 1 × 10 cm.

To diagnose the electron beam character during each discharge of the generator, both diode current and voltage were monitored. The diode current monitor is a low inductance resistive belt which is placed circumferentially at the cathode-anode gap in the wall of the diode (see Fig. 47). The voltage monitor is a capacitive divider formed by a metal band and the wall of the diode (see Fig. 47). The voltage monitored is that of the cathode shank. Inductive corrections to this signal are also made. Typical diode current and voltage data are shown in Fig. 51.

In addition to diode current and voltage, separate experiments were performed to assess analytical techniques used to determine the degree of ionization created in the neck. These experiments consisted of measuring current transmitted through the neck and the energy per gram or dose created by the electrons in a dosimeter also at the back of the neck. The transmitted current was measured using a Faraday cup. The dose measurement was made with blue cellophane dosimetry. A typical transmitted current measurement is also shown in Fig. 51. Figure 52 is a blue cellophane map of the current density distribution as determined from a calibration against dose at the back of the neck, which clearly indicates the uniformity of the electron beam that the SPI-PULSE machine produced.

For monitoring the quantity of hydrogen fluoride produced through the rapid reaction (88), the absorption of the $1P_4$ transition of a HF pulsed laser was measured. The probe HF laser was an Avco C950 nitrogen laser,

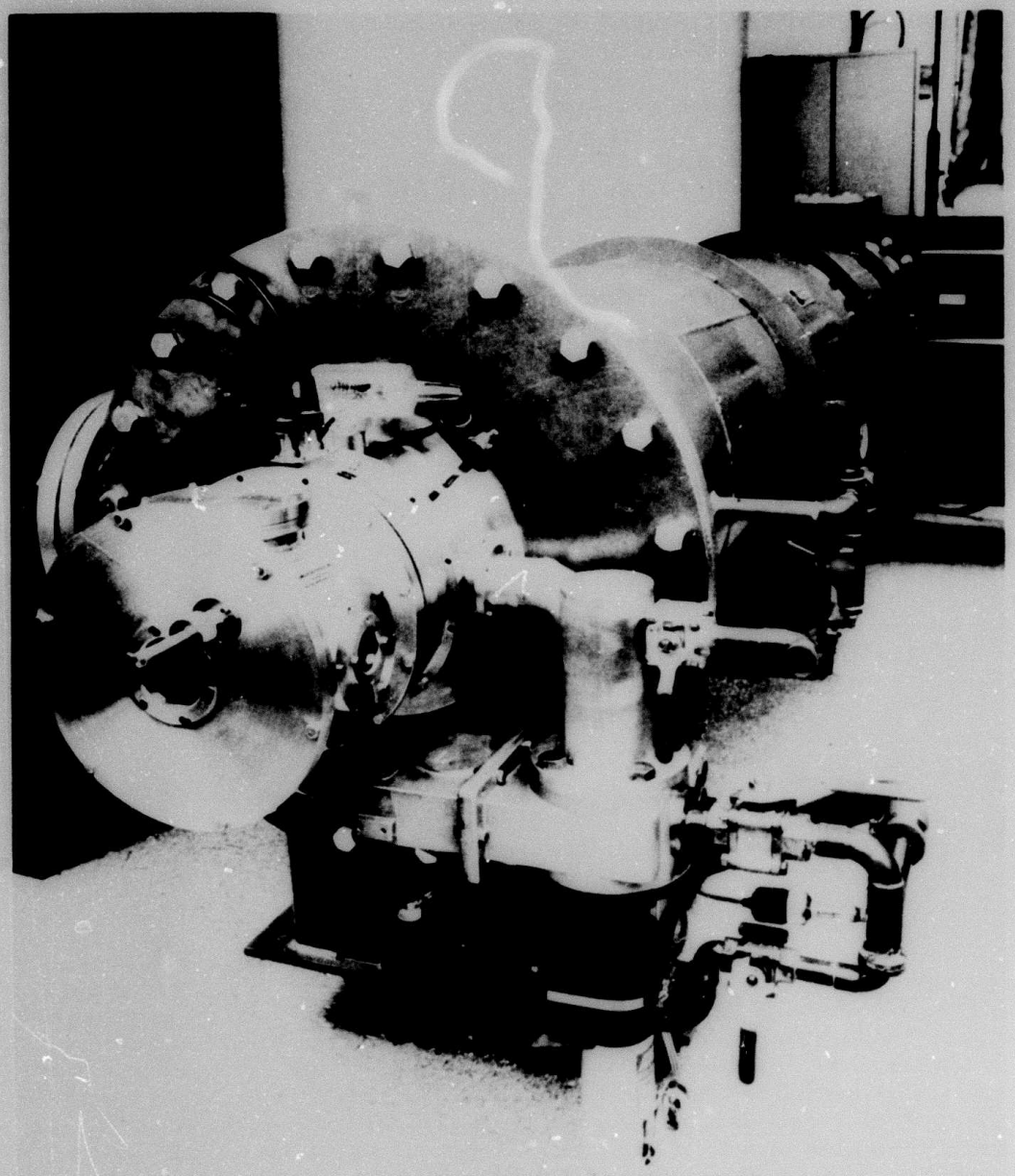

D4593

Fig. 46 SPI PULSE™ Model 2500 Electron Beam Generator

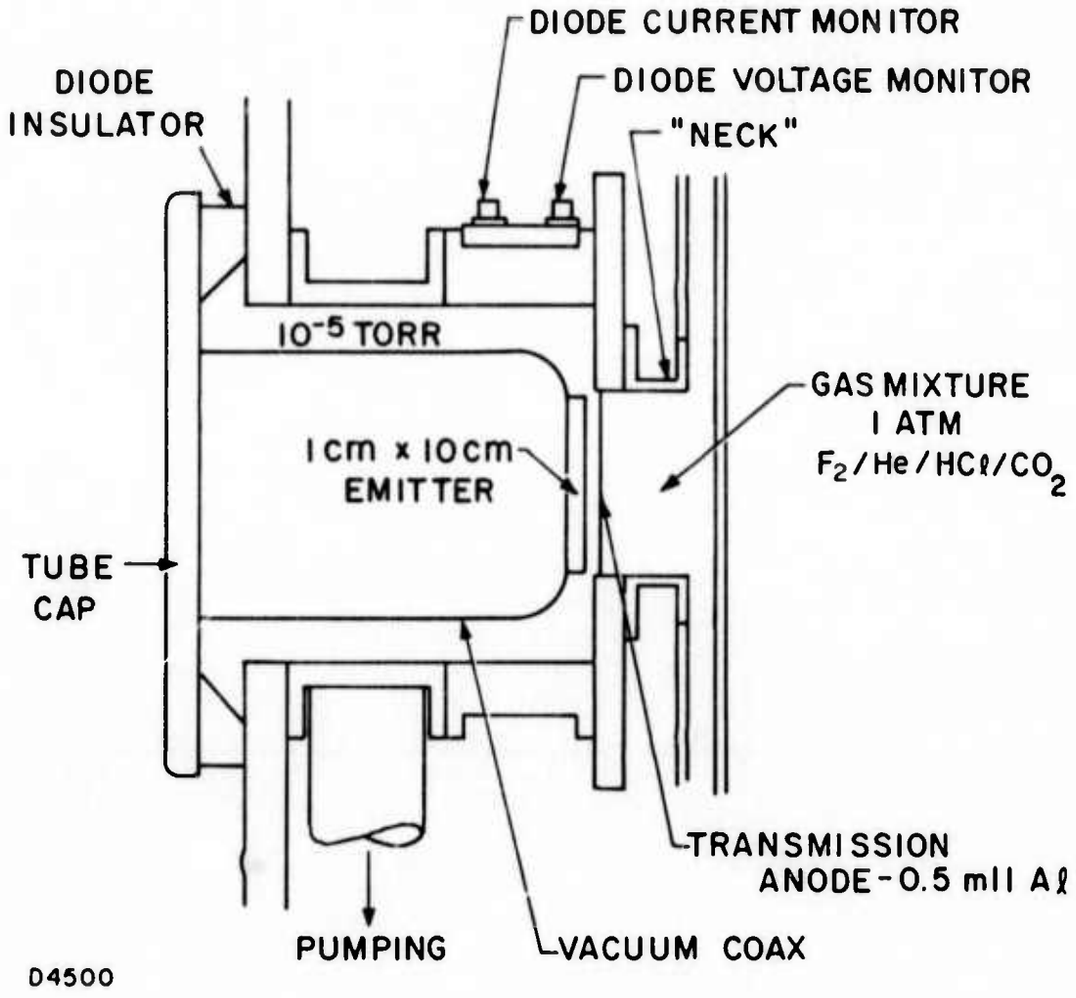

Fig. 47 Experimental Geometry for Gas Excitation Experiment.

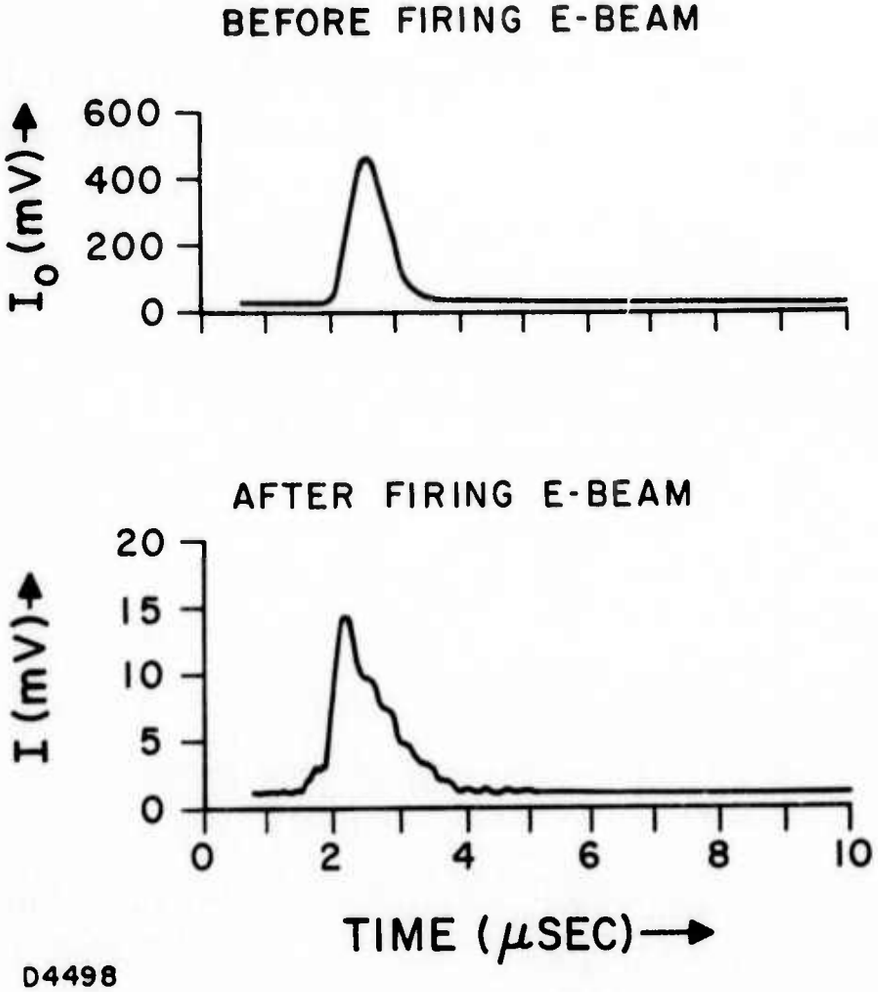

Fig. 48 Typical $1P_4$ Laser Pulses, Monitored by a Ge Au Photoconductor. The upper trace is the intensity of $1P_4$ line before the HF absorption. The lower trace is the intensity of that after the IR absorption of HF. The optical pathlength is 10 cm. A ratio of $I/i_o = 0.03$ is observed which represents a partial pressure of 0.06 torr of HF in the mixture studied. The charging voltage was 100 kV. The gaseous composition was 4% F_2, 1% HCl, 1% CO_2 and 94% He at a total pressure of 800 torr.

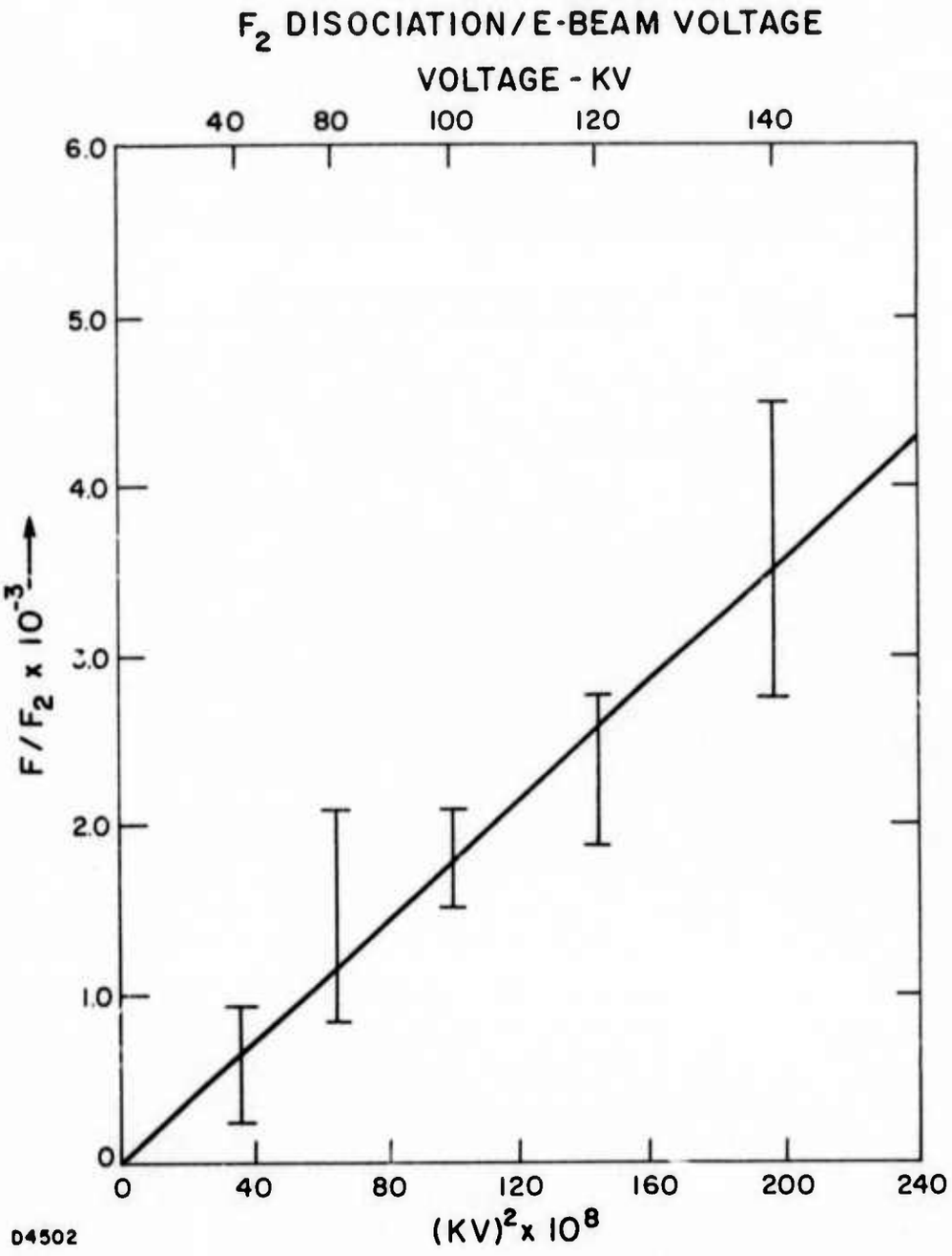

Fig. 49 The Experimentally Determined F/F_2 Ratio for Various Electron Beam Discharging Voltages. The gaseous composition was 4% of F_2, 1% HCl, 1% CO_2 and 94% He at a total pressure of 800 torr.

modified to operate on SF_6 and H_2 to produce HF laser pulses. Figure 48 shows typical $1P_4$ laser pulses, monitored by a GeAu detector through a 0.5-meter Jarrel Ash monochromator, showing the absorption of the HF molecules in the interaction chamber before and after firing the E-beam. Due to the possible mismatch between the line center of IR absorption and laser emission, the absorption coefficient of the $1P_4$ line of HF was calibrated against the actual absorption of a known HF/He mixture in a separate experiment. Figure 51 shows the measured F/F_2 ratio as determined from the $1P_4$ absorption for various electron beam discharge voltages. The scatter in F/F_2 ratio observed is caused mainly by fluctuations in power of the $1P_4$ probe laser transition from shot to shot.

A diagram illustrating the overall sequence of timing and triggering is shown in Fig. 50. Initially the fast acting valves are opened and the gases begin to flow. Approximately 100 msec later the mixed gases are entering the interaction chamber. The electron gun is fired at about 200 msec after the valves opened; about 150μsec later the probe HF laser is fired. This latter period is needed to assure that the HF, produced vibrationally excited by reaction (88), has relaxed. This point is discussed further in the next section. During this 150 msec the gas in the interaction chamber has moved only 1-2 mm, so that for all purposes the gas sampled by the E-beam and laser probe are identical.

1.6.4.3 Dissociation and Analysis Scheme

A primary high energy electron incident upon a gas molecule may lose energy in three ways: ionization, excitation, and dissociation of the target molecule. The debris produced by a high energy electron beam then consists of a swarm of electrons and ions, together with excited molecules and molecular fragments. Since our gas is mainly helium, presumably most of the impacts will lead to the ionization and/or excitation of helium atoms, i.e.,

$$e_p + He \rightarrow He^+ + e_p + e_s \qquad (89)$$

$$\rightarrow He^* + e_p \qquad (90)$$

where e_p and e_s are the primary and secondary electrons, respectively, and He^* stands for electronically excited species, which could be any of the ($2\,^3S$, $2\,^1S$, $2\,^1P$, $2\,^3P$) states. Landshoff and Magee[27] have shown that, in the case of air, the primary electron mainly undergoes ionizing collisions, rather than dissociative collisions, resulting in secondary electrons with approximately 22 eV energy. A 90 keV primary electron would be capable of producing 4×10^3 secondary electrons, which clearly indicates that the number of secondary electrons must be 10^3 times that of the primary electrons. Thus for the F_2/He mixtures studied, dissociation of F_2 will probably be caused mainly by the secondary electrons. The processes which could lead to the ionization and/or dissociation of the F_2 molecule during the electron-molecule collisions are

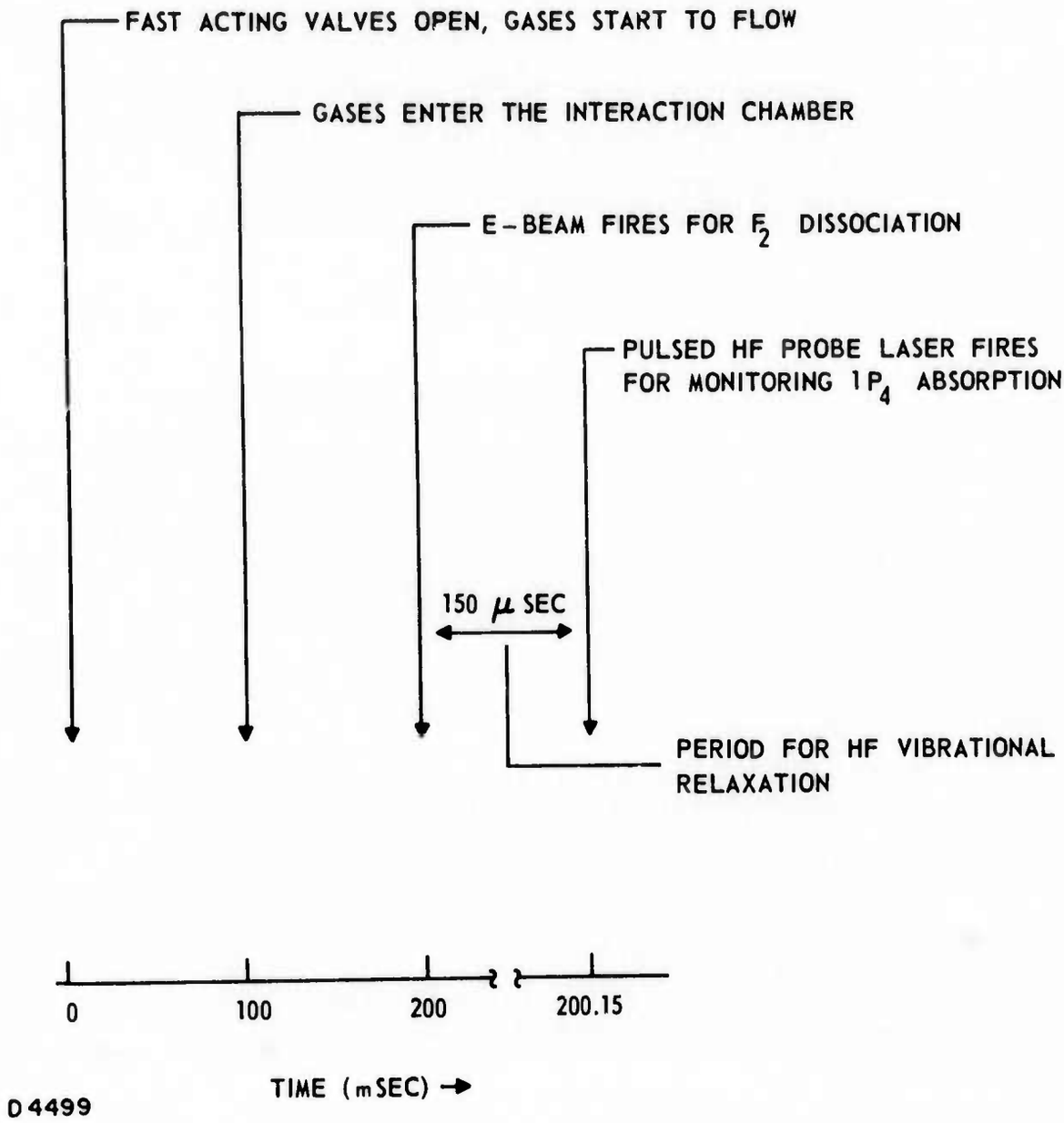

Fig. 50 Schematics of Overall Experimental Timing and Triggering.

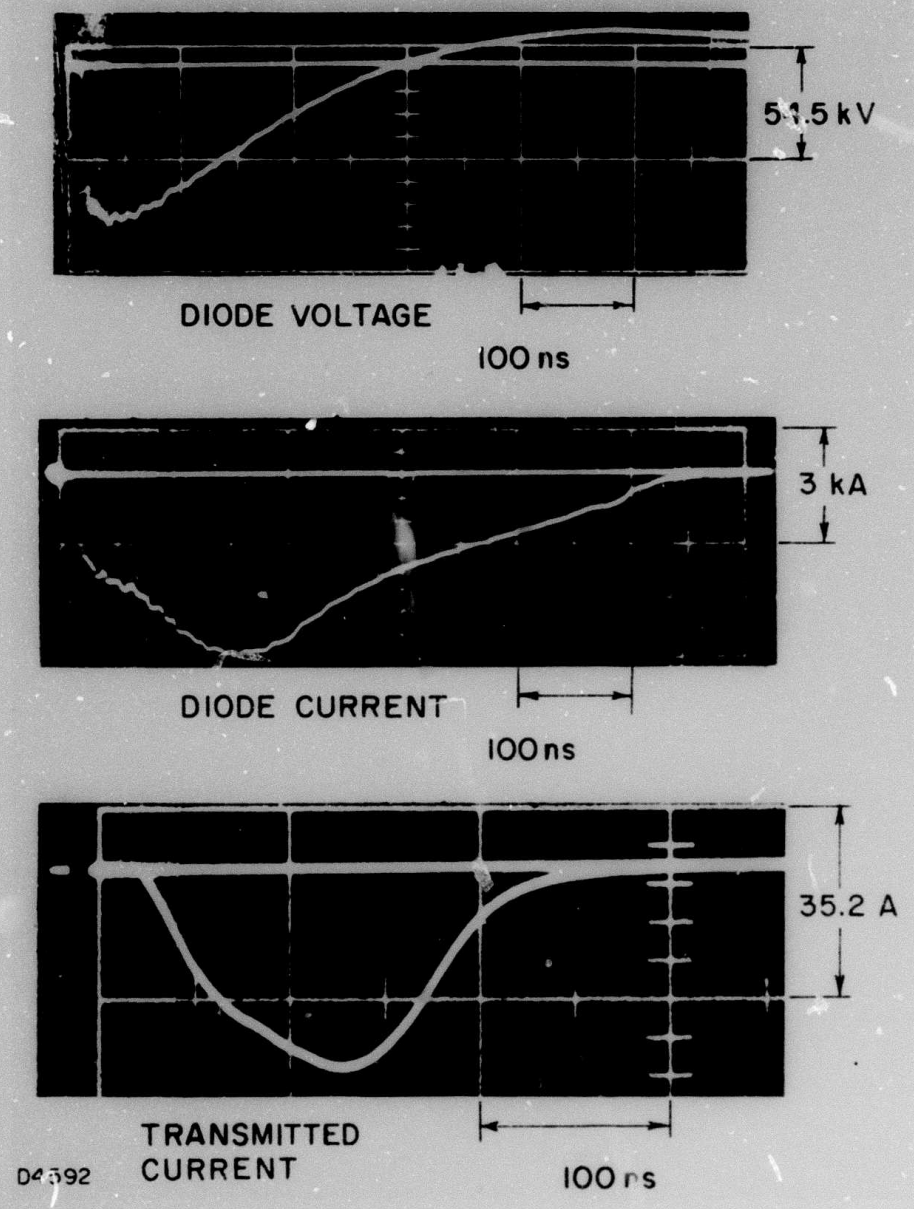

Fig. 51 Representative Diode Current, Voltage and Transmitted Current Data. The charging voltage was 120 kV and cathode area is 1 cm x 10 cm.

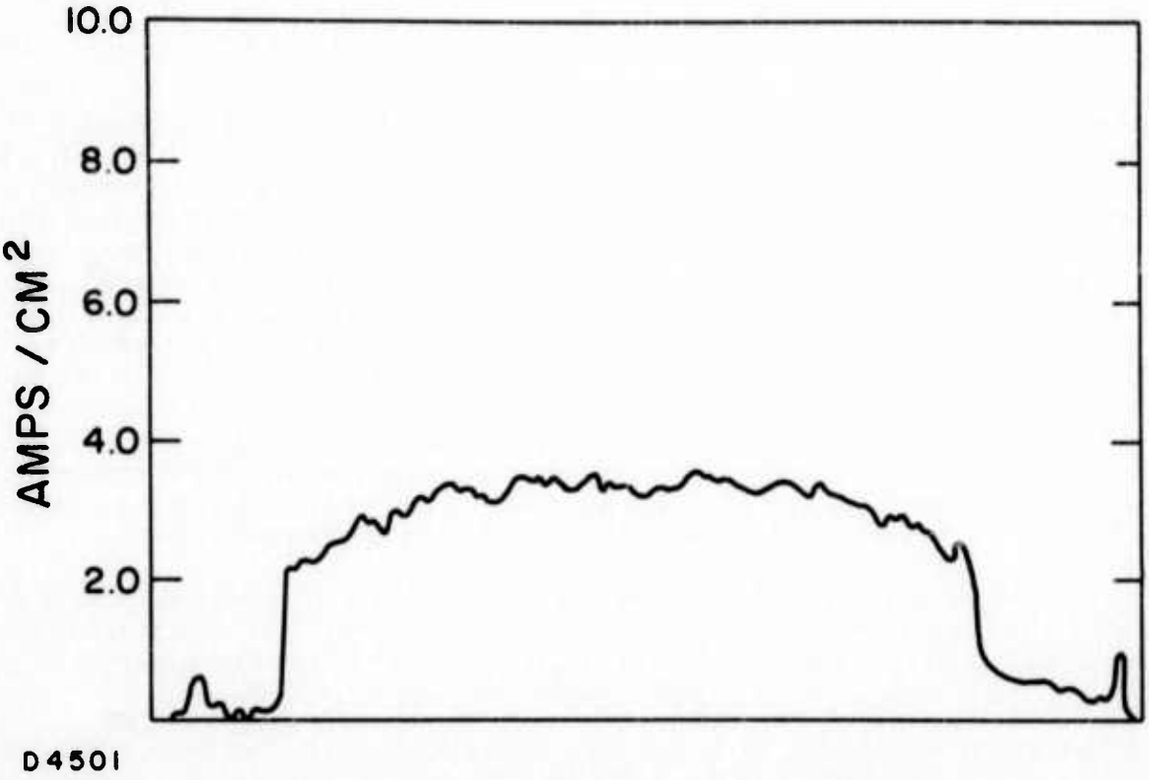

Fig. 52 Current Density Distribution Behind Gas Channel. The charging voltage is 120 kV, and cathode area is 1 cm x 10 cm.

$$F_2 + e \rightarrow F_2^{-*} \rightarrow F + F^- \qquad A_0 = -1.9 \text{ eV} \qquad (91)$$

$$\rightarrow F_2^+ + 2e \qquad A_0 = 16.6 \text{ eV} \qquad (92)$$

$$\rightarrow F^+ + F + 2e \qquad A_0 = 19.0 \text{ eV} \qquad (93)$$

$$\rightarrow F^+ + F^- + e \qquad A_0 = 15.4 \text{ eV} \qquad (94)$$

$$\rightarrow 2F + e \qquad A_0 = 1.5 \text{ eV} \qquad (95)$$

where A_0 is the minimum energy required for the forward reaction, i.e., the minimum energy that would have to be supplied by the colliding electrons. For processes (92), (93) and (94), impacts with electrons of moderate energy are required. For processes (89) and (95), collisions with electrons of only low energy are necessary. Since process (91) is 1.9 eV exothermic and requires small (or no) activation energy, it is expected to be relatively fast. Using a shock tube technique, Mandl[28] has measured the associative detachment rate for the reaction $F + F^- \rightarrow F_2 + e - 1.9$ eV, i.e., the reverse of (91). A rate constant of 10^{-12} cm^3 sec^{-1} at 4000°K was observed. The reaction rate estimated from Mandl's data for reaction (91) at room temperature indicates that reaction (91) must be fast and has a cross section of the order of 10^{-15} cm^2. Fox[29] and coworkers have actually measured the cross section for dissociative electron attachment of the I_2 molecule. A value of 3×10^{-15} cm^2 was observed, comparable to our estimate for reaction (91).

Processes like charge transfer or Penning ionization from He could also be of importance for F_2 dissociation, since for every secondary electron liberated from helium there is also an accompanying ion.

$$He^+ + F_2 \rightarrow F_2^+ + He \qquad A_0 = -8.0 \text{ eV} \qquad (96)$$

$$He^* + F_2 \rightarrow F_2^+ + He + e \qquad A_0 = -3.1 \text{ eV} \qquad (97)$$

$$He^* + F_2 \rightarrow F_2^* \rightarrow 2F + He \qquad A_0 = -18.2 \text{ eV} \qquad (98)$$

Here, He^* stands for metastable Helium atom. The reaction of ionic recombination or neutralization,

$$F_2^+ + F^- \rightarrow F + F + F \qquad (99)$$

could generate additional fluorine atoms. It is rather unfortunate that none of these reactions have been studied. At the present stage, we can only suspect that reactions (91), (92) and (99) are most likely the important processes involved in making F-atoms via high energy electron bombardment of F_2.

The reaction between an F-atom and an HCl molecule has been thoroughly studied by many investigators. A recent report by Kompa and Wanner[30] has indicated that the reaction

$$F + HCl \rightarrow HF + Cl \qquad (88)$$

is fast and possesses a rate constant of 1.5×10^{13} cm^3 mole^{-1} sec^{-1} at 300°K. Thus for gaseous mixtures that we have studied, the titration reaction should take only a few hundred nsec to reach completion. Furthermore, the recombination of F-atoms is too slow and unimportant under our conditions.

For a quantitative and accurate measurement of the concentration of F-atoms originating from the electron beam dissociation, any side reactions that might lead to the formation of HF must also be considered or corrected for. Since there are by necessity a significant number of HCl molecules present in the mixtures studied, ionization or dissociation of HCl would lead to further complication of our titration scheme. The cross section for dissociative electron-attachment for HCl has been carefully studied by Christophorou,[31] et al. It is found that the overall cross section for the reaction

$$HCl + e \rightarrow HCl^{-*} \rightarrow H + Cl^-, \qquad A_0 = 0.81 \text{ eV} \qquad (100)$$

is 7.4×10^{-18} cm^2 eV and peaks at an impact energy of 0.81 eV with a maximum cross section of 1.85×10^{-17} cm^2. If this cross section is much larger than that of reaction (91) for F_2, reaction

$$H + F_2 \rightarrow HF + F \qquad (101)$$

plus reaction (88) would lead to the formation of two additional HF molecules for every dissociative electron-attachment of HCl. Although reaction (101) is about seven times slower than that of reaction (88), the measurements were made on samples enriched with molecular F_2 ($[F_2]/[HCl] \approx 4$), therefore it is not all that clear whether contributions from reaction (100) to the overall formation of HF molecules are negligible. Other side reactions like charge transfer, Penning ionization of HCl, and ionic recombinations,

$$He^+ + HCl \rightarrow HCl^+ + He \qquad A_0 = -11.8 \text{ eV} \qquad (102)$$

$$He^* + HCl \rightarrow HCl^+ + He + 3 \qquad A_0 = -6.9 \text{ eV} \qquad (103)$$

$$HCl^+ + F^- \rightarrow HF + Cl \text{ or } H + F + Cl \qquad (104)$$

would further hamper the interpretation *of the experi*mental data. Since reaction (91) is likely to be a hundred times faster than any of the above side reactions mentioned, we conclude that the analysis should be simple and straightforward.

Since HF molecules generated from either reaction (88) or (101) are vibrationally excited, CO_2 gas was added to the mixture to shorten the

vibrational relaxation time of HF. Then, the $1P_4$ absorption measurement could be performed on ground state HF. Hancock and Green[32] have recently measured the rate of vibrational relaxation of HF by CO_2. They find that the reaction

$$HF\ (v = 1) + CO_2 \rightarrow HF\ (v = 0) + CO_2\ (n,\ 1^0,\ m) \qquad (105)$$

has a cross section of 0.27×10^{-16} cm^2 or a rate constant of 5.9×10^4 sec^{-1} torr^{-1}. For mixtures with 8 torr of CO_2, HF vibrational relaxation should take only a few μsec. Since we have delayed our absorption experiment for about 150 μsec after the E-beam pulse (see Fig. 52), the amount of IP_4 absorption should give us a direct measurement of the concentration of ground state HF molecule produced.

1.6.4.4 Results and Discussion

Table VIII lists the composition of the gaseous mixtures studied and the amount of F-atoms (or HF molecules) observed for various F_2/HCl/CO_2/He mixtures for five different electron-impact energies. For a fixed gas composition of F_2/HCl/CO_2/He = 1/0.25/0.25/23.5, the amount of F-atoms produced varies linearly with the amount of electron energy deposited in the gas as indicated in Fig. 51. In order to obtain a gross figure on the efficiency of F_2 dissociation by electron impact, the number of ionizing collisions produced in the gas by the electron beam has to be estimated.

For a monoenergetic electron beam, if the stopping power and the average energy loss per ionizing collision for the gas sample are known, one can correlate the number of ionizing collisions per cm^3, N_{coll} by

$$N_{coll} = \int_0^{\tau} j(t) \left\{\frac{1}{W} \frac{dE}{dx}\right\} dt \qquad (106)$$

where $j(t)$ is the total current density (in electrons/cm^2 sec) as a function of time, t. τ is the pulse duration of the electron beam. W is defined as the average energy loss per ionizing collision that the primary electrons suffer. The energy degradation per unit path (dE/dx) can be expressed as

$$\frac{dE}{dx} = \sum_i S_i(E)\, \rho_i \qquad (107)$$

where $S_i(E)$ is the stopping power for molecule i at an electron-impact-energy of E. ρ_i is the density for the gas molecule i and the summation is over all gaseous species.

To determine the electron beam energy spectra and electron energy deposition profile for these experiments, a separate calibration experiment and detailed computation were performed. For simplicity, the approach used is summarized as follows:

TABLE VIII

ELECTRON BEAM DISSOCIATION OF FLUORINE IN F_2, HCl, CO_2 AND He MIXTURES AT A TOTAL PRESSURE OF 800 TORR

X_{F_2}	X_{HCl}	X_{CO_2}	X_{He}	keV[a]	$j\tau$[b] electrons/cm^2	N_{coll}[c] collisions/cm^3	F[d] atoms/cm^3	F/N_{coll} atoms/ionizing collisions
0.06	0.008	0.008	0.924	60	5.4×10^{13}	1.3×10^{15}	5.2×10^{15}	4
0.03	0.008	0.008	0.954	60	5.4×10^{13}	1.2×10^{15}	3.7×10^{15}	3
0.02	0.009	0.009	0.962	60	5.4×10^{13}	1.2×10^{15}	3.6×10^{15}	3
0.03	0.016	0.008	0.946	60	5.4×10^{13}	1.2×10^{15}	4.4×10^{15}	3
0.03	0.008	0.008	0.954	50	2.9×10^{13}	0.8×10^{15}	2.4×10^{15}	3
0.03	0.008	0.008	0.954	40	1.8×10^{13}	0.3×10^{15}	2.1×10^{15}	7

a. The values represent the average energy of electrons that was injected into the sample. A 60 keV energy was obtained from a shot of 140 kV charged gun-voltage. The energy of 50 and 40 keV was obtained from the shots of 120 kV and 100 kV respectively.

b. The values represent the products of the effective average current density and the average duration of the electron pulse that is injected into the sample studied.

c. This is calculated by Eq. (19) in the text where values W_{He} = 30 eV, W_{F_2} = 36 eV, W_{HCl} = 25 eV, W_{CO_2} = 34 eV were adopted.

d. The average values with a possible error up to $\pm$ 25%.

(1) Measure diode current and voltage.

(2) Calculate the electron beam spectrum using the EBSPEC code.[33]

(3) Calculate the energy deposited in the gas mixture and the current density transmitted through the mixture by the electron beam using the Monte Carlo transport code ELTRAN.[33]

(4) Measure the transmitted charge and compare it to that calculated to determine the fraction of current lost to the walls by scattering in passing through the neck and into the channel.

(5) Use this fraction to correct the calculated energy deposited for the wall losses.

(6) Measure the energy deposited at the back of the neck using blue cellophane dosimetry and compare to the corrected calculation to verify the analysis.

Figures 53a, 53b and 53c show a typical experimental diode voltage (corrected for inductance) and diode current and the calculated electron beam spectrum determined by EBSPEC for the generator charging voltages of 100, 120 and 140 kV employed in this experiment.

These spectra were then used to calculate both (1) the electron beam energy deposition profiles through the experimental package by using ELTRAN, and (2) the number of ionizing collisions per cm^3, N_{coll} by Eq. (106). As is clearly shown in Figs. 53a, 53b and 53c, the electron beam energy injected into the gas sample is not monoenergetic. The distribution function f(E) is thus inserted into Eq. (106) which becomes

$$N_{coll} = \int_0^{E_{max}} \int_{0^-}^{\tau} f'(E)\, j(t) \sum_i S_i(E)\, \frac{\rho_i}{W_i}\, dt\, dE \qquad (108)$$

Figures 54a, 54b and 54c show the calculated electron energy deposition profiles for the charging voltages of 140, 120 and 100 kV, respectively. All these profiles have been normalized to unit energy fluence at the anode.

Table VIII lists the values of N_{coll} obtained through numerical integration of Eq. (108) by using ELTRAN and by adopting the corrected calculated energy deposition as shown in Table IX. The values of S_{He} and S_{CO_2} were taken from Berger and Seltzer,[34] and the values of W_{He} and W_{CO_2} from Bartner and Hurst.[35] The value of W_{HCl} was taken from Christophorou.[31] For helium, due to possible excitation effects,[31] the value of W_{He} used is the value appropriate for helium with added gas, not

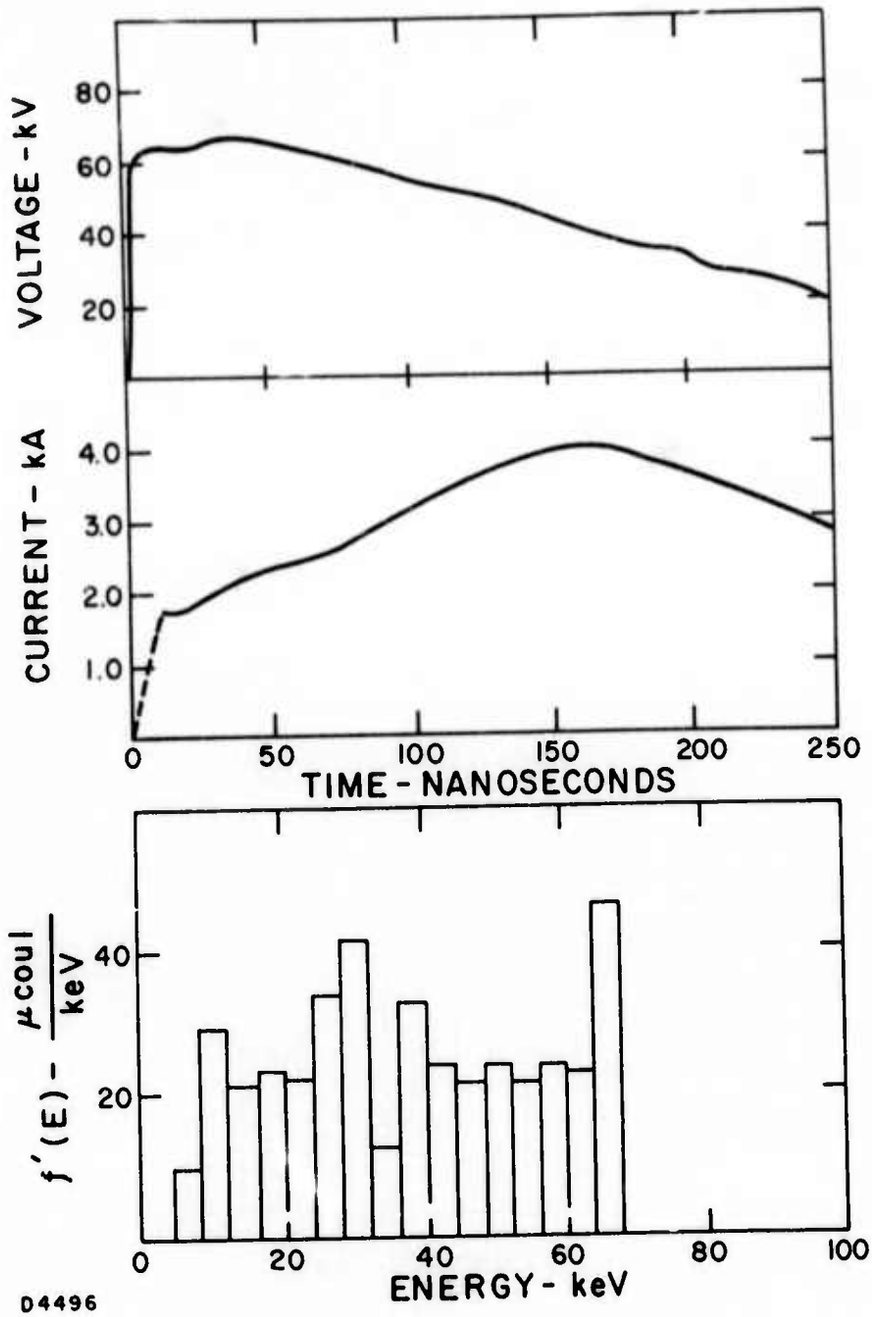

Fig. 53a Typical Electron Beam Spectrum for a Charging Voltage of 100 kV. The cathode area is 1 cm x 10 cm and gap is 8 mm.

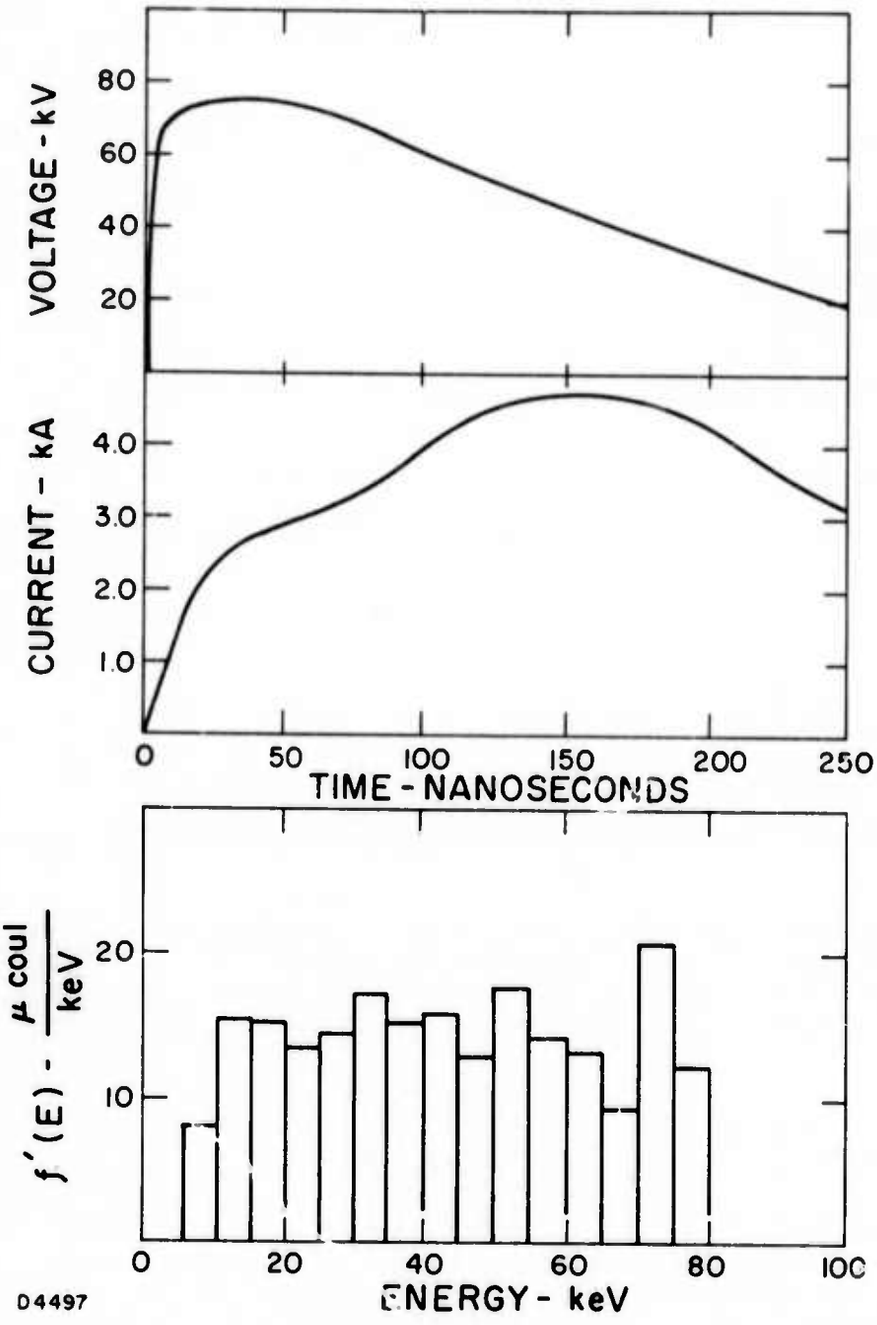

Fig. 53b Typical Electron Beam Spectrum for a Charging Voltage of 120 kV. The cathode area is 1 cm x 10 cm and gap is 8 mm.

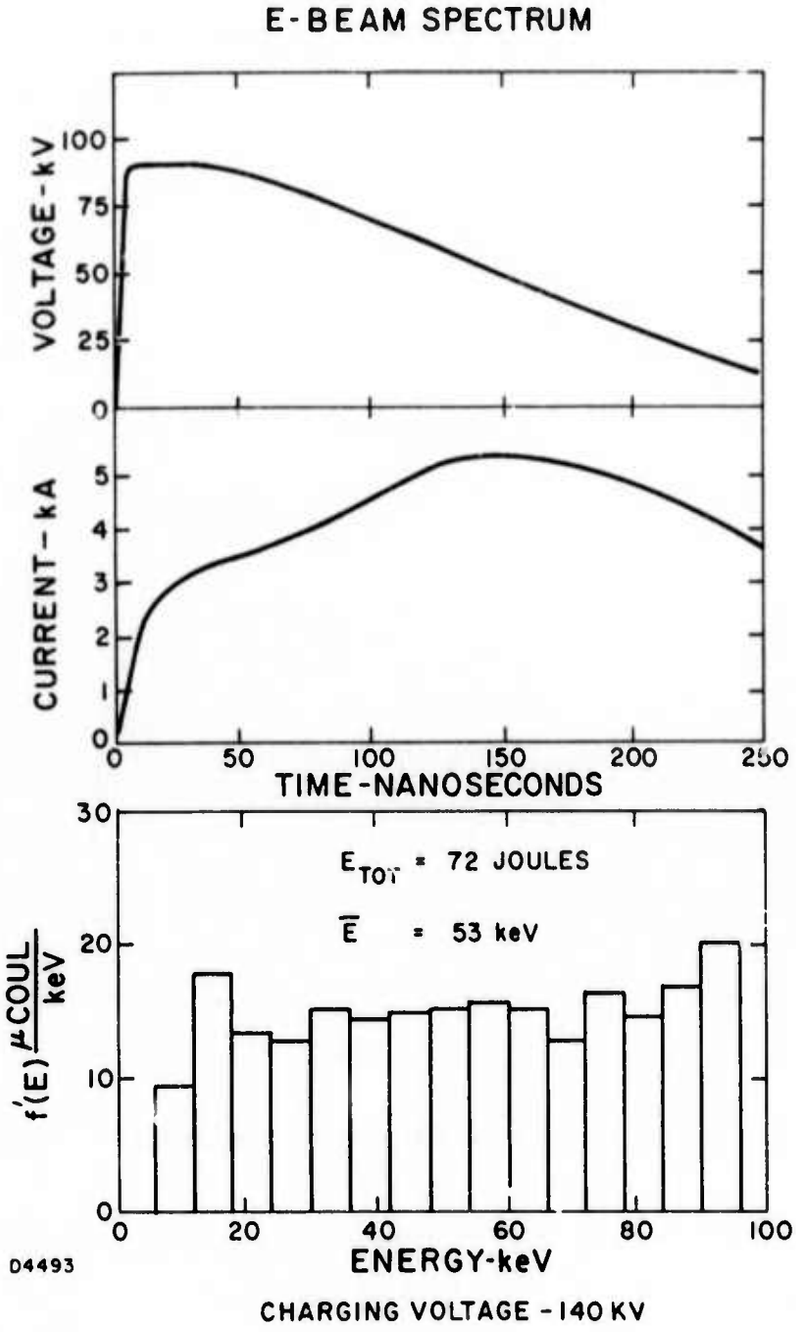

Fig. 53c Typical Electron Beam Spectrum for a Charging Voltage of 140 kV. The cathode area is 1 cm x 10 cm and gap is 8 mm.

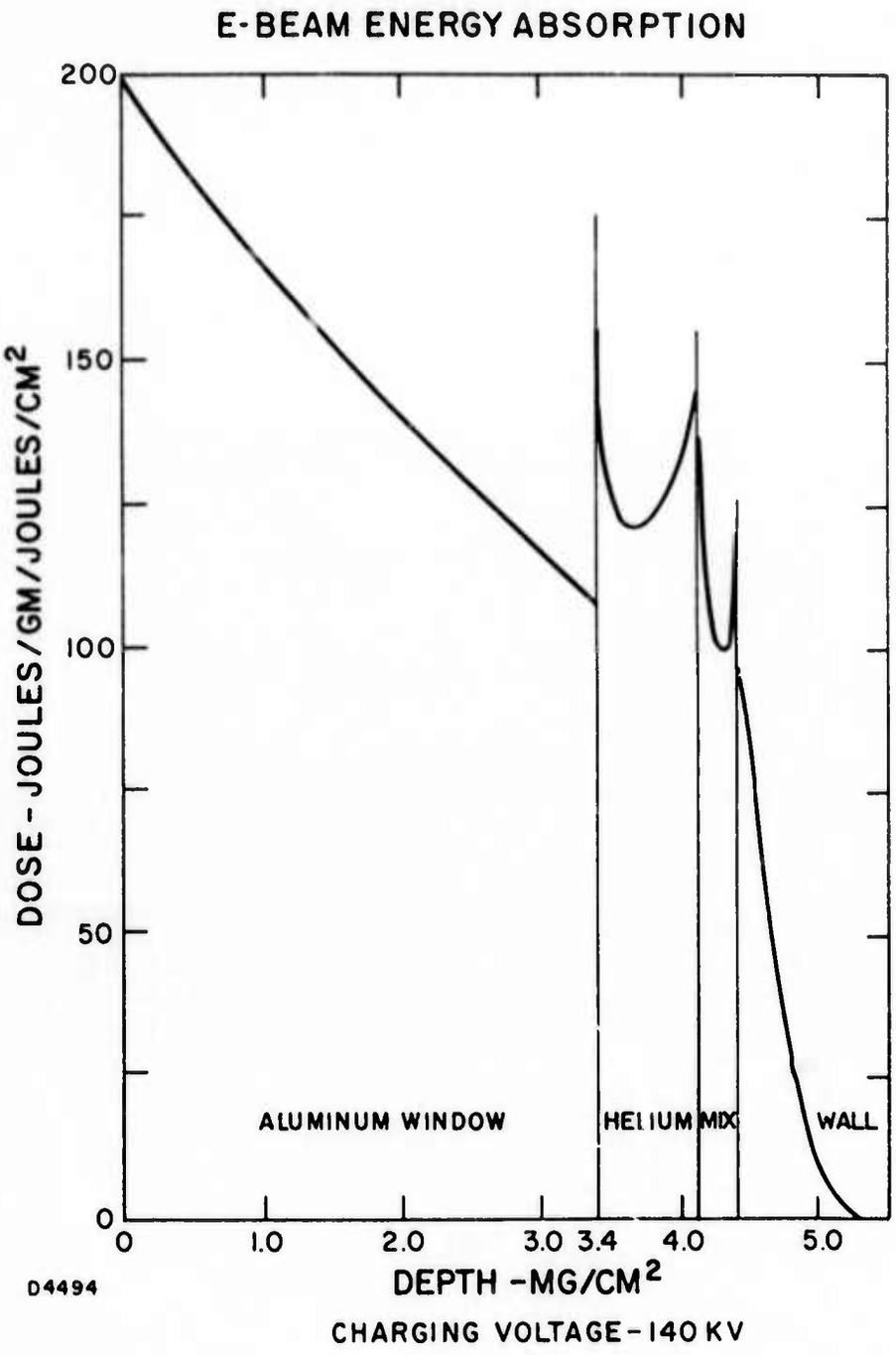

Fig. 54a Typical Electron Beam Energy Deposition Profile for the Experiment with a Charging Voltage of 140 kV.

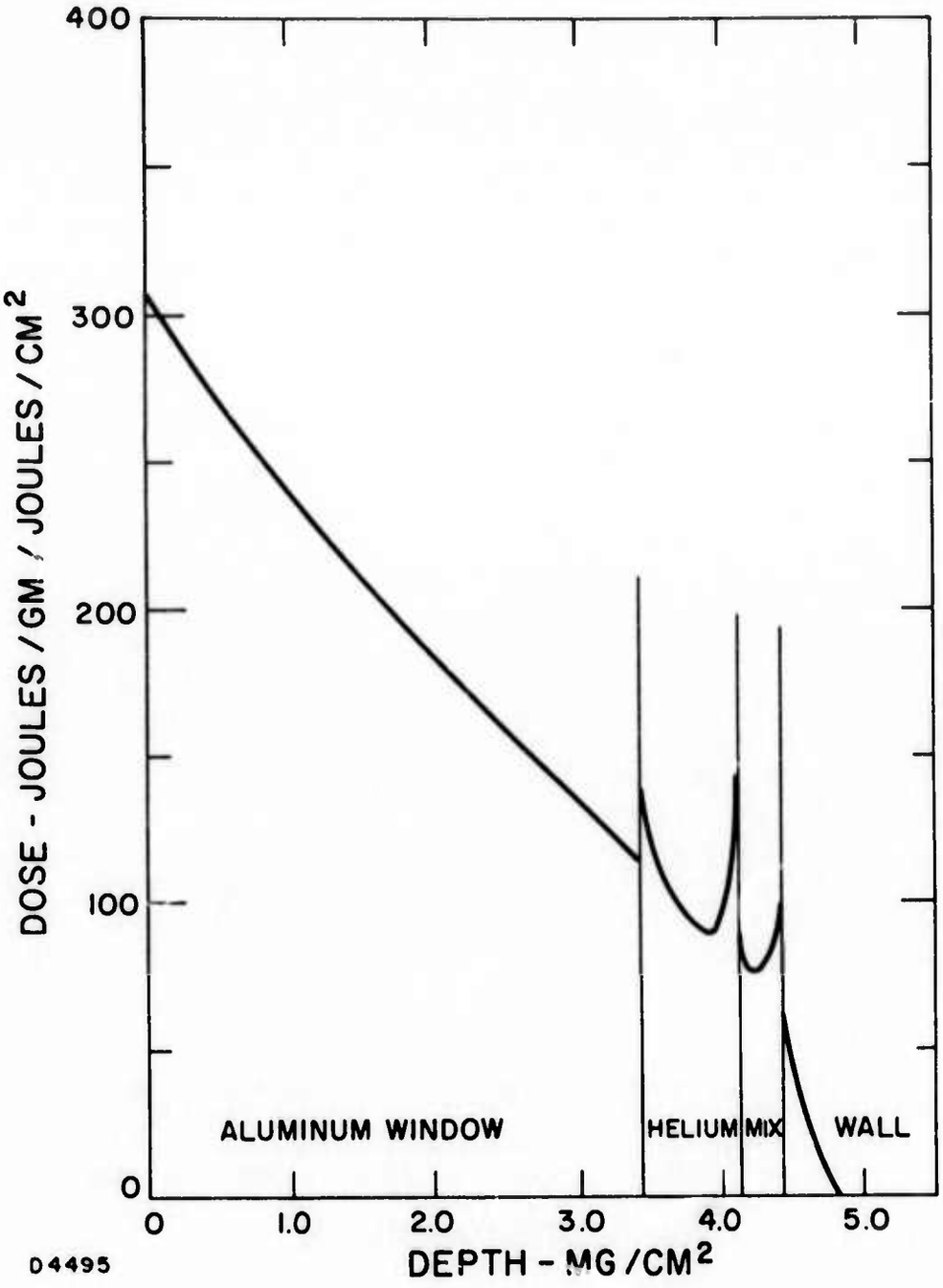

Fig. 54b Typical Electron Beam Energy Deposition Profile for the Experiment with a Charging Voltage of 120 kV.

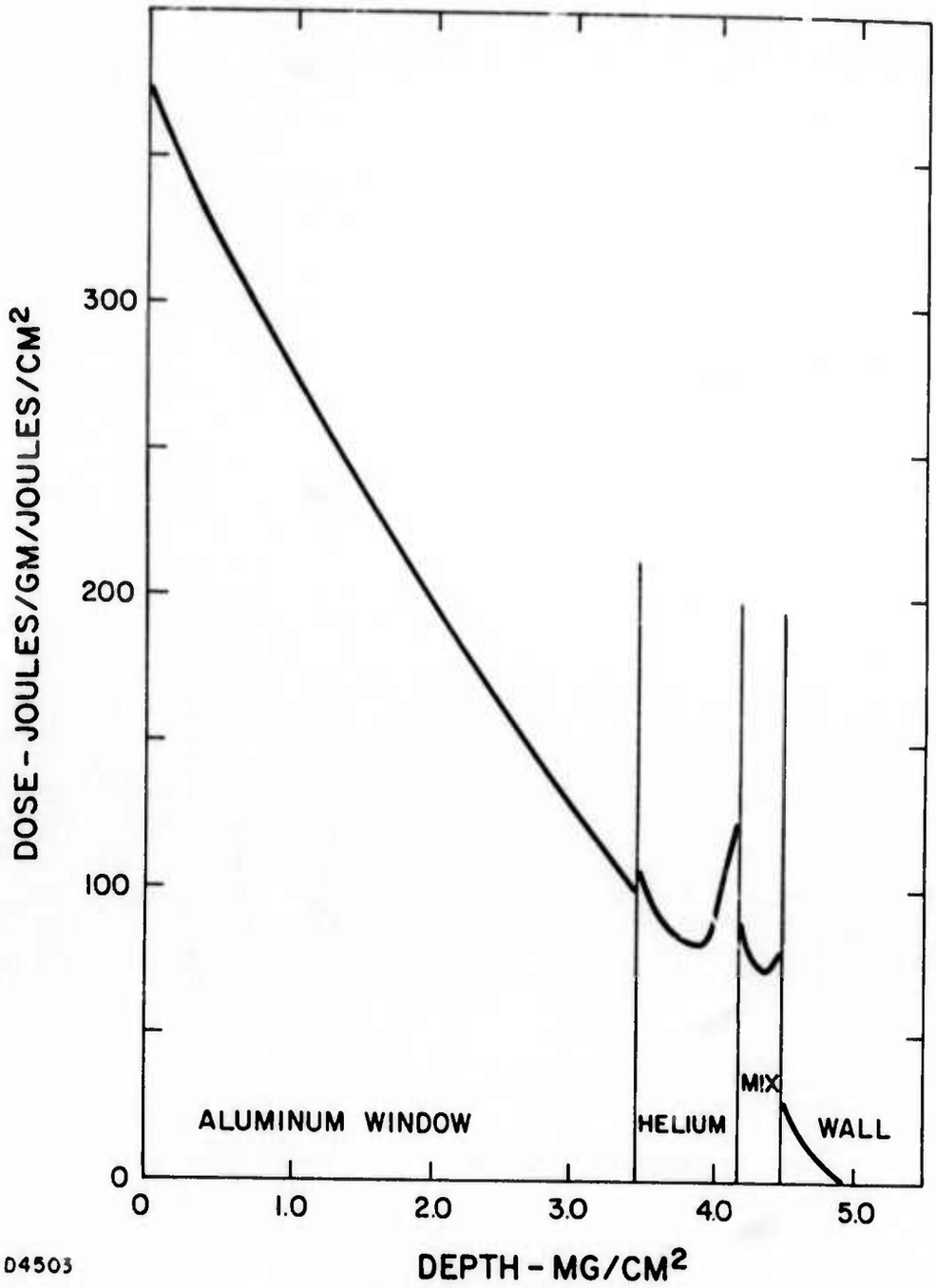

Fig. 54c Typical Electron Beam Energy Deposition Profile for the Experiment with a Charging Voltage of 100 kV.

TABLE IX

DATA SUMMARY FOR ELECTRON BEAM EXCITATION EXPERIMENT

Parameter	Charging Voltage		
	100 kV	120 kV	140 kV
Average Electron Energy in Diode from EBSPEC keV	39	43	53
Fluence Before Screen cal/cm^2	0.93	1.11	1.72
Fluence After Screen (75%) cal/cm^2	0.63	0.75	1.16
Average Dose to "Mix" - Calculated by ELTRAN cal/gr	45.8	64.1	1<5
E_{TOTAL} in Diode joules	38.7	43.3	72.0
Q_{TOTAL} in Diode μc	1000	1075	1350
Q_{TOTAL} After Screen (75%)	750	806	1012
Q Transmitted from Channel-Calculated by ELTRAN μc	132	187	383
Q Transmitted from Channel-Measured μc	5.1	13.5	21.9
$\frac{\text{Q Transmitted Measured}}{\text{Q Transmitted Calculated}}$	0.39	072	057
Dose "Mix" = $\frac{Q_{TM}}{Q_{TC}} \times$ Dose/cal cal/gr	1.8	4.6	7.1
Average Dose to "Mix" - Measured cal/gr	1.9	7.3	8.8
N_{coll} electron collisions/cm^3	3×10^{14}	7.6×10^{14}	11.8×10^{14}

the value for pure helium. The value of W_{F_2} is not known, but the fluorides BF_3 and SF_6 have a value of 36 eV, as do other diatomic molecules, so this value was assumed for fluorine. Both S_{F_2} and S_{HCl} values are not known either, the values corresponding to Ne and Ar were chosen, respectively.

Table IX summarizes the results, most of which are self-explanatory. As discussed, the approach was to get an empirical correction factor for the calculated energy deposited in the mixture by ratioing the measured to the calculated transmitted charge. Applying this correction to the calculated energy deposited brought the value close to that measured as is shown in Table IX. This agreement gave confidence to the analytical approach taken. Table VIII lists the values of N_{coll} calculated and the corresponding number of F-atoms observed. A consistent ratio of $[F]/N_{coll} \approx 3$ is indicated. Thus, the comparison between the experiment and the calculation suggests that about three fluorine atoms are produced for each electron-molecule collision. If one assumes that high energy electrons lose 35 eV per inelastic collision, it then costs approximately 12 eV for every F-atom produced.

Since the dissociation scheme is obviously quite complicated, at the present time with our limited information, it is not possible to draw any conclusions regarding the mechanism of dissociation or the percentage of contribution from each individual reaction.

1.6.4.5 Conclusion

The experiments described have determined the efficiency for electron beam dissociation of F_2 molecules in HCl, CO_2 and He gaseous mixtures. An efficiency of three F-atoms per electron-molecule collision is observed. If one assumes that high energy electrons lose 35 eV per inelastic collision, it costs approximately 12 eV for every F-atom produced. Thus, an electron beam does appear to be an efficient means for initiation of HF chemical lasers. A few possible processes that might lead to F_2 dissociation were suggested. However, due to the lack of knowledge on rate constants, it is not possible to give any firm or quantitative conclusion on the mechanism or the relative importance of each individual process involved in the reaction. Nevertheless, the information obtained from the experiment should be useful to the further development of electron beam dissociated chemical lasers, and hopefully will stimulate additional detailed studies of high energy electron kinetics in various gases.

1.7 CONCLUDING REMARKS

At the beginning of this Contract the future of the high energy, high pressure, pulsed HF laser did not appear bright. Although mixture stability had been achieved, there were problems of reproducibility. Although laser action had been demonstrated, the efficiencies were very poor, and more discouraging was the apparent lack of understanding of the data obtained. Certainly the progress achieved during the past year and reported in this Final Technical Report is impressive and definitely suggests the potential of this type of device for future military applications.

The laser performance demonstrated on a small scale - 8 joules in a 100 cc flash initiated device for a mixture of 10% F_2/10% H_2/80% He at a total cavity pressure of 1.1 atm - is a milestone in pulsed chemical laser technology. This performance scales to 80 J/l-atm and a specific energy of 100 kJ/lb which is certainly as good or better than demonstrated by any other laser; electric, gas dynamic, or other chemical system.

Another important milestone that has been achieved is the development of a kinetic model that has provided considerable insight into the detailed chemistry and physics and performance of this laser system. There are still a number of important areas of disagreement between model prediction and observed laser characteristics, but, considering the complexity of this system, the significance of the agreements far over shadows the areas of uncertainty. There are obvious areas of future research that should be pursued in theoretical model development.

The third significant achievement under this program was the first experimental measurement of the efficiency of producing fluorine atoms from F_2 via a high energy electron beam. A value of 12 eV/F-atom was obtained. This measurement is important because it indicates that electric discharge techniques can be attractive volumetric, high efficiency initiation techniques for large scale devices. This statement is supported by pin discharge initiated laser experiments done under this Contract and elsewhere that have achieved high electric efficiency (~ 100%) in small volumes.

The future developments in this area seem clear. In order to obtain the high power levels necessary for eventual applications, it will be necessary to scale to larger volumes. The inherent high gain of this type of laser will make the extraction of high powers from large devices a non-trivial task. In order to achieve high efficiency it will be necessary to find a volumetric, scalable discharge scheme for initiation of the laser. Finally, since this device operates on a pulsed basis, for high power applications, it will be necessary to repetitively fire the laser. This requirement will necessitate quenching the chemical reaction in the cavity volume, and refilling with fresh gas without preignition. In addition, the acoustic waves generated from the initation pulse and reaction must be damped for reasonable medium homogeneity. A recent RFP has been issued by AFWL to address some of these considerations.

In conclusion it is our opinion that a new area of chemical laser development is beginning, and the work and achievements reported herein have, in large measure, contributed to that birth.

SECTION II

PROPAGATION TASK

2.1 PULSE PROPAGATION

2.1.1 Introduction

Evaluation of the propagation characteristics of a laser beam through an absorbing fluid is a problem in non-linear optics. The interaction of the laser with the medium is through the index of refraction which has both a real and imaginary part giving rise to absorption and phase changes associated with the density changes of the atmosphere. The interaction is non-linear because the index of refraction depends upon the intensity of the propagating wave through the hydrodynamic equations. The non-linear interaction process which has been treated in this investigation is absorption of a pulsed laser beam in a medium in which the pulse time is of the order of the hydrodynamic time, i.e., the time required for a signal traveling at the sound velocity to cross the beam.

Earlier work[36] has been devoted to a study of the steady-state situation which is obtained when a transverse wind is present to remove the absorbed energy. This present work is an extension to the time regime before the wind has an effect. The next step in the development is the inclusion of wind in the time dependent problem in order to study the intermediate times between beam turn on and the steady-state regime.

This study is restricted to collimated Gaussian beams in the limit where linearized hydrodynamics applies. Comparison will be made with analytical theory for situations where the theory is valid. In addition, results for cases for which the analytic theory is known to be a poor approximation will be presented.

2.1.2 Interaction of a Pulsed Laser Beam with an Absorbing Atmosphere

In this section the dependence of the gas density on the irradiance distribution of the laser beam is calculated. The density response is determined from the linearized equations of mass, momentum, and energy. Viscosity and heat conduction are neglected and times of interest are restricted to be less than the time required for free convection to set in. This latter restriction allows the problem to be solved in cylindrical symmetry, giving the following set of equations for the changes in the hydrodynamic variables,

$$\frac{\partial \rho}{\partial t} + \rho_o \nabla \cdot \vec{v} = 0 \qquad (109)$$

$$\rho_o \frac{\partial \vec{v}}{\partial t} = -\nabla p \tag{110}$$

$$\rho_o \frac{\partial h}{\partial t} - \frac{\partial p}{\partial t} = \alpha I \tag{111}$$

$$h = \frac{\gamma}{\gamma - 1} \frac{p}{\rho} \tag{112}$$

where p, ρ, $\vec{v}$, α, I, h are, respectively, the pressure, density, and velocity changes, total absorption coefficient, beam intensity and enthalpy, and where subscript zero refers to ambient values.

The above set of equations can be reduced to the following single equation involving only the density:

$$\left(\frac{\partial^2}{\partial t^2} - c_s^2 \nabla^2 \right) \frac{\partial \rho}{\partial t} = (\gamma - 1)\, \alpha \nabla^2 I \tag{113}$$

where $c_s = \sqrt{\gamma p_o / \rho_o}$ is the sound velocity. Equation (113) is subject to the following initial conditions

$$\rho = 0, \ \partial\rho/\partial t = 0, \ \partial^2\rho/\partial t^2 = 0 \tag{114}$$

which are also the initial conditions of Eqs. (109), (110) and (111), respectively.

For a pulse length t_p which is much shorter than the hydrodynamic time t_H ($t_H \equiv R_m/c_s$ where R_m is the laser beam radius) the density dependence is given by,

$$\rho = (\gamma - 1)\, \alpha I \int_0^{t_p} \frac{(t - t')^2}{3} \nabla^2 I dt' + 0\left(\frac{t_p c_s}{R_m} \right)^2 \tag{115}$$

For t_p much longer than t_H, the density dependence is given by

$$\rho = - \frac{(\gamma - 1)\alpha}{c_s^2} \int_0^{t_p} I \, dt' . \qquad (116)$$

If the true situation is modeled by assuming that the heating of the gas is done by a non-varying beam having a Gaussian shape, Eqs. (115) and (116) become[37]

$$\rho = (\gamma - 1)\, \alpha t^3\, \nabla^2\, I_o / 6 \qquad (117)$$

for the short time behavior and

$$\rho_1 = - \frac{(\gamma - 1)\, \alpha t I_o}{c_s^2} \qquad (118)$$

for the long time behavior where I_o denotes the Gaussian beam intensity in a vacuo. It is clear that for short enough times the density will always change according to Eq. (117) for beams of arbitrarily high intensity, but it is only for small values of $\alpha I_o t_p$ that Eq. (117) will be obeyed out to times as long as t_H. If the density as given by Eqs. (117) and (118) are equated and solved for t one can thereby define an intermediate time t_c which separates the two time regimes for those cases where the beam is not highly distorted throughout the early regime. This time is $t_c = \sqrt{3 t_H}$. Thus, for those cases which result only in a slightly modified profile at times greater than t_c, the beam follows Eq. (117) for times close to t_H and follows Eq. (118) for times greater than about $3\, t_H$. In the intermediate regime at about $2\, t_H$ the detailed behavior of the beam and the fluid is best studied self-consistently by numerical procedures. Furthermore, interesting cases will include those for which the beam is highly distorted from its initial Gaussian profile for $t \ll t_H$. For these situations *self*-consistent numerical techniques are necessary.

In the optical frequency range, Maxwell's equations can be approximated by a parabolic equation. The electric field is taken to be of the form

$$E = A\,(r, z, t)\, \exp\,(ikn_o z - \alpha z/2) \quad k = 2\,\pi/\lambda \qquad (119)$$

and the index of refraction, n, is related to the gas density changes by

$$n = n_o + \frac{n_o}{\rho_o} (\rho - \rho_o) \tag{120}$$

The diffracted amplitude A is complex and the irradiance I is defined to be AA^*. The amplitude obeys the following paraxial approximation to the scalar wave equation(37)

$$2ik \frac{\partial A}{\partial z} + \frac{1}{r} \frac{\partial}{\partial r} \left(r \frac{\partial A}{\partial r} \right) + k^2 (n^2 - n_o^2) e^{-\alpha z} A = 0 \tag{121}$$

The derivatives in time $(2\ ik/c)\ \partial A/\partial t$, in Eq. (121) are neglected since the time dependence of the index of refraction is on the scale of t_H.

Since the initial beam is assumed to be collimated at the laser face, the appropriate boundary conditions for the diffracted amplitude are:

$$A(r,\ 0,\ t) = e^{-r^2}$$

$$A(r,\ z,\ t) \to 0 \quad \text{as} \quad r \to \infty \tag{122}$$

A uniform square pulse in time is studied.

2.1.3 Numerical Results

Equation (121) has been programmed using the stable, explicit, numerical technique of Ref. (36). For $r \neq 0$, derivatives in the r-direction are replaced by the central difference approximation

$$\frac{\partial^2 A}{\partial r^2} + \frac{1}{r} \frac{\partial A}{\partial r} = \frac{1}{\Delta_r^2} \left\{ A_{i+1,k,s} \left(1 + \frac{\Delta_r}{2r} \right) - 2A_{i,k,s} + A_{i-1,k,s} \left(1 - \frac{\Delta_r}{2r} \right) \right\} \tag{123}$$

where $A_{i,k,s} \equiv A(r, z, t)$ and $r = i\Delta r$, $z = k\Delta z$, and $t = s\Delta t$. At $r = 0$,

$\partial A/\partial r = 0$ and the central difference approximation becomes

$$\frac{\partial^2 A}{\partial r^2} + \frac{1}{r}\frac{\partial A}{\partial r} = \frac{4}{\Delta_r^2}(A_{1,k,s} - A_{0,k,s}) \qquad (124)$$

The derivative in the propagation direction z is replaced by the symmetric difference quotient

$$\frac{\partial A}{\partial z} = \frac{(A_{i,k+1,s} - A_{i,k-1,s})}{2\Delta z} \qquad (125)$$

where Δz is the width of the mesh in the propagation direction. This differencing scheme for Eq. (121), is stable under the condition[38]

$$\frac{4\Delta z}{\Delta_r^2}\left\{1 + \frac{\Delta_r^2}{2} k^2 e^{-\alpha z}(n^2 - n_o^2)\right\} \leq 1.0 \qquad (126)$$

The initial value hydrodynamic problem can be completely formulated in terms of a Green's function but computationally it is far simpler to use the standard finite difference equations for a hyperbolic system of equations rather than to complete the Green's function quadratures numerically. Differencing of the hydrodynamics wave equation, Eq. (113), in the spatial coordinate, r, is identical to Eqs. (123) and (124). Differencing in the time direction is accomplished by central differences

$$\frac{\partial \rho}{\partial \rho} \quad \frac{1}{2\Delta t}(\rho_{i,\,s+1} - \rho_{i,\,s-1})$$

$$\frac{\partial^2 \rho}{\partial t^2} = \frac{1}{(\Delta t)^2}(\rho_{i,\,s+1} - 2\rho_{i,s} + \rho_{i,\,s-1}) \qquad (127)$$

where $\rho_{i,s} \equiv \rho(r,t)$ and $r = i\Delta r$, $t = s\Delta t$. This differencing is stable[38] under the condition that

$$\frac{c_s \Delta t}{\Delta_r} < 1.0$$

Both the set of equations, Eqs. (109), (110), (111), (112), and the resultant Eq. (113) have been programmed successfully using central differences in time, and give identical results. If forward differencing in time is used, the equations are unstable unless the concept of artificial viscosity is introduced.

There are two methods for determining the spatial and time variation of the irradiance distribution. The first method integrates in propagation distance z at a fixed time and repeats this process until times of interest have evolved. The second numerical procedure computes the index change as a function of time and space for each propagation level $z = k\Delta z$ starting with the known initial profile at $z = 0$. The governing equation for the electromagnetic field is computed for all time and space at $z = (k + 1)\Delta z$ using the previous computed values $A_{i, k, s}$. The procedure is then repeated for all propagation levels and a complete spatial and time history is obtained.

This latter method, which was chosen for this work, is used to advantage when fewer steps in time are required than steps in range. This can be seen by reference to Table X where the storage locations required for each method are enumerated.

The table assumes that central differencing in both range and time is used. This explains the entries of the number 3 in Table X.

The two methods are seen to require comparable storage when $n_z = n_t$. This condition is met when studying pulses of a few hydrodynamic times at ranges which are appreciable fractions of the far field range. For times much longer than this the inclusion of wind becomes necessary. Wind introduces an asymmetry which effectively replaces n_r by $n_r^2/2$ in the above enumeration making storage requirements prohibitively large.

2.1.4 Results

Figure 55 shows the time evolution of the gas density perturbation for a case where the laser beam is never highly distorted throughout the pulse. A compressive wave propagates away from the beam and its strength decreases as $r^{-1/2}$. The dashed curves in Fig. 55 represent the approximate analytic relations for the short and long time limit. The early time solution is valid for times shorter than t_H and the long time limit is valid for times longer than $3t_H$, as discussed above.

A series of plots of normalized intensity vs normalized range at five different times after pulse initiation for four ranges is shown in Fig. 56 Times are given in units of t_H. Ranges are given in units of the Rayleigh range kR_M^2. As expected, the central irradiance decreases with time and increases to a peak at the edge of the beam. This enhancement can be understood from a geometrical optics argument which predicts that the rays near the center of the beam will deflect outward to the region of higher index.

TABLE X

ENUMERATION OF STORAGE REQUIREMENTS
FOR ALTERNATIVE COMPUTING METHODS

Variable	Method I (march in z, fixed t)			Method II (march in t, fixed z)		
	r	z	t	r	z	t
Re A	n_r	3	0	n_r	3	n_t
Im A	n_r	3	0	n_r	3	n_t
ρ	n_r	n_z	3	n_r	0	3
v	n_r	n_z	3	n_r	0	3
p	n_r	n_z	3	n_r	0	3
TOTALS	$(6 + 9n_z)\, n_r$			$(6n_t + 9)\, n_r$		

(n_r, n_z, n_t = number of samples in r, z, t respectively).

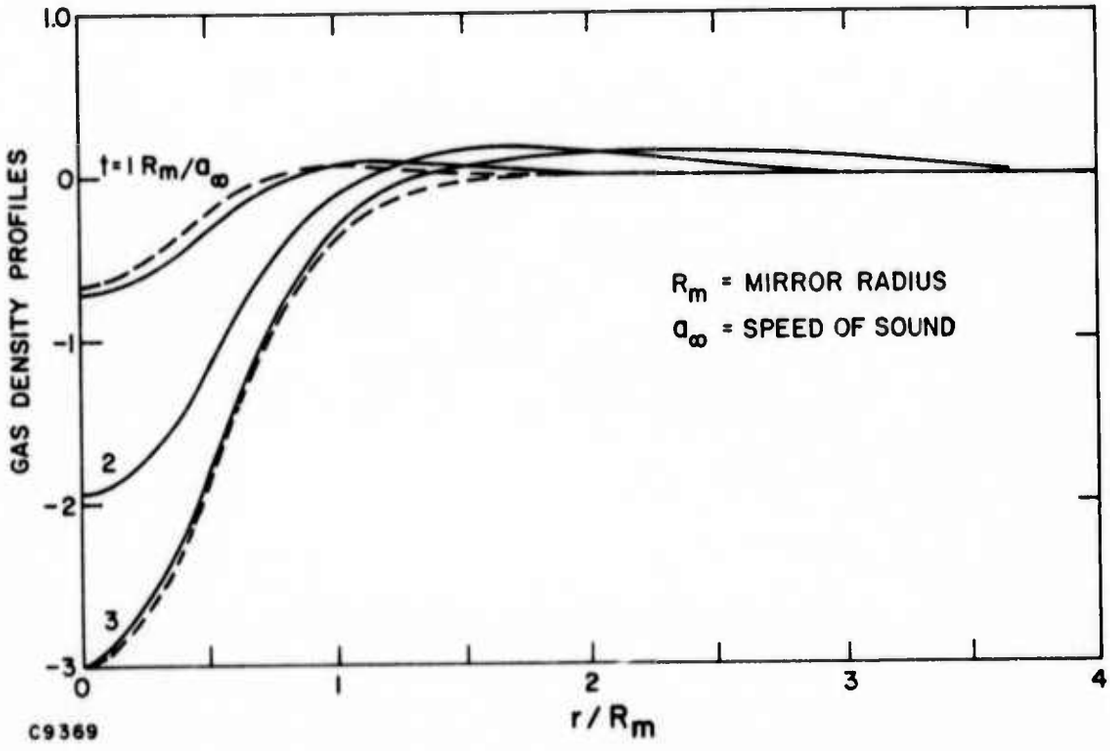

Fig. 55 Time Dependence of the Normalized Density Distribution for a Gaussian Irradiance

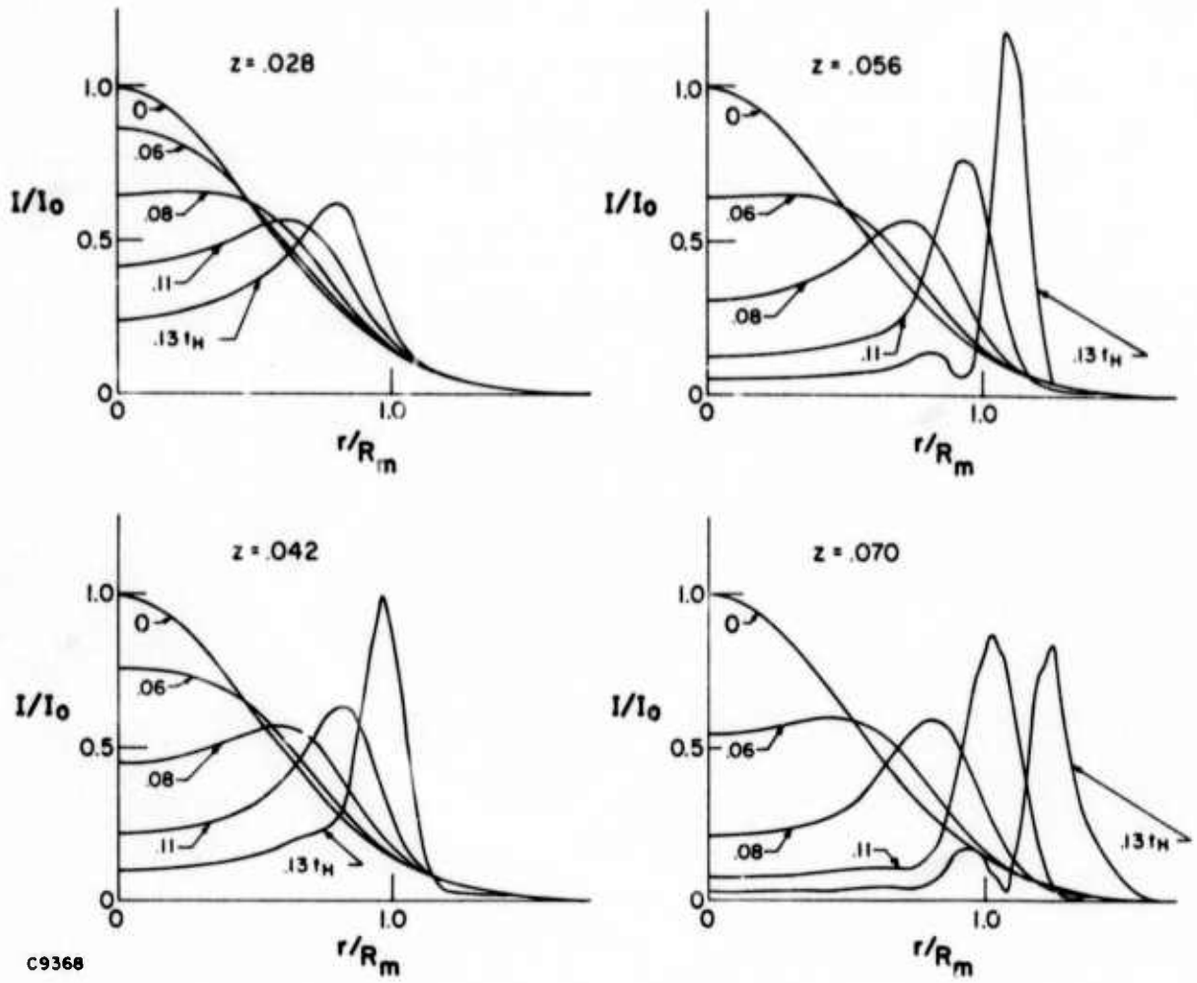

Fig. 56 Time Dependence of the Irradiance Distribution for a $P\tau_p = 1.0$ and $\tau_p = .133\ R_m/a_\infty$

A comparison of two very different cases at the same Rayleigh range is shown in Fig. 57. The upper plot is taken from Fig. 56 while the lower plot depicts a case where the power and beam size were chosen to increase the average irradiance by a factor of 4. The power was decreased by a factor of 100 and the beam radius was decreased by a factor of 20. Thus, for the same elapsed real time the smaller beam pulse is twenty times longer measured in units of t_H. In spite of this higher power per unit area and longer time evolution with respect to t_H the lower beam is clearly less distorted. The difference can be attributed to the large difference in energy which has been deposited in the volume $\pi R_m^2/\alpha$. This energy is responsible for the heating of the gas and the changes in the index of refraction. For the case considered the upper beam received 100 times as much energy as the lower beam at the end of their respective pulses, and 2000 times the energy of the lower beam at .13 of the respective hydrodynamic times. The energy delivered per unit volume per unit (hydrodynamic) time was in the ratio of 5 to 1, upper beam to lower beam, using original beam volumes for the calculation.

The behavior of the time averaged irradiance is plotted in Fig. 58 for three cases where t_p was varied but the product $\alpha t_p p$ was held constant. The time averaged results for the longest pulse duration corresponds to a loss of 30 percent of the average far field brightness (after correction for absorption effects). Up to .07 t_H, the time averaged irradiance effectively defines a beam whose radius is only slightly larger than the undistorted average radius. The .13 t_H curve corresponds to the profiles shown in Fig. 56.

2.1.5 Conclusions

The nonlinear problem of laser propagation through an absorbing gas has been studied using a stable, convergent numerical algorithm. The study was restricted to collimated Gaussian beams in the limit where linearized hydrodynamics applies. The computer results agree in detail for those cases where both long and short pulse analytical theory is known to be valid. Results for situations for which the analytic theory is known to be poor approximation have been presented (i.e., $t_p \sim R_m/a_\infty$). The distortion of the beam is a strong function of the energy deposited in a time of the order of the hydrodynamic time. Irradiance distributions which have been averaged over a pulse length indicate that even for beams which are highly distorted by the end of the pulse, the average degradation of pulse shape can be relatively small.

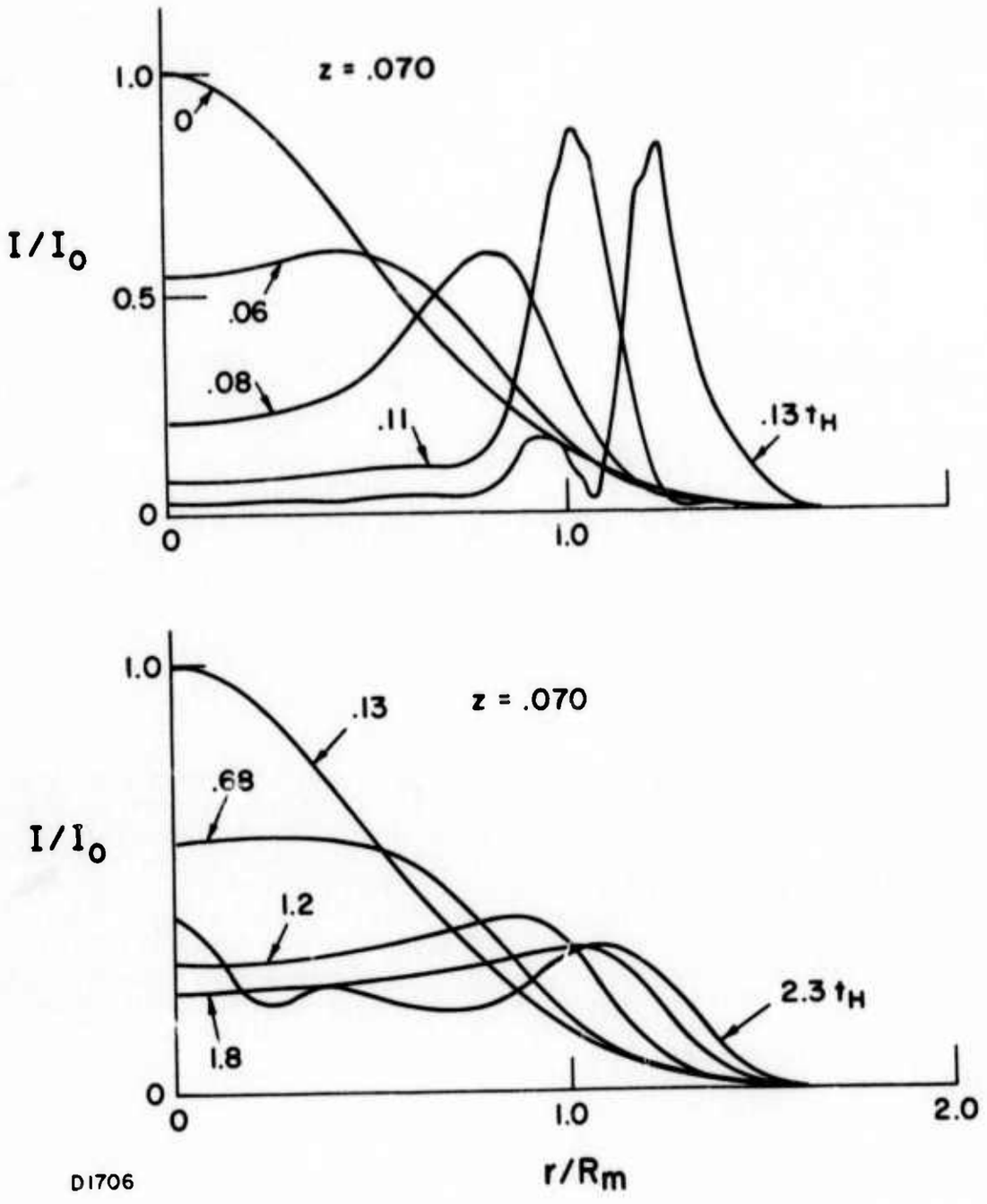

Fig. 57 Comparison of Irradiance Distributions for Two Beams with very Different Characteristics at the same Rayleigh Range for each Beam

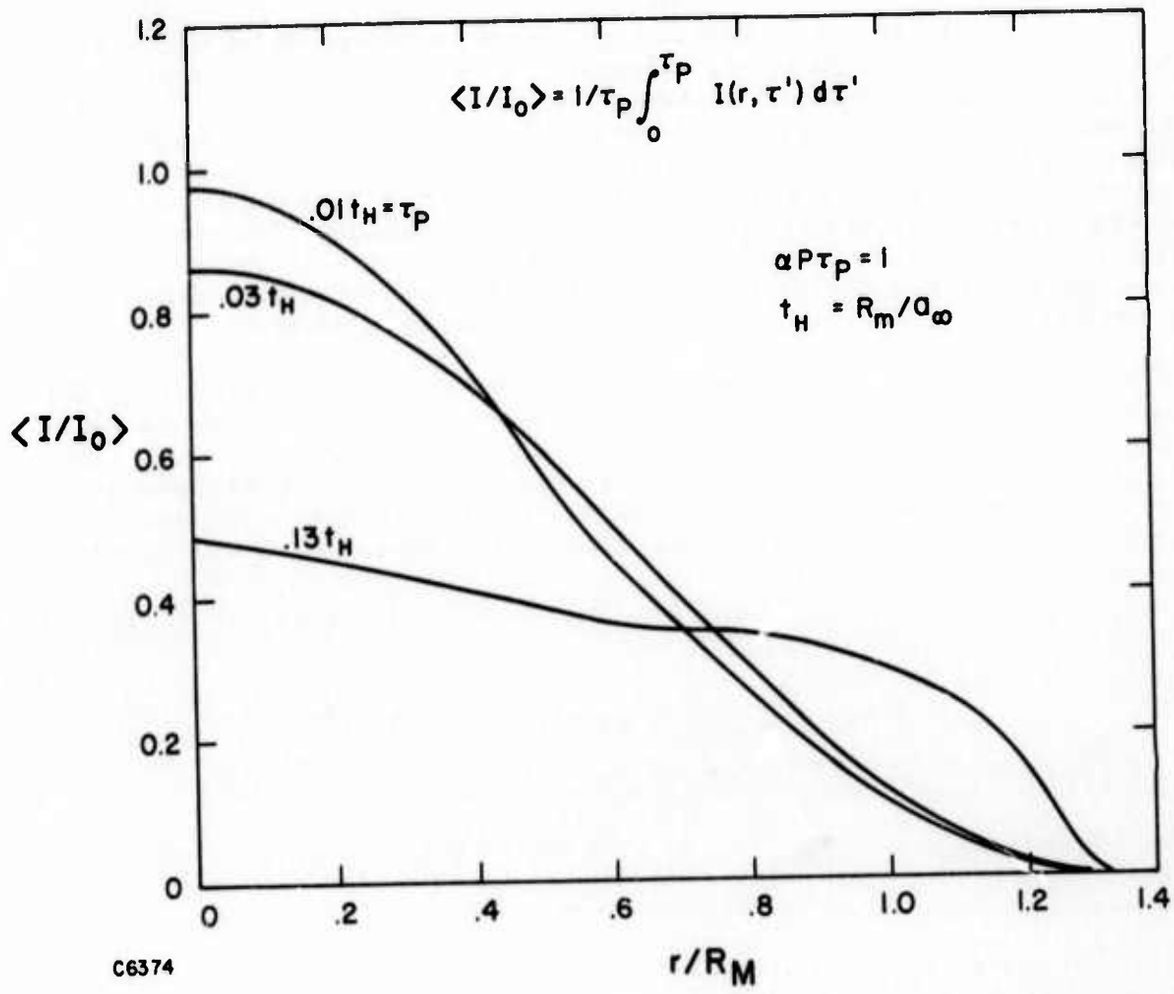

Fig. 58 Time Averaged Irradiance Distribution as a Function of the Pulse Duration τ_p for $\alpha P \tau_p = 1.0$

2.2 PRELIMINARY STUDY ON PROPAGATION CHARACTERISTICS OF UNSTABLE RESONATORS

2.2.1 Introduction

Unstable resonators at high output coupling are an efficient means of extracting high power in lasers. Thus a study on their propagation characteristics was undertaken. This study is preliminary in nature and was undertaken using present finite difference methods. The problem with sharply truncated beams is that they introduce infinite second derivative at the edges into the analysis. It is not clear on how appropriate or accurate these schemes are in treating truncated beams. Nonetheless, we proceeded to make an analysis using the stable explicit finite differencing scheme. However, future work in this area will require a totally new numerical approach to resolve the computational uncertainties.

Unstable resonators have a relatively flat irradiance (Fig. 59) distribution and this irradiance distribution should reduce somewhat the blooming transverse to the wind. No matter how flat the irradiance distribution is in circular unstable resonators these resonators have an astigmatic component due to the combination of a circular irradiance distribution and a flow. The density distribution at $z = 0$ associated with a circular unstable resonator is

$$\frac{\Delta\rho}{\rho} = \int_{-\sqrt{1 - y^2}}^{x} I_o \, dx' = I_o \left(x + \sqrt{1 + y^2}\right)$$

The linear term in x is simply a ray deflection term which does not introduce any significant defocusing effect. However the y-dependence introduces an astigmatic component and we can expect crescents.

If we have a square or rectangular unstable resonator at high output coupling the density distribution is simply linear without a gradient in y. At first glance in the near field this should introduce just a bending term without much irradiance degradation in the near field. This, however, is not borne out in the detailed numerical calculation. In fact, the diffraction effects of the edges introduce such peaking of the irradiance distribution that rectangular and/or square unstable resonators have density distributions with more severe gradients than either circular unstable resonators or Gaussian beams.

2.2.2 Theoretical Analysis

In the optical range, the circular frequency of oscillation of the electromagnetic field is very great and Maxwell's equation admits an asymptotic series expansion in powers of $1/kR_M$. The first term in this

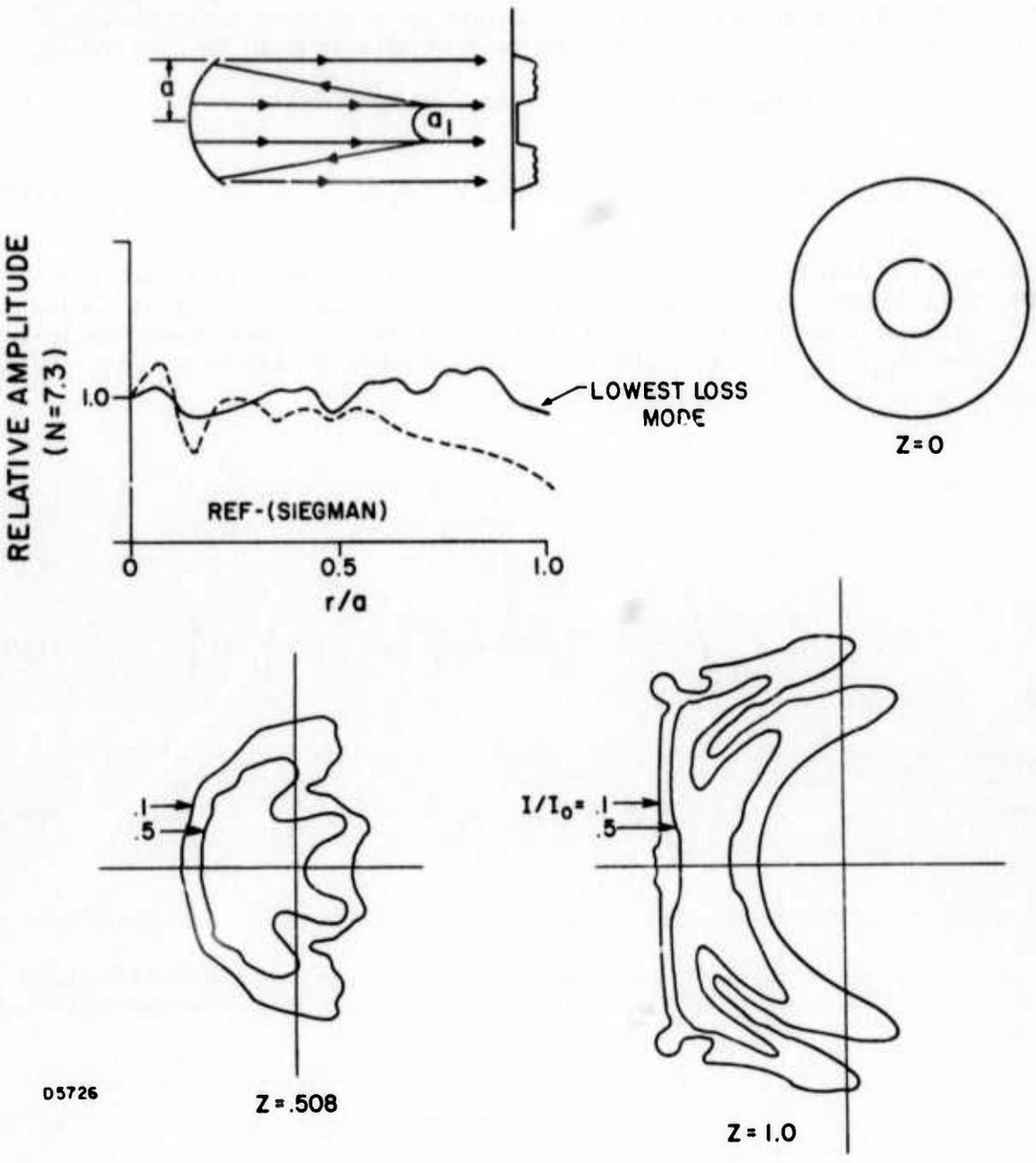

Fig. 59 Irradiance Distribution for a Circular Unstable Resonator for a Beam Focused at 1 km with a Power of 10^5 watts and a Velocity U_∞ Transverse to the Propagation Direction z of 2 Meters/Second

asymptotic expansion gives geometric optics. Geometric optics, by replacing Maxwell's equations by two first-order partial differential equations, is a considerable simplification. Geometric optics gives infinite irradiance at certain singular points or curves such as foci and caustics; at these singularities, diffraction effects must be considered.

To include diffraction effects, we put

$$E = A(x, y, z) \exp(ikn_\infty z + a_t z/2); \quad k = 2\pi/\lambda, \tag{128}$$

where A, the diffraction amplitude, has both a real and imaginary part. The irradiance I (x, y, z) is defined to be the A times the complex conjugate A^*. Substitution of Eq. (128) into Maxwell's equation and neglecting terms of order R_M^2/z_o^2 ($\sim 10^{-6}$) gives, in the normalized variables x/R_M, y/R_M, z/z_o, $A(R_M^2 \pi/P)^{1/2}$

$$2iA_z + \epsilon (A_{xx} + A_{yy}) - \frac{2 e^{-a+z}}{\epsilon 0}$$

$$X\ A \left\{ \int_{-\infty}^{x} AA^* \left\{ 1 - \delta \exp\left[-(x - x')/\beta \right] \right\} dx' \right\} = 0, \tag{129}$$

where

$$\epsilon_0 = z_0/kn_\infty R_M^2 . \tag{130}$$

The nondimensional quantity kR_M^2/z_0 is related to the Fresnel number.

We assume that we have a light beam whose rays are focused at $z = z_f$. The appropriate boundary conditions for the diffracted amplitude are

$$A(x, y, 0) = Ai(x, y), \tag{131a}$$

$$A(x, y, z) = 0 \quad \text{as} \quad x, y \to \pm \infty \tag{131b}$$

The governing equation has been programmed using the stable, explicit numerical technique of Ref.(38). We replace derivatives in the s, y direction

by the central difference

$$A_{xx} + A_{yy} = \frac{1}{(\Delta)^2} (A_{i+1,j,k} + A_{i-1,j,k} + A_{i,j+1,k} + A_{i,j-1,k} - 4A_{i,j,k}) \quad (132)$$

where Δ is the width of the mesh perpendicular of the propagation direction. The derivative in the propagation direction z is replaced by the symmetric difference quotient

$$A_z = \frac{(A_{i,j,k+1} - A_{i,j,k-1})}{2\Delta z} \quad (133)$$

where Δz is the width of the mesh in the propagation direction. This differencing scheme is stable under the condition

$$\frac{4\epsilon \Delta z}{\Delta^2} \left\{ 1 + \frac{\Delta^2}{2\epsilon^2} \int_{-\infty}^{x} AA^* \left\{ 1 - \delta \exp\left[-(x - x')/\beta \right] \right\} dx' \right\} < 1.0 \quad (134)$$

The second derivative in Eq. (128) at the edge is very large and gives rise to a solution which oscillates extremely fast near z = 0. This requires an extremely small grid structure to accurately calculate the complex amplitude. Thus, calculations with relatively small Fresnel number are the only ones which can be computed with any degree of confidence.

2.2.3 Discussion and Results

We now present calculations for a circular unstable resonator focused at 1 km and compare with an infinite Gaussian beam also focused at 1 km. The unstable resonator at the focal point z = 1.0 has a far field brightness reduced by a factor of 2 over a Gaussian beam. The peak irradiance is a maximum for both beams at $z = .50_f$ (minimum waste). The phase changes associated with the heating simply does not allow the beam to be focused any smaller. The physical reason for the unstable resonator having less irradiance at the focal point is due to the fact that diffraction for a truncated beam is much greater as we approach z = 1. This reduces the far field brightness over the infinite Gaussian beam as shown in Fig. 60.

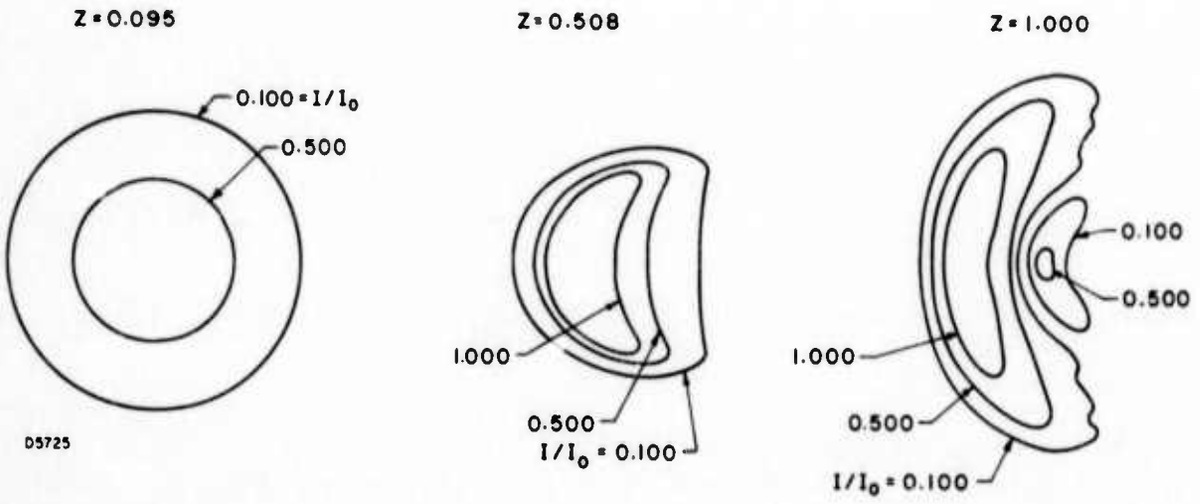

Fig. 60 Irradiance Distribution of an Infinite Gaussian Beam Focused at 1 km with a Power of 10^5 watts and a Velocity of 2 Meters/Second

Summarizing, for those calculations which are accessible (relatively low Fresnel number) using the present explicit finite difference scheme, unstable resonators do not propagate as well as infinite Gaussian beams. Since neither shape is acceptable as far as far field brightness is concerned, new emphasis must be put on beam shaping which minimize these effects. Also, further computational procedures must be developed in order to calculate propagation characteristics of beams with high Fresnel numbers. High Fresnel number beams (i.e. large radius) are one other way to minimize these refractive effects.

APPENDIX I

THE METHOD USED FOR NUMERICAL EVALUATION OF THE INTEGRAL $\int_0^\infty R_\ell (kr)\, R_\ell (k'r)\, V(r)\, dr$

In this appendix we describe a method for obtaining approximate solutions R_ℓ to the equation

$$\frac{d^2 R_\ell (kr)}{dr^2} + \left[k^2 - \frac{\ell (\ell + 1)}{r^2} - \frac{2\mu}{\hbar^2} V(r) \right] R_\ell (kr) = 0 \qquad (135)$$

where we take

$$V(r) = D \left[e^{-2\beta (r - R_0)} - 2e^{-\beta (r - R_0)} \right], \qquad (136)$$

i.e., assume a Morse type potential with well depth D at $r = R_0$ and range parameter β. The solutions of interest to us satisfy two boundary conditions

$$\lim_{r \to 0} R_\ell (kr) = 0 \qquad (137)$$

and

$$R_\ell (kr) \sim \cos (kr + \delta) \quad \text{for } r \geq r_1 \qquad (138)$$

where r_1 is determined by the condition that

$$\frac{2\mu}{\hbar^2} \left| V(r_1) \right| \ll k^2 - \frac{\ell (\ell + 1)}{r_1^2} \qquad (139)$$

We also point out that we are interested in solution of Eq. (135) to be able to evaluate the integrals of the type

$$\int_0^\infty R_\ell (kr)\, R_\ell (k'r)\, f(r)\, dr \tag{140}$$

where $f(r)$ is a smooth function of r which goes to zero at large r. If $k < k'$ and R_1 and R_2 are defined such that

$$\frac{2\mu}{\hbar^2} V(R_1) + \frac{\ell(\ell+1)}{R_1^2} = k'^2 \tag{141}$$

and

$$\frac{2\mu}{\hbar^2} V(R_2) + \frac{\ell(\ell+1)}{R_2^2} = k^2 , \tag{142}$$

the integral (140) can be approximated as

$$\int_{R_1 - \epsilon_1}^{R_2 + \epsilon_2} R_\ell (kr)\, R_\ell (k'r)\, f(r)\, dr \tag{143}$$

where ϵ_1 is the number of the order of 1 A while ϵ_2 may equal several angstroms depending upon k, k' and f (r). The reason is that for $r < R_1 - \epsilon_1$, $R_\ell (kr)$ and $R_\ell (k'r)$ are fast decaying functions while for $r > R_2 + \epsilon_2$, the product $R_\ell (kr)\, R_\ell (k'r)$ oscillates approximately as $\cos((k - k')\, r)$. In the latter case the Expression (143) is good approximation to integral (135) if (i) $f(R_2 + \epsilon_2) << f(R_1)$, i.e., if $f(r)$ goes to zero rapidly enough with increasing r or (ii) $|k - k'|\, r >> 1$ so that the product $R_\ell (kr)\, R_\ell (k'r)$ oscillates rapidly and $|f(r)|$ is monotonically decreasing function of r for $r \geq R_2 + \epsilon_2$. In this appendix we restrict ourselves to the case $\ell = \ell'$ and compare our approximate results with those obtained by numerical integration of Eqs. (135) and (141) for the case that $f(r) = V(r)$.

To obtain the approximate solution of Eq. (135) we write

$$\frac{1}{r^2} \approx -2.46 \times 10^{17}\, e^{-2\beta r} + 4.74 \times 10^{16}\, e^{-\beta r} + 4.33 \times 10^{14} \tag{144}$$

Figure 61 shows a graph of right-hand side of Eq. (144) and shows that the above approximation is a reasonable one for $2 \times 10^{-8} \leq r \leq 5 \times 10^{-8}$ = cm. Now we define

$$a_\ell \equiv \frac{2\mu D}{\hbar^2} e^{2\beta R_0} - 2.46 \times 10^7 \ \ell\,(\ell + 1) \tag{145}$$

$$\beta_\ell \equiv \frac{4\mu D}{\hbar^2} e^{\beta R_0} - 4.74 \times 10^{16} \ \ell\,(\ell + 1) \tag{146}$$

and $$k \equiv k^2 - 4.33 \times 10^{14} \ \ell\,(\ell + 1) \tag{147}$$

We will restrict our approximate method to the case for which

$$a_\ell \geq 0. \tag{148}$$

Equation (135) can now be written as

$$\frac{d^2 R_\ell}{dr^2} + \left[k_\ell^2 + a_\ell e^{-2\beta r} + \beta_\ell e^{-\beta r}\right] R_\ell = 0 \tag{149}$$

Restriction (148) makes $V(r) \approx a_\ell e^{-2\beta r}$ for $r \ll 0$ and permits us to alter the boundary condition (137) to

$$\lim_{r \to -\infty} R_\ell (kr) = 0. \tag{150}$$

The solution of (149) which satisfies boundary conditions (148) and (150) is

$$R_\ell (z) = \frac{1}{2} \left| \frac{\Gamma\left(\frac{1}{2} - \kappa + i\gamma\right)}{\left|\Gamma\ (2i\gamma)\right|} \right| z^{-1/2} W_{\kappa,\, i\gamma}(z)$$

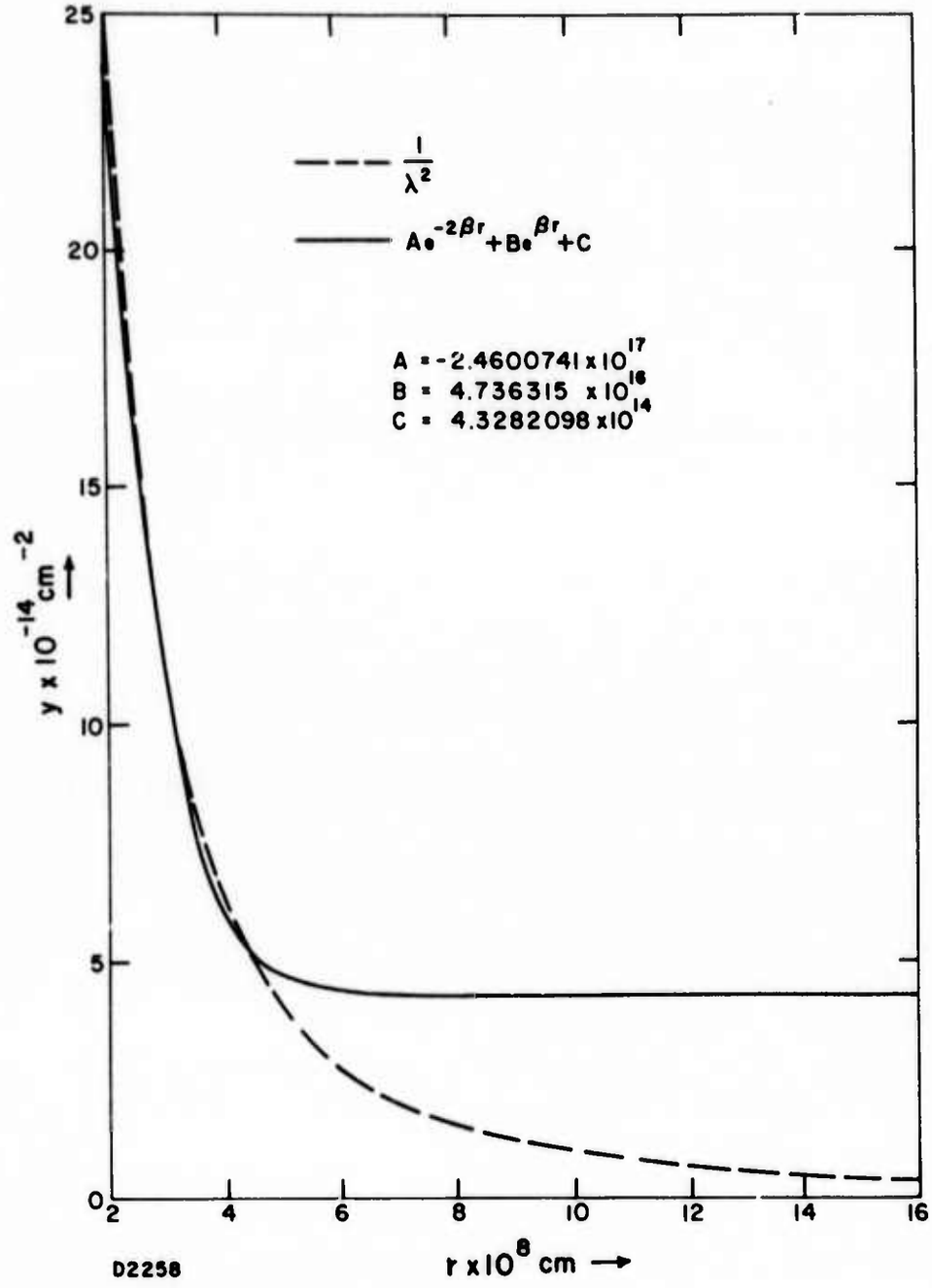

Fig. 61 Comparison of $1/r^2$ - - - with the Approximate Form Used in Solving the Wave Equation

where

$$\gamma \equiv \frac{k_\ell}{\beta} \tag{151}$$

$$\kappa \equiv \frac{\beta_\ell}{2\beta} \, (a_\ell)^{-1/2} \tag{152}$$

and

$$z \equiv \frac{2}{\beta} \, (a_\ell)^{1/2} \, e^{-\beta r} \tag{153}$$

Γ in Eq. (150) is gamma function and W is a Whittaker function.

The appropriate form of integral is

$$\int_0^\infty R_\ell (kr) \, R_\ell (k' r) \, V (r) \, dr \tag{153}$$

$$\simeq D \, e^{2\beta R_0} \, I_1 - 2D \, e^{\beta R_0} \, I_2$$

where

$$I_1 = \frac{\beta}{16 \, a_\ell} \quad \frac{\left|\Gamma\left(\frac{1}{2} - \kappa + i\gamma\right)\right| \left|\Gamma\left(\frac{1}{2} - \kappa + i\gamma'\right)\right|}{\left|\Gamma (2i\gamma)\right| \left|\Gamma(2i\gamma')\right|} \, I_3 \tag{155}$$

and

$$I_3 = \int_0^\infty W_{\kappa, i\gamma} (z) \, W_{\kappa, i\gamma'} (z) \, dz$$

$$= \frac{2\pi^2}{\cosh (2\pi\gamma) - \cosh (2\pi\gamma')} \tag{156}$$

$$\left[\frac{\gamma^2 - \gamma'^2 + 2\kappa}{\left|\Gamma\left(\frac{1}{2} - \kappa + i\gamma\right)\right|^2} + \frac{\gamma^2 - \gamma'^2 - 2\kappa}{\left|\Gamma\left(\frac{1}{2} - \kappa + i\gamma'\right)\right|^2}\right] \quad \text{if } \gamma' \neq \gamma.$$

$$I_3 = \frac{4\pi}{\sinh(2\pi\gamma)} \frac{1}{\left|\Gamma\left(\frac{1}{2} - \kappa + i\gamma\right)\right|^2} \left(\gamma + \kappa \operatorname{Im} \psi\left(\frac{1}{2} - \kappa + i\gamma\right)\right)$$

if $\gamma' = \gamma$. (157)

where $\psi(z) = \frac{\Gamma'(z)}{\Gamma(z)}$ is psi function.

$$I_2 = \frac{1}{8(a_\ell)^{1/2}} \frac{\left|\Gamma\left(\frac{1}{2} - \kappa + i\gamma\right)\right|}{|\Gamma(2i\gamma)|} \frac{\left|\Gamma\left(\frac{1}{2} - \kappa + i\gamma'\right)\right|}{|\Gamma(2i\gamma')|} I_4 \quad (158)$$

$$I_4 = \int_0^\infty \frac{1}{z} W_{\kappa, i\gamma}(z) W_{\kappa, i\gamma}(z)\, dz$$

$$= \frac{|\Gamma(1 + i\gamma + i\gamma')|^2 |\Gamma(1 + i\gamma - i\gamma')|^2}{\left|\Gamma\left(\frac{1}{2} - \kappa + i\gamma\right)\right|^2 \left|\Gamma\left(\frac{1}{2} - \kappa + i\gamma'\right)\right|^2} \frac{1}{\gamma^2 - \gamma'^2}$$

$$\times \left(\left|\Gamma\left(\frac{1}{2} - \kappa + i\gamma'\right)\right|^2 - \left|\Gamma\left(\frac{1}{2} - \kappa + i\gamma\right)\right|^2\right) \text{ if } \gamma \neq \gamma' \quad (159)$$

and

$$I_4 = \frac{1}{\gamma} \frac{|\Gamma(1 + i\gamma + i\gamma')|^2 |\Gamma(1 + i\gamma - i\gamma')|^2}{\left|\Gamma\left(\frac{1}{2} - \kappa + i\gamma\right)\right|^2} \operatorname{Im} \psi\left(\frac{1}{2} \kappa + i\gamma\right)$$

if $\gamma' = \gamma$ (160)

Equation (154) gives the approximate value of the integral when the classical turning points (Eqs. (141) and 142)) are less than 5 Å. For values of ℓ and k such that one of the two turning points is greater than 5 Å, we approximate the solution of (135) by Bessel functions, i.e., we ignore V (r) term in Eq. (135). In this approximation

$$R_\ell (kr) = kr\, j_\ell (kr) \tag{161}$$

where j_ℓ ' s are spherical Bessel functions. The integral to be evaluated now is

$$kk' \int_0^\infty j_\ell (kr)\, j_\ell (k'r)\, V(r)\, r^2\, dr$$

$$= \frac{\pi}{2} D (kk')^{1/2} \left[e^{2\beta R_0} \int_0^\infty J_{\ell + 1/2} (kr)\, J_{\ell + 1/2} (k'r)\, re^{-2\beta r} dr \right.$$

$$\left. - 2 e^{\beta R_0} \int_0^\infty J_{\ell + 1/2} (kr)\, J_{\ell + 1/2} (k'r)\, e^{-\beta r}\, rdr \right] \tag{162}$$

Writing

$$\int_0^\infty J_{\ell + 1/2} (kr)\, J_{\ell + 1/2} (k'r)\, r\, e^{-\beta r}\, dr$$

$$= - \frac{d}{d\beta} \int_0^\infty J_{\ell + 1/2} (kr)\, J_{\ell + 1/2} (k'r)\, e^{-\beta r}\, dr$$

$$= - \frac{1}{\pi} (kk')^{-1/2} \frac{d}{d\beta} Q_\ell \left(\frac{\beta^2 + k^2 + k'^2}{2kk'} \right)$$

$$= - \frac{\beta}{\pi} (kk')^{-3/2} Q'_\ell (z) \tag{163}$$

where Q_ℓ is Legendre function of the second kind, $Q'_\ell(z) = d/dz\, Q_\ell(z)$ and $z = \beta^2 + k^2 + k'^2/2kk'$. Using the recursion relation

$$Q'_\ell(z) = (z^2 - 1)^{-1} (\ell + 1) \left[Q_{\ell+1}(z) - z Q_\ell(z) \right] \tag{164}$$

one can write

$$kk' \int_0^\infty j_\ell(kr)\, j_\ell(k' r)\, r^2\, e^{-\beta r}\, dr$$

$$= -\frac{\beta}{2} \frac{(\ell + 1)}{(z^2 - 1)} \left[Q_{\ell+1}(z) - z Q_\ell(z) \right] \tag{165}$$

Similarly,

$$kk' \int_0^\infty j_\ell(kr)\, j_\ell(k' r)\, r^2\, e^{-2\beta r}\, dr$$

$$= -\beta \frac{(\ell + 1)}{\left(z_1^2 - 1\right)} \left[Q_{\ell+1}(z_1) - z_1 Q_\ell(z_1) \right] \tag{166}$$

where $z_1 \equiv 4\beta^2 + k^2 + k'^2/2kk'$.

Using Eqs. (165) and (166), we can write

$$kk' \int_0^\infty j_\ell(kr)\, j_\ell(k' r)\, V(r)\, r^2\, dr$$

$$= \beta D (\ell + 1) e^{\beta R_0} \left[(z^2 - 1)^{-1} (Q_{\ell+1}(z) - z Q_\ell(z)) \right.$$

$$\left. - e^{\beta R_0} (z_1^2 - 1)^{-1} (Q_{\ell+1}(z_1) - z Q_\ell(z)) \right] \tag{167}$$

Table XI compares the results obtained for the left-hand side of Eq. (154) by numerical integration (Col. a) with the approximate expression given on the right-hand side of Eq. (154) (Col. b). Column c is that obtained by Takayanagi's modified wave number approximation while Col. d is obtained using Eq. (167). The potential parameters used are $\beta = 1.4 \times 10^{8}$ cm^{-1}, $R_0 = 4 \times 10^{-8}$ cm and $D = 5 \times 10^{-14}$ ergs. The potential parameters are considered appropriate for H-Ar interaction. The results show that the numerical results and the approximate expression on the L.H.S. of Eq. (154) agree well before the former changes sign. After the change of sign the numerical integral agrees well with that obtained using Eq. (167). The physical basis of this result is that a change in sign of the integral occurs when the attractive term in the Morse potential becomes more important. At that point the trajectory is hardly deflected and one can approximate R_ℓ (kr) by kr j_ℓ (kr). Operationally during a calculation we switched over from Col. b to Col. d when Col. d changed sign. Takayanagi's results agree well with the numerically obtained ones when $k \approx k'$. When $k \neq k'$, the Takayanagi modified wave number approximation appears to be valid for low values of ℓ.

Table XII demonstrates the smoothness of the transition when change from Col. b to d is made when d changes sign.

For $\ell = 49$ and 50 the sign of the results in Cols. b and d differs from that in Col. a. This disagreement should not be taken seriously. The absolute value of the integral for these partial waves is about an order of magnitude smaller than the nearby ones with the result that their contribution to the cross section is negligible.

TABLE XI

VALUES OF THE INTEGRAL $\int_0^\infty R_\ell(kr)\, R_\ell(k'r)\, V(r)\, dr$ OBTAINED BY DIFFERENT METHODS

$k = 1.35\times10^{9}\,cm^{-1}$

	$k' = 1.43\times10^{9}\,cm^{-1}$				$k' = 1.90\times10^{9}\,cm^{-1}$				$k' = 3.23\times10^{9}\,cm^{-1}$			
ℓ	a	b	c	d	a	b	c	d	a	b	c	d
0	1.45×10^{-21}	1.45×10^{-21}	1.45×10^{-21}	5.86×10^{-18}	1.87×10^{-22}	1.87×10^{-22}	1.87×10^{-22}	1.28×10^{-18}	1.85×10^{-27}	1.85×10^{-27}	1.85×10^{-27}	1.18×10^{-19}
10	1.38×10^{-21}	1.36×10^{-21}	1.34×10^{-21}	1.38×10^{-18}	1.68×10^{-22}	1.68×10^{-22}	1.69×10^{-22}	6.24×10^{-20}	1.47×10^{-27}	1.45×10^{-27}	1.56×10^{-27}	4.86×10^{-23}
20	1.16×10^{-21}	1.10×10^{-21}	1.04×10^{-21}	2.14×10^{-19}	1.23×10^{-22}	1.20×10^{-22}	1.24×10^{-22}	1.79×10^{-21}	7.25×10^{-28}	7.06×10^{-28}	9.54×10^{-28}	1.00×10^{-26}
30	8.06×10^{-22}	7.26×10^{-22}	6.11×10^{-22}	2.82×10^{-20}	6.58×10^{-23}	6.34×10^{-23}	7.06×10^{-23}	4.55×10^{-23}	1.95×10^{-28}	1.89×10^{-28}	4.04×10^{-28}	1.83×10^{-30}
40	3.65×10^{-22}	3.20×10^{-22}	1.89×10^{-22}	2.84×10^{-20}	2.07×10^{-23}	2.07×10^{-23}	2.82×10^{-23}	1.11×10^{-24}	2.05×10^{-29}	2.15×10^{-29}	1.16×10^{-28}	3.16×10^{-34}
50	-2.98×10^{-23}	2.30×10^{-23}	-3.22×10^{-23}	1.07×10^{-23}	2.11×10^{-24}	2.57×10^{-24}	5.02×10^{-23}	2.62×10^{-26}	3.87×10^{-31}	5.61×10^{-31}	1.88×10^{-28}	5.30×10^{-38}
60	-1.28×10^{-22}	-2.15×10^{-23}	-2.28×10^{-22}	-1.25×10^{-22}	2.54×10^{-26}	1.81×10^{-26}	6.64×10^{-23}	6.06×10^{-28}	3.42×10^{-34}	4.01×10^{-34}	3.79×10^{-27}	8.74×10^{-42}
80	-2.21×10^{-23}	-9.77×10^{-24}	-1.60×10^{-23}	-2.16×10^{-23}								
100	-2.44×10^{-24}	-4.14×10^{-24}		-2.44×10^{-24}								

1, Potential used is $V(r) = 5\times10^{-14}\left[e^{1.2}e^{-2.8r} - 2e^{5.6}e^{-1.4r}\right]$.

a, Result of numerical integration

b, Present calculation

c, Takayanagi modified wavenumber approximation

d, Bessel function approximation

TABLE XII

COMPARISON ON THE NUMERICAL VALUES OBTAINED BY METHODS OF EXACT INTEGRATION, BESSEL APPROXIMATION AND THE PRESENT THEORY

$k = 1.35 \times 10^9$ $k' = 1.43 \times 10^9$

ℓ	a	b	c
40	3.65×10^{-22}	3.20×10^{-22}	2.84×10^{-21}
42	2.75×10^{-22}	2.47×10^{-22}	1.66×10^{-21}
44	1.88×10^{-22}	1.79×10^{-22}	9.16×10^{-22}
46	1.06×10^{-22}	1.18×10^{-22}	4.53×10^{-22}
48	3.26×10^{-23}	6.54×10^{-23}	1.73×10^{-22}
49	-1.85×10^{-25}	4.29×10^{-23}	8.06×10^{-23}
50	-2.91×10^{-23}	2.30×10^{-23}	1.10×10^{-23}
51	-5.59×10^{-23}	5.89×10^{-24}	-4.03×10^{-23}
52	-7.83×10^{-23}	-8.31×10^{-24}	-7.73×10^{-23}
54	-1.11×10^{-22}	-2.76×10^{-23}	-1.20×10^{-22}
56	-1.29×10^{-22}	-3.53×10^{-23}	-1.35×10^{-22}
58	-1.34×10^{-22}	-3.22×10^{-23}	-1.34×10^{-22}
60	-1.28×10^{-22}	-2.15×10^{-23}	-1.25×10^{-22}

(a) Numerical integration

(b) Present results

(c) Bessel approximation

APPENDIX II

THE DERIVATION FOR THE EXPRESSION OF $\langle \chi_B' \left| e^{-i\underline{q} \cdot \underline{r}_{\nu c}} \right| \chi_B \rangle$

In this appendix we evaluate the matrix elements $\langle \chi_f \left| e^{-i\underline{q} \cdot \underline{r}_\nu} \right| \chi_i \rangle$, where χ_i and χ_f are wave functions for the rotational and vibrational motion, $\underline{q}$ is the momentum exchanged during the collision and $\underline{r}_\nu$ is the distance of the νth atom of the molecule from the center of mass of the molecule. We consider only diatomic molecules. In this case $\underline{r}_1 = m_2/m_1 + m_2\, \underline{r}$ and $\underline{r}_2 = -m_1/m_1 + m_2\, \underline{r}$, where m_1 and m_2 are the masses of the atom 1 and 2, respectively, and $\underline{r}$ is the internuclear distance. Further we write $\underline{r} = \underline{b} + \underline{u}$, where $\underline{b}$ is the equilibrium internuclear distance and $\underline{u}$ is the vibrational displacement. We also write $\chi_i = \phi_i(u) \times Y_{j_i m_i}(\hat{b})$ where ϕ_i is harmonic-oscillator wave function for vibrational level i and $Y_{j_i m_i}$ are the spherical harmonics.

$$\langle \chi_f \left| e^{-i\underline{q} \cdot \underline{r}_1} \right| \chi_i \rangle$$

$$= \langle Y_{j_f m_f} \left| \langle \phi_f \left| e^{-i\underline{q} \cdot \underline{r}_1} \right| \phi_i \rangle \right| Y_{j_i m_i} \rangle$$

$$= \langle Y_{j_f m_f} \left| \langle \phi_f \left| e^{-i \frac{m_2}{M} \underline{q} \cdot \underline{u}} \right| \phi_i \rangle e^{-i \frac{m_2}{M} \underline{q} \cdot \underline{b}} \right| Y_{j_i m_i} \rangle \qquad (168)$$

$$\langle \phi_f \left| e^{-i \frac{m_2}{M} \underline{q} \cdot \underline{u}} \right| \phi_i \rangle = 4\pi \sum_{\ell_1, m_1} (-)^{\ell_1} Y_{\ell_1 m_1}(\Omega_q)\, Y^*_{\ell_1 m_1}(\Omega_b)$$

$$\times \int_{-\infty}^{+\infty} \phi_f^*\, j_{\ell_1}\left(\frac{m_2}{M} q u\right) \phi_i \, du \qquad (169)$$

In Eq. (169) we have written $Y^*_{\ell_1 m_1}(\Omega_b)$ for $Y^*_{\ell_1 m_1}(\Omega_u)$ because $\underline{b}$ and $\underline{u}$ are collinear, j_ℓ are spherical Bessel functions and $M \equiv m_1 + m_2$.

The vibrational wave functions have the property

$$\phi_v(-u) = (-)^v \phi_v(u) \tag{170}$$

Since the spherical Bessel Functions have the same parity as the order of the Bessel Function, i.e.,

$$j_{\ell_1}(-x) = (-)^{\ell_1} j_{\ell_1}(x), \tag{171}$$

the integral over the wave functions vanishes unless $i + f + \ell_1$ is an even number. We can therefore write

$$\int_{-\infty}^{+\infty} \phi_f^* j_{\ell_1}\left(\frac{m_2}{M} q u\right) \phi_i \, du = \left[1 + (-)^{f+i+\ell_1}\right] \times \int_0^{+\infty} \phi_f j_{\ell_1}\left(\frac{m_2}{M} q u\right) \phi_i \, du \tag{172}$$

Using the relation

$$\phi_v(u) = \left(\frac{\mu\omega}{\sqrt{\pi}\,\hbar (v!)\, 2^v}\right)^{1/2} \exp\left[-\frac{\mu\omega}{2\hbar} u^2\right] H_v\left(\left(\frac{\mu\omega}{\hbar}\right)^{1/2} u\right) \tag{173}$$

where $\mu = m_1 m_2/M$ is the reduced mass and ω is the frequency (radians/sec) of the oscillator and H_v are Hermite Polynomials of order v, we can write

$$\int_0^{\infty} \phi_f^* \, j_{\ell_1}\left(\frac{m_2}{M} q u\right) \phi_i \, du = \left[\pi (i!) (f!) 2^{i+f}\right]^{-1/2}$$

$$\times \int_0^{\infty} j_{\ell_1}(a_1 u) \exp(-u^2) H_i(u) \times H_f(u) \, du \tag{174}$$

where

$$a_1 \equiv \frac{m_2}{M}\left(\frac{\hbar}{\mu\omega}\right)^{1/2} q \tag{175}$$

Using the relation

$$H_n(x) = n! \sum_{m=0}^{\left[\frac{n}{2}\right]} \frac{(-)^m (2x)^{n-2m}}{m!\,(n-2m)!} \tag{176}$$

where $[n/2]$ is the largest integer less than or equal to $n/2$, Eq. (174) can be rewritten as

$$\int_0^\infty \phi_f^* \, j_{\ell_1}(a_1 u)\, \phi_i \, du = \left(\frac{(i!)\,(f!)\,2^{i+f}}{\pi}\right)^{1/2} \sum_{m=0}^{\left[\frac{i}{2}\right]} \sum_{n=0}^{\left[\frac{f}{2}\right]} \left(\frac{-1}{4}\right)^{m+n}$$

$$\times \left[m!\,(i-2m)!\,(n!)\,(f-2n)!\right]^{-1} \int_0^\infty du\, j_{\ell_1}(a_1 u)\, e^{-u^2}\, (u)^{i+f-2m-2n}$$

$$= \left((i!)\,(f!)\,2^{i+f}\right)^{1/2} (2a_1)^{-1/2} \sum_{m=0}^{\left[\frac{i}{2}\right]} \sum_{n=0}^{\left[\frac{f}{2}\right]} \left(\frac{-1}{4}\right)^{m+n}$$

$$\times \left[m!\,(i-2m)!\,(n!)\,(f-2n)!\right]^{-1} \int_0^\infty du\, J_{\ell_1+1/2}(a_1 u)\, e^{-u^2}\, u^{i+f-2m-2n-\frac{1}{2}}$$

$$= R_1(\ell_1, i, f, q) \tag{177}$$

where $R_1(\ell_1, i, f, q)$

$$\equiv \frac{1}{4} e^{-\frac{a_1^2}{4}} \left(\frac{a_1}{2}\right)^{\ell_1} \left[\Gamma\left(\ell_1 + \frac{3}{2}\right)\right]^{-1} \left[(i!)\,(f!)\,2^{i+f}\right]^{1/2}$$

$$\times \sum_{m=0}^{\left[\frac{i}{2}\right]} \sum_{n=0}^{\left[\frac{f}{2}\right]} \left(\frac{-1}{4}\right)^{m+n} \left[m!\;(i-2m)!\,(n!)\,(f-2n)!\right]^{-1} \tag{178}$$

$$\times \Gamma\left(\frac{i+f-2m-2n+\ell_1+1}{2}\right) {}_1F_1\left(\frac{\ell_1 - i - f + 2m + 2n + 2}{2}; \ell_1 + \frac{3}{2}; \frac{a_1^2}{4}\right)$$

where ${}_1F_1(a; b; z) = 1 + \frac{a}{b} z + \frac{a(a+1)}{b(b+1)} \frac{z^2}{2!} + \ldots$ is confluent hypergeometric function.

Substituting Eqs. (177), (178), and (172) in Eq. (169) we get

$$\langle \phi_f \left| e^{-i \frac{m_2}{M} \underline{q} \cdot \underline{u}} \right| \phi_i \rangle = 4\pi \sum_{\ell_1, m_1} (-i)^{\ell_1} Y^*_{\ell_1 m_1}(\Omega_q)\, Y_{\ell_1 m_1}(\Omega_b)$$

$$\times \left(1 + (-)^{i+f+\ell_1}\right) R_1(\ell_1, i, f, q) \tag{179}$$

Using the expansion for the planewave and standard relations between spherical harmonics we can write

$$e^{-i\frac{m_2}{M}\,\underline{q}\cdot\underline{b}} \left\langle \phi_f \right| e^{-i\frac{m_2}{M}\,\underline{q}\cdot\underline{u}} \left| \phi_i \right\rangle$$

$$= (4\pi)^{3/2} \sum_{\ell_1,\ \ell_2,\ \ell} (-i)^{\ell_1+\ell_2}\ \hat{\ell}_1\hat{\ell}_2\ C^2(\ell_1\ \ell_2\ \ell{:}00)$$

$$(1+(-)^{i+f+\ell_1})\, j_{\ell_2}\left(\frac{m_2}{M}\ q\ b\right) R_1(\ell_1,\ i,\ f,\ q)$$

$$\times \sum_m Y^*_{\ell m}(\Omega_q)\, Y_{\ell m}(\Omega_b) \qquad (180)$$

where $\hat{\ell} \equiv (2\ell+1)$, etc.

Substituting (180) in (168) we get

$$\left\langle \chi_f \right| e^{-i\underline{q}\cdot\underline{r}_1} \left| \chi_i \right\rangle$$

$$= 4\pi\,(\hat{j}_i)^{1/2}\ (-)^{j_i-m_i} \sum_{\ell_1,\ \ell_2,\ \ell} (-i)^{\ell_1+\ell_2}\ \hat{\ell}_1\hat{\ell}_2$$

$$C^2(\ell_1\ \ell_2\ \ell;\ 00)\ C(j_i\ \ell\ j_f;\ 00)\ (1+(-)^{i+f+\ell_1}) \qquad (181)$$

$$j_{\ell_2}\left(\frac{m_2}{M}\ q\ b\right) R_1(\ell_1,\ i,\ f,\ q) \sum_m Y^*_{\ell m}(\Omega_q)\, C(j_1\ j_f\ \ell;\ m_i,\ m-m_i)\, R_1$$

REFERENCES

1. Pimentel, G. C. and Kasper, J. V. V., "HCℓ Chemical Laser," Phys. Rev. Letters 14, 352 (1965).

2. Batovskiy, O. M., Vasilyev, G. K., Makarov, Ye. F. and Talroze, V. L., "Chemical Laser Based on a Branched Chain Reaction of Fluorine with Hydrogen," Zhurnal eksperimental' noy i teoreticheskoy fiziki, Vol 9, No. 6 p 341-343 (1969).

3. Polanyi, J. C. and Woodall, K. B., "Energy Distribution among Reaction Products VI. F+H_2, D_2," J. Chem. Phys. 57, 1574 (1972); Polanyi, J. C. and Sloan, J. J., "Energy Distribution among Reaction Products VII. H+F_2," J. Chem. Phys. 57, 4988 (1972).

4. Wilson, J. and Stephenson, J. C., "Atmospheric Pressure Pulsed Chemical Laser," Applied Phys. Letters 20, 64 (1972).

5. Wilson, J., et al, "Exploratory Development Work in Support of the High Power/Energy Laser Program (U)," Final Report under Contract F29601-70-C-0073 prepared for Air Force Weapons Laboratory, Kirtland Air Force Base, New Mexico, July 1971.

6. Ksander, Yuri, "Soviet Chemical Laser Research," ARPA Report 189-1 (1971).

7. Kapralova, G. A., Trofimova, E. M., Shilou, A. E., Kinetika i Kataliz, 6, 977 (1965).

8. Levy, J. B. and Copeland, B. K. K., "The Kinetics of the Hydrogen Fluorine Reaction III The Photochemical Reaction," J. Phys. Chem. 72, 3168 (1968).

9. Hancock, J. K. and Green, W. H., "Laser Excited Vibrational Relaxation Studies of HF," J. Chem. Phys. 56, 2474 (1972).

10. Hess, L. D., "HF Chemical Laser Studies, Use of MoF_6 to Increase Reaction Rates in H_2 - F_2 Mixtures," J. Appl. Phys. 43, 1157 (1972).

11a. Fried, S., Wilson, J., and Taylor, R., "Temperature Dependence of HF Vibrational Relaxation," presented at 3rd Conf. on Chemical and Molecular Laser, St. Louis (1972) in press.

11b. Polanyi, J. C., "Vibrational Rotational Population Inversion," Appl. Opt. Suppl. 2, 109 (1965).

12. Deutsch, T. F., "Laser Emission from HF Rotational Transitions," Appl. Phys. Letters 11, 18 (1967).

13. Cohen, N., Tech. Rept. TR-0172 (2779)-2 The Aerospace Corporation, Sept. 1971.

14. Airey, J. R., "Cl + HBr Pulsed Chemical Laser; A Theoretical and Experimental Study," J. Chem. Phys. 52, 156 (1970).

15. Meredith, R. E., Spellieg, R. L. and Smith, F. G., "Strengths and Collision Widths in the Second Overtone Band of Hydrogen Fluoride," J. Chem. Phys. 57, 5119 (1972).

16. Airey and Smith, "Quenching of IR Chemilumenescence; Rates of Energy Transfer from HF ($V \leq 5$) to CO_2 and HF, and from DF ($V \leq 3$) to CO_2 and HF," J. Chem. Phys. 57, 1669 (1972).

17. Rigord, W. W., "Saturation Effects in High Gain Lasers," J. Appl. Phys. 36, 2487 (1965).

18. Polanyi, J. C. and Woodall, K. B., "Mechanism of Rotational Relaxation," J. Chem. Phys. 56, 1563 (1972).

19. Suchard, S. N., Kerber, R. L., Emanuel, G., and Whittier, J. S., "Effect of H_2 Pressure on Pulsed H_2+F_2 Laser, Experiment and Theory," J. Chem. Phys. 57, 5065 (1972).

20. Krogh, O. D. and Pimentel, G. C., "Chemical Lasers from the Reaction of ClF and ClF_3 with H_2 and CH_4. A Possible Chain Branching Chemical Laser," J. Chem. Phys. 56, 969 (1972).

21. Gensel, P., Kompa, K. L. and Wammer, J., "IF_5 - H_2 Hydrogen Fluorine Chemical Laser Involving A Chain Reaction," Chem. Phys. Letters 5, 179 (1970).

22. Gregg, D. W., Krawetz, B., Pearson, R. K., Schleicher, B. R., Thomas, S. J., Huss, E. B., Pettipiece, K. J., Cheighton, J. R., Niver, R. E., and Pan, Y. L., "Electron Beam and Flashlamp Initiation of a Pulsed Hydrogen Fluoride Chemical Laser," Chem. Phys. Letters 8, 609 (1971).

23. Wilson, J., and Stephenson, J. C., "Atmospheric Pressure Pulsed Chemical Laser," App. Phys. Letters Vol 20, pp 64-66 (1972).

24. Airey, J. R., "Cl + HBr Pulsed Chemical Laser: A Theoretical and Experimental Study," J. Chem. Phys. Vol 52, pp 156-167 (1970)

25. Airey, J. R. and McKay, S. F., "A Supersonic Mixing Chemical Laser," Appl. Phys. Letters 15, 401 (1969).

26a. Wilson, J., Stephenson, J. C., and Northam, D., "Exploratory Development Work in Support of the High Power/Energy Laser Program (U)," Final Report under Contract F29601-70-C-0073 prepared for Air Force Weapons Lab. and Advanced Research Projects Agency, July 1971.

26b. Wilson, J., Northam, D. and Lewis, P., "HF Laser Action above the Second Explosion Limit," paper presented at 3rd Symposium on Chemical and Molecular Lasers, St. Louis, April 1972.

27. Landshoff, R. K. and Magee, J. L., "Thermal Radiation," Lockheed Report 3-27-67-1 Vol 4, Nov. 1967, DASA 1917-4.

28. Mandl, A., AVCO Everett Research Laboratory, private communication.

29. Fox, R. E., "Dissociative Attachment of Electrons in I_2," Phys. Rev. 109, 2008 (1958).

30. Kompa, K. L. and Wanner, J., "Chem. Phys. Letters 5, 179 (1970).

31. Christophorou, L. G., "Atomic and Molecular Radiation Physics," Wiley-Interscience, New York (1971).

32. Hancock, J. K. and Green, W. H., "Laser Excited Vibrational Relaxation Studies of HF," J. Chem. Phys. 56, 2472 (1972).

33. Wilson, J., Chen, H-L, Fyfe, W., Taylor, R. L., Little, R. and Lowell, R., "Electron Beam Dissociation of Fluorine, J. Chem. Phys. to be published.

34. Berger, J. J. and Seltzer, S. M., "Tables of Energy Losses and Ranges of Electrons and Positrons," Paper 10, NAS-NRC Publication 1133 (1964), also NASA SP-3012 (1964).

35. Bortner, T. E. and Hurst, G. S., "Ionization of Pure Gases and Mixtures of Gases by 5-Mev Alpha Particles," Phy. Rev. Vol 93, pp 1236-1241 (1954).

36. Hayes, J. N., Ulrich, P. B., and Aitken, A. H., "Effects of the Atmosphere on the Propagation of 10.6 μ Laser Beams," Appl. Opt. 11, 257 (1972).

37. Hayes, J. N., "Thermal Blooming of Laser Beams in Fluids," Appl. Opt. 11, 455 (1972).

38. Harmuth, H. F., "On the Solution of the Schroedinger and the Klein-Gordon Equations by Digital Computers," J. Math. Phys. 36, 269 (1957).